Response to Referee #1 (Andreas Zuend) on "Influence of Organic Compound Functionality on Aerosol Hygroscopicity: Dicarboxylic Acids, Alkyl-Substituents, Sugars and Amino Acids"

Aleksandra Marsh[1], Rachael E. H. Miles[1], Grazia Rovelli[1], Alexander G. Cowling[1], Lucy Nandy[2], Cari S. Dutcher[2] and Jonathan. P Reid[1]
[1] School of Chemistry, University of Bristol, Bristol, BS8 1TS, UK
[2] Department of Mechanical Engineering, University of Minnesota, 111 Church Street SE, Minneapolis, MN 55455, USA

Correspondence to: Jonathan. P. Reid j.p.reid@bristol.ac.uk

The authors would like to thank Andreas Zuend (Referee #1) for his generally positive comments on the manuscript. We respond to the specific comments made by the referee below and identify the changes we have made to the manuscript.

On consideration of the comments, all predictions generated by AIOMFAC-web have been repeated with careful consideration of the functional groups used. Methyl malonic acid, 3-methyl adipic acid, dimethyl malonic acid, 2,3-dimethyl succinic acid and pimelic acid were found to differ marginally from the original predictions. All figures (Figure 2, 4, 5 and 7), supporting information and tabulated data have been updated to reflect these changes. Although the corrections lead to slight numerical changes, they do not alter the overall conclusions of the manuscript.

Response to general comments

Referee Comment: *Section 2. Methods and Materials. While the reader is referred to Rovelli et al. (2016) and Davis et al. (2013) for a detailed description of the CK-EDB method, a general description of the chemicals used, their purities and solution preparation is missing. Some of that information is provided in the SI 2 only. I suggest that a brief description is also given in the main text and that the reader should be informed about additional information on this in the SI.*

Response: As recommended by the referee, we have added a brief comment on P4 L21-23 to refer the reader to the detailed information in the SI: 'Purity and supplier for all compounds is presented in the supplementary information. Further, all measurements presented in this work are taken at 293.15 K. All solutions are prepared using HPLC grade water (VWR Chemicals).'

Referee Comment: *Temperature range and droplet temperatures. In the first paragraph of page 4 it is highlighted that the temperature in the EDB trapping region can be controlled well over a ~75 K range, however, throughout the main text information about the actual temperature used is missing (including tables and figures). As far as I can tell from the temperature information given in the SI, all experiments and model calculations were carried out at 293.15 K. Were hygroscopicity measurements at other temperatures considered (which would be useful, e.g. for improved, temperature-dependent thermodynamic model parameterisations given the temperatures were sufficiently different)?*

Response: We have now noted the temperature of all measurements (see previous response). We have conducted temperature dependent hygroscopicity experiments for a number of organic systems presented in this work and for a number of additional inorganic systems. However, these will be detailed in a subsequent publication due to the length of this manuscript and the length of discussion involved on the effect of temperature on hygroscopicity.

Referee Comment: *...a discussion on the EDB temperature range used and the actual droplet surface temperature during the evaporation experiments will require some discussion. From Rovelli et al. (2016) it seems clear that the time scale of the evaporation will lead to deviations between droplet and surrounding gas phase temperature. Moreover, given that the evaporation rate from a relatively concentrated solution droplet*

is different from the evaporation rate of the probe droplet, a discussion of such temperature related issues with respect to the retrieval of the sample droplet's water activity at a particular temperature seems appropriate.

Response: We agree with the referee that accounting for the temperature suppression is important when retrieving the hygroscopic growth curve. We have provided an extensive discussion of this in our recent paper (Rovelli et al. 2016, as identified by the referee) where we provided considerable evidence to validate and benchmark the technique. Having previously provided this information in great detail, we feel that any further discussion provided here would be rather insubstantial and inferior to our previous discussion. Instead, we feel it is important that the reader be referred to the comprehensive account in our earlier report, with all procedures used in this manuscript carefully following our earlier recommendation. On P7 L11 we add the following comment: "It is imperative that the evaporative cooling be accounted for as this suppresses the apparent vapour pressure at any instant, particularly at early time when the mass flux is larger. Indeed, equation (5) explicitly accounts for the latent heat lost from the droplet. At very early times and when evaporating into low RH, the temperature suppression can be sufficient (>3 K) so as to reduce the accuracy of approximations made when deriving equation 5. Under these circumstances, when the temperature suppression is larger than this limit, we do not infer equilibrium water activities, but instead only retrieve the equilibrium hygroscopic growth when the temperature suppression is smaller than 3 K. This procedure has been discussed and verified in detail in our earlier work, and the reader is referred to Rovelli et al. (2016) for further details."

Referee Comment: In contrast to the inorganic solutes used in Rovelli et al. (2016), the present study involves organic solutes, some of which may cause a significant increase in mixture viscosity with decreasing droplet water content during evaporation in the EDB. In this context, the time scale of 10 s for the evaporation from the droplets may become an issue for droplets > 10 µm radius, potentially impeding the droplet-gas mass transfer (e.g. Koop et al., 2011) and potentially violating assumptions about a homogeneous, concentration-gradient-free mixing of water and organic compound within sample droplets aside from a developing temperature gradient within a rapidly evaporating droplet. The authors discuss the viscosity concern in Section 3.3, where it is mentioned that for many compounds measurements unimpeded by kinetic limitations were not possible below 80 % RH. Because this consideration may not only apply to sugars and alcohols, but to many of the multifunctional organics of higher molar mass, a more general discussion of kinetic limitations and consequences for the CKEDB data processing should be provided in Section 2 where the method is described. If a relatively viscous binary aqueous droplet is exposed to low RH and evaporates water quickly, there may be insufficient time for homogeneous mixing in the droplet bulk compared to the near-surface volume of the droplet, which could lead to a concentration gradient and a higher solute concentration in the surface region of the droplet, affecting the local water activity there. Under such conditions, an organic solute may appear as more hygroscopic than it would be under actual gas-particle equilibrium conditions. Did the authors consider such effects in their method and the data processing? It is also not clear whether the authors considered a longer measurement time scale with slower evaporation settings for systems where substantial kinetic limitations may occur (and for which organic evaporation may not be a concern). Please discuss.

Response: We have added the following discussion and Figures to the SI, "The kinetic modelling framework used in the analysis of the droplet evaporation events is valid only in the absence of a bulk-kinetic limitation on near surface composition, i.e. the particle must be assumed to be homogeneous in composition. Such a limitation was obvious for hygroscopicity measurements of trehalose, galactose and sorbitol at RH's lower than 80 %. To ensure the measurements are not compromised by bulk diffusion, we consider two important factors.

Firstly, the impact of viscosity on the hygroscopicity retrievals becomes very obvious when we consider the consistency and uncertainty in the raw hygroscopic growth curves determined from different droplets evaporating into differing RHs. Droplets drying into different RHs reach different compositions at different times, and will retain different amounts of water because of different drying rates. This leads to an artificially low MFS at a particular RH which then slowly returns to the equilibrium curve overtime. Thus, an inconsistency is apparent between retrieved hygroscopic growth curves (or MFS vs a_w) when drying into different RHs. An example of this is shown in Figure S39.1, where we report unbinned hygroscopicity data for alanine (a non-viscous amino acid) and trehalose (viscous at RHs lower than 80%). It is clear here that the different portions of the hygroscopic curves retrieved from measurements at different RHs are consistent for alanine but not for trehalose. A further easy way to identify this retention of water in a particle that is not fully

equilibrated is simply to measure the much longer time-dependence in size once the initial evaporation of water has stopped. In droplets that have reached a bulk diffusion limitation, the existence of a kinetic limitation is apparent in a steadily decreasing size as water continues to leave over a timescale longer than 10 s.

Fig S39.1 a) Unbinned hygroscopicity data for the compound alanine. b) Unbinned hygroscopicity data for the compound trehalose. At 50 % RH trehalose has a viscosity of 3.8 x 10^5 Pa.s (Song et al. 2016).

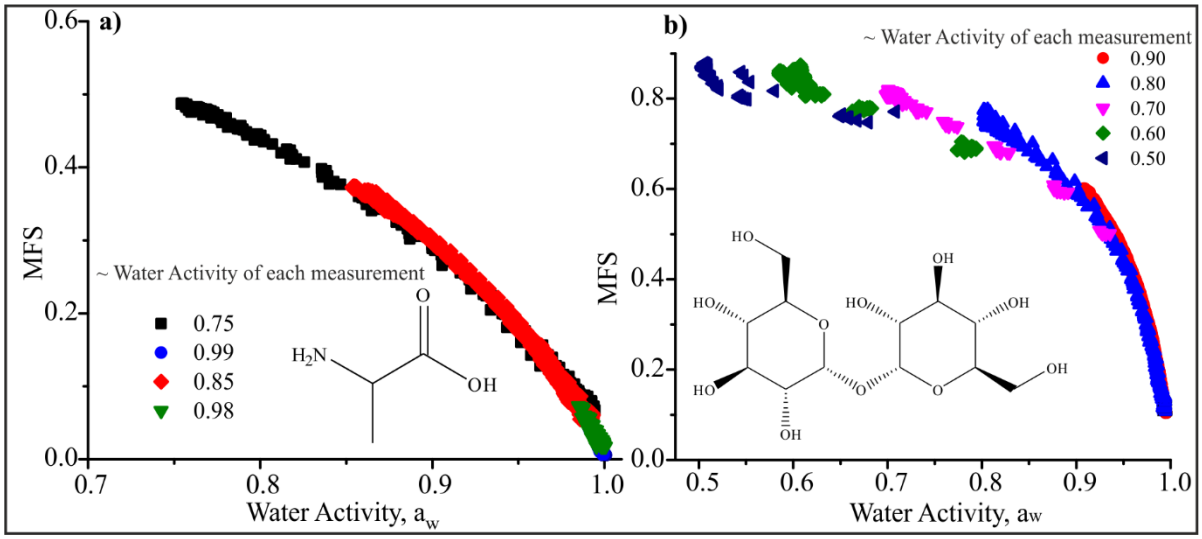

Secondly, we can determine the expected conditions under which we might expect problems to arise in retrieving hygroscopic growth curves from an evaporation measurement. Considering again trehalose at 80 % RH, an aqueous-trehalose droplet has a viscosity of 0.5 Pa.s, increasing to 3.8 × 10^5 Pa.s at 50 % RH (Song et al. 2016). Therefore, as the RH of the gas phase for the evaporation measurement is lowered, we can expect the increasing viscosity/decreasing diffusivity to become increasingly important. By contrast, for aqueous-carboxylic acid droplets, the viscosity never gets above 1 Pa s even at the driest RHs considered here (Song et al. 2016).

With these known dependencies of viscosity on water activity, we can estimate the timescale for diffusional mixing within a droplet, assuming that this provides an estimate of the timescale for an evaporating droplet to form a homogeneous mixture. This timescale must be considerably shorter than the evaporation timescale for our hygroscopicity estimations to be valid. First, the Stokes-Einstein equation is used to estimate the diffusion constant of water at varying viscosity (varying RH).

$$D = \frac{k_B T}{6\pi r_{mol} \eta} \qquad (1.1)$$

D is the diffusion constant, k_B is the Boltzmann constant, T is temperature, r_{mol} is the molecular radius of water (taken as 1.375 Å) and η is the viscosity. It should be noted that equation (1.1) is likely to provide a significant underestimate of the diffusion constant due to the failure of the Stokes-Einstein equation. At a viscosity of 100 Pa s, the diffusion constant for water in sucrose is already more than one order of magnitude larger than estimated from the viscosity (Power et al. 2013). However, using diffusion constants estimated from (1.1) will provide an upper limit on the diffusional mixing timescale. The timescale for diffusional mixing, τ, is then estimated using the expression

$$\tau = \frac{a^2}{\pi^2 D} \qquad (1.2)$$

where a is the droplet radius (set as 10 microns in this calculation).

We compare the diffusional mixing timescales for aqueous droplets of trehalose, NaCl, $NaNO_3$ and glutaric acid in the newly added supplemental Figure S39.2 (and repeated below). Given that we have been able to report accurate hygroscopic growth curves for $NaNO_3$ down to 50 % RH (see Rovelli et al. 2016 and the

response to referee 2), it is clear that a final viscosity at 50 % of ~ 0.1 Pa.s (Baldelli et al.) is insufficient to impede accurate measurement of the hygroscopicity. Indeed, this suggests that water transport in any aerosol droplet that maintains a viscosity lower than 0.1 Pa.s during drying should remain sufficiently fast to avoid a bulk diffusion limitation, permitting accurate hygrosocpicity measurements. As an example of the diacarboyxlic acids considered in this study, glutaric acid has a considerably lower viscosity at 50 % RH of ~ 0.01 Pa.s (Song et al. 2016), indicative of what we might expect for all such similar systems. By contrast, aqueous-trehalose droplets cross the 0.1 Pa.s viscosity threshold at a water activity of ~0.85 (Song et al. 2016), commensurate with the deviation and increased scatter in the hygroscopicity measurements reported above for this compound.

Again, we must reiterate that the true diffusion constants are generally found to be much larger than values estimated from the Stokes-Einstein equation. A droplet with a viscosity of 0.1 Pa s takes ~0.3 s to mix by diffusion based on our analysis here, but this is an upper limit on the timescale.

Based on the two considerations above and to indicate clearly the water activity ranges over which we consider the hygroscopicity measurements to be valid for trehalose (S30), galactose (S31) and sorbitol (S29), we have added a dashed line to indicate where the data appear to become kinetically limited. We have added the following words to the captions of these Figures: "Data taken at RHs lower than indicated by the dashed black line show increased error in hygroscopicity retrieval due to the imposition of a kinetic limitation on water transport."

Fig S39.2 a) Viscosity of Trehalose, NaCl, NaNO3 and Glutaric Acid as a function of RH. b) Estimated diffusion constant as a function of RH. c) Timescale for diffusional mixing at the RH shown on x-axis. Dashed green line represents 1 second timescale for diffusional mixing.

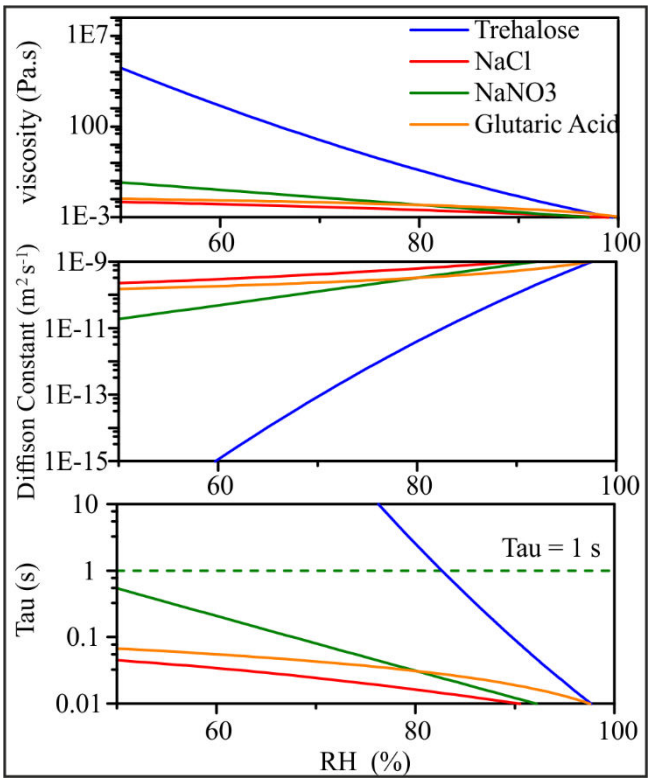

A. Baldelli, R. M. Power, R. E. H. Miles, J. P. Reid and R. Vehring *Effect of crystallization kinetics on the properties of spray dried microparticles,* Aerosol Science and Technology, 2016, 50:7, 693-704, DOI:10.1080/02786826.2016.1177163

R. M. Power, S. H. Simpson, J. P. Reid and A. J. Hudson, *The transition from liquid to solid-like behaviour in ultrahigh viscosity aerosol particles,* Chemical Science, 2013, 4 , 2597, DOI: 10.1039/c3sc50682g

Y. Chul Song, A. E. Haddrell, B. R. Bzdek, J. P. Reid, T. Bannan, D. O. Topping,, C. Percival, and C. Cai *Measurements and Predictions of Binary Component Aerosol Particle Viscosity* J. Phys. Chem. A 2016, 120, 8123−8137, DOI: 10.1021/acs.jpca.6b07835"

Referee Comment: *UNIFAC models – three general comments and clarifications:*
1. The authors compare many of the measurements to predictions by "the" UNIFAC model, however, the information about the specific model version used and its parameterisation for some of the compounds is incomplete in the manuscript. While the original UNIFAC model theory by Fredenslund et al. (1975) is mentioned on page 2, several UNIFAC modifications 3 (changes to model equations, e.g. UNIFAC-Dortmund, UNIFAC-Lyngby, etc.) and several revisions of UNIFAC parameter tables applicable to certain UNIFAC versions have been published in the past 40 years. For example, the AIOMFAC model (Zuend et al., 2008; 2011), which includes a UNIFAC model based on the original theory of Fredenslund et al. (1975), relies mostly on the revised parameter set by Hansen et al. (1991). However, Zuend et al. (2011) discuss several modifications of the parameter database, including the use of improved interaction parameters determined by Marcolli and Peter (2005) for alcohols and multifunctional compounds containing hydroxyl groups, as well as modified interaction parameters by Peng et al. (2001) for a subset of interactions involving carboxylic acid groups. These modifications are detailed in Zuend et al. (2011) and are used in the online version of the AIOMFAC model (which was used for several comparisons with measurements in the present paper; see also www.aiomfac.caltech.edu/about.html). Similarly, the online UNIFAC versions in UManSysProp (http://umansysprop.seaes.manchester.ac.uk; Topping et al., 2016), which includes AIOMFAC and a UNIFAC version, and the E-AIM website's UNIFAC (www.aim.env.uea.ac.uk/aim/aim.php) contain modified parameter sets from Peng et al. (2001) and from other sources of UNIFAC parameter revisions (see also http://www.aim.env.uea.ac.uk/aim/phpmain/edit_help.php#section100 for details on UNIFAC in E-AIM). While some of these newer parameterisations lead to only slight changes to predicted water activities compared to the original UNIFAC by Fredenslund et al. (1975) with the Hansen et al. (1991) parameters, others are significant – and e.g. in the case of AIOMFAC, the description of alcohols and sugars is substantially modified by the introduction of specific subgroups and main groups in the model for these compounds (of relevance for the comparisons with CK-EDB data made in this study). Therefore, to provide sufficient detail for clarity and reproducibility, it is necessary to specify which models and parameterisations were actually applied (e.g. in the Methods section).

Response: All UNIFAC model predictions presented in this paper for dicarboxylic acids, sugars and alcohols were performed using AIOMFAC-web. This has been specified both in section 3.1. (Hygroscopic Response of Dicarboxylic Acids of Varying Complexity) and section 3.3. (Sugars and Alcohols) and in all relevant captions (Figure 2, 3, 5 and 10). We have added the following to ensure clarity:

P8 L11: 'All calculations for dicarboxylic acids were performed using the AIOMFAC-web model.'
P2 L33: 'AIOMFAC-web implements several improved parameters which are detailed by Zuend et al. (2011).'
P10 L13: With regard to amino acid modelling we have added the following: 'Hence UNIFAC (AIOMFAC-web) thermodynamic model predictions for amino acids were generated using E-AIM, using the UNIFAC model with Peng et al. parameterization (Peng et al., 2001) and Model III (Clegg et al., 1998).'

Referee Comment: *2. Contrary to the statements on page 2, lines 30 – 32 and on page 8, lines 20-21, UNIFAC (and AIOMFAC) actually account for the molecular structure and for certain differences between branched and straight-chain dicarboxylic molecules of the same molar mass – albeit in a limited way. For example, via the differing number in hydrogen atoms on CH_2, CH, and C subgroups, which leads to different values of the relative Van der Waals volume and surface area terms in the combinatorial part of the UNIFAC model for these alkyl subgroups (affecting predicted activity coefficients). For this reason, the UNIFAC subgroup assignments, as listed in Table S0 of the SI, are incomplete/incorrect in the case of the dicarboxylic acids. For example, CHn is not a UNIFAC/AIOMFAC subgroup and as such does not sufficiently characterise the compound; instead the appropriate subgroups need to be stated. For example, correct subgroup assignments show that the three distinct C7- dicarboxylic acids (see also Table 3 of Zuend et al. (2011): 3-methyl adipic acid, (CH3)(CH)(CH2)3(COOH)2, 3,3-dimethylglutaric acid, (CH3)2(C)(CH2)2(COOH)2, and pimelic acid, (CH2)5(COOH)2, have slightly different subgroup formulas in UNIFAC/AIOMFAC and consequently there should be distinct model curves in Fig. 5b and UNIFAC structure formulas in Table S0 of the SI. Although,*

this reviewer agrees that the differences between UNIFAC predictions for such similar dicarboxylic acids are likely small.

Response: We have amended P2 L 31 to read: 'In this approach, molecules are divided into characteristic molecular subgroups and the activity coefficients derived from group contributions with limited consideration for molecular structure.' Further, we have removed the text on P8 L20-21 that reads: '…a consequence of representing all CH, CH2, and CH3 substituents by CHn (Zuend et al., 2008).'

We would like to apologise because these AIOMFAC-web predictions were labelled incorrectly in the previous version of Figure 5(b) and have been corrected in the new Figure 5(b). The caption now reads: "….where the AIOMFAC-web prediction for 3-methyl adipic acid, $[(CH_3)(CH)(CH_2)_3(COOH)_2]$, 3,3-dimethylglutaric acid, $[(CH_3)_2(C)(CH_2)_2(COOH)_2]$, 2,2-dimethylglutaric acid, $[(CH_3)_2(C)(CH_2)_2(COOH)_2]$ is represented by the blue dashed line. Note that the equilibrium curves for the first 4 compounds are in such close agreement and indistinguishable on this scale that only one curve is shown for clarity. The prediction for pimelic acid $[(CH_2)_5(COOH)_2]$ is shown as a black solid line."

With respect to the AIOMFAC web prediction for 3-methyl adipic acid $[(CH_3)(CH)(CH_2)_3(COOH)_2]$, 3,3-dimethylglutaric acid $[(CH_3)_2(C)(CH_2)_2(COOH)_2]$, 2,2-dimethylglutaric acid $[(CH_3)_2(C)(CH_2)_2(COOH)_2]$ and diethyl malonic acid $[(CH3)_2(CH2)_2(C)(COOH)_2]$, the predicted equilibrium activity curves (mfs vs water activity) are so similar that they are indistinguishable, as shown in the figure below. As a consequence, only one curve is used to represent all four compounds in Fig. 5.

We have now explicitly included all functional groups used in the prediction of the AIOMFAC–web curves in Table S0 of the SI as suggested by the referee.

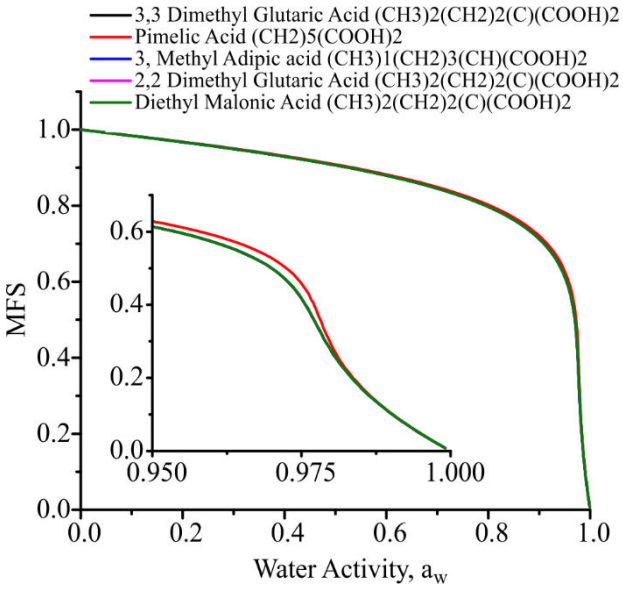

Referee Comment: 3. The UNIFAC group-contribution method also offers another way to account for proximity effects by neighboring subgroups in organic molecules: specific subgroups can be assigned to larger sections of a molecular structure and that has been proposed for modified UNIFAC parameterisations in the case of amino acids. For example, Gupta and Heidemann (1990) introduced a specific "proline" UNIFAC subgroup (including a subset of determined interaction parameters for aqueous solutions of amino acids). Kuramochi et al. (1997) introduced a series of new functional groups and determined UNIFAC parameters for the description of most amino acids, including histidine, for a modified UNIFAC version based on "Larsen's UNIFAC". Thus, statements like (page 10, line 15): "UNIFAC predictions cannot be performed for all amino acids examined here; in particular, the ring structures found in proline and histidine, cannot be represented as subgroups in the current version of UNIFAC." are not generally correct – the UNIFAC parameterisation by Kuramochi et al. covers most amino acids studied experimentally in this work. However, it is correct that those "specialized" UNIFAC modifications are not implemented in the online versions of AIOMFAC and UNIFAC in E-AIM (see point (1) above), so they are not conveniently available for

calculations, which is likely what is meant by the authors' statement. Such general statements should therefore be revised accordingly and the work by Gupta and Heidemann (1990), Kuramochi et al. (1997) and others mentioned. Consider also that parameter sets that were determined for different UNIFAC model versions are typically not compatible and the use of specific subgroups with only a limited set of interaction parameters determined, e.g. for aqueous mixtures of amino acid solutions only, disqualifies the applicability of such models for predictions of complex, multi-component and multifunctional mixtures of interest in atmospheric aerosol chemistry (as discussed in Section 5.4 of Zuend et al., 2011).

Response: We have amended section 3.2. P10 L14 now reads: "Amino acids form zwitterions in solution, supressing the vapour pressure of the acid, and this presents a challenge to current thermodynamic models with most not allowing the inclusion of nitrogen amine containing groups (e.g. AIOMFAC-web). AIOMFAC-web only allows for the inclusion of organonitrate and peroxy acyl nitrate sub groups. Hence, model predictions for amino acids were generated using E-AIM, using the UNIFAC model with Peng et al. parameterization (Peng et al., 2001) and Model III (Clegg et al., 1998). Even then UNIFAC predictions cannot be performed for all the amino acids examined here. In particular, the ring structures found in proline and histidine cannot be represented as subgroups in the current version of E-AIM, although these could be represented with the further parametrisations reported by Kuramochi et al. (1997b) or Gupta and Heidemann (1990)."

Specific comments and technical corrections

Referee Comment: Abstract, first sentence and page 4, line 9: "Hygroscopic data" should be "Hygroscopicity data" (the data itself is likely not hygroscopic).
Response: Corrected to: 'Hygroscopicity data for 36 organic compounds'

Referee Comment: P3, line 7: correct spelling of "Köhler"
Response: Corrected to: 'Köhler'

Referee Comment: P3, l. 11 – 13: "Values are typically determined from sub-saturated hygroscopic growth measurements and reported at the highest accessible RH (Pajunoja et al., 2015). The value of κ can also be inferred from measurements of the critical supersaturation required for CCN activation, a measurement in a super-saturated regime (Carrico et al., 2008)." It would be appropriate to state that κ values determined at different RH and, to a lesser extent temperature, can vary substantially, especially when comparing κ determined from CCN activation data at water super-saturation compared to sub-saturation conditions, as, e.g., discussed by Hodas et al. (2016) and references mentioned therein.
Response: P3 L15 We have added 'Further, κ values reported at different RHs can vary significantly and can also differ substantially from measurements in the supersaturated regime (Hodas et al., 2016).'

Referee Comment: P3, l. 33: correct "(approaching [values] very close to 1)"
Response: We have amended to read "(approaching values very close to 1)"

Referee Comment: P4, l. 25: clarify the accuracy statement: "with a greater accuracy (< ± 0.2 % at water activities > 0.8…" do you mean < ± 0.2 % error in water activity or in hygroscopic growth factor or MFS?
Response: We have clarified the statement to read: "accuracy (<±0.2 % error in water activity at water activities > 0.8 and ±1 % error in water activity at water activities < 0.8) than can be achieved in conventional approaches"

Referee Comment: P6, l. 5: "with most solutes instead", better: "with most pure organic compounds instead" since this is not about a solution but about the pure components.
Response: We have amended to read: 'corresponds to that of the pure sub-cooled melt with most pure organic compounds'

Referee Comment: *P6, title 2.3: Replace "hygroscopic" by hygroscopicity*
Response: We have amended to read '2.3. Extraction of Hygroscopicity properties'

Referee Comment: *P7, l. 2: "In this equation, the gradient in water partial pressure is the difference between the RH and aw, the instantaneous water activity at the droplet surface." First, given the evaporation setup with an RH profile dependent on the distance from the droplet, it needs to be stated which RH (and measured where) is meant, i.e. is it the RH at the droplet surface or the RH (sufficiently) far away from the droplet. Second, the difference (RH - aw) or rather saturation ratio S – aw) (as in Rovelli et al., 2016) alone does not constitute a "gradient". Also, since the component subscript "i" in Eq. (5) denotes water (i.e. subscript "w" as in aw), it would seem better to use "w" instead of "i".*

Response: We have added the following sentence to clarify that the probe droplet is trapped in exactly the same position as the sample droplet: "In this study, the probe droplets are trapped in exactly the same position within the gas flow as the sample droplets which allows the measurement of the RH in situ. The probe droplets are either pure water (for the RH range 80 – 99 %) or aqueous NaCl (for the RH range 50 – 80 %)."

When referring to gradient in the text, we are referring to the gradient in water partial pressure and we believe this is correct. We do not refer to a gradient formed from (RH-a_w). To be consistent with our previous publications, we have removed the subscript *i* entirely from the equation but not replaced it with *w*.

Referee Comment: *P7, l. 9: "is the latent heat of vaporization"; add "of water" at temperature T_∞(?).*
Response: Added 'L is the latent heat of vaporization of water at T_∞.'

Referee Comment: *P8, l. 10: "using Peng corrections" the meaning of this is unclear. Also, as detailed above, the UNIFAC models likely used by the authors actually include further modifications in terms of the used parameter sets and/or subgroup assignments.*
Response: All UNIFAC predictions (with the exception of amino acids) were performed using AIOMFAC-web and we hope we have now made this clear in the manuscript.

Referee Comment: *P8, l. 20: "In addition, the UNIFAC predictions become less accurate as the added substituent becomes larger, a consequence of representing all CH, CH2, and CH3 substituents by CHn (Zuend et al., 2008)." There seems to be a misunderstanding about the UNIFAC (AIOMFAC) way of group contribution calculations, see the general comment above. Only group-group interactions in the residual UNIFAC expressions are common for all CHn subgroups (with n = 0,1,2,3), but the volume and surface area terms (combinatorial part) are not. This is the case in all variants of UNIFAC.*
Response: We have removed 'a consequence of representing all CH, CH2, and CH3 substituents by CHn (Zuend et al., 2008).'

Referee Comment: *P9, l. 20 and l. 17: There are actually more than two distinct UNIFAC group formulas for the different C7-dicarboxylic acids, see the general comment above. Also, given that the UNIFAC (AIOMFAC) model predictions of water activity show a deviation from the CK-EDB data for the straight-chain pimelic acid, the model-measurement deviations shown in Fig. 5b are expected and at least consistent in that sense. Related to the statement on line 17, the observed similarity in hygroscopicity of the different C7-dicarboxylic acids suggests that the degree of branching and/or lengths of alkyl substituents may not always play a substantial role, in particular above a water activity of 0.8. This seems to be a counter-example to the trends observed for the smaller dicarboxylic acids with alkyl substitutions (and a hint for a general underestimation of the hygroscopicity contribution by the CHn groups as represented in UNIFAC/AIOMFAC).*

Response: We have now included all functional groups used for AIOMFAC-web predictions in the table in the SI for each compound. The referee makes an interesting observation about the general consequences of the observation of the underestimation of the contribution from CHn groups.

Referee Comment: P10, l. 15: The sentence should be revised as certain nitrogen containing compounds are available in most UNIFAC models (including in AIOMFAC for organics + water systems) since the parameter set by Hansen et al. (1991) includes amine, amid, nitro, nitrile and pyridine groups and some version include organonitrate groups (Compernolle et al., 2009; Zuend and Seinfeld, 2012) and proline and histidine groups Kuramochi et al. (1997).

Response: We have amended the section on P10, 3.2. Hygroscopic Response of Amino Acids, to read: "Amino acids form zwitterions in solution, supressing the vapour pressure of the acid, and this presents a challenge to current thermodynamic models with most not allowing the inclusion of nitrogen amine containing groups (e.g. AIOMFAC-web). AIOMFAC-web only allows for the inclusion of organonitrate and peroxy acyl nitrate sub groups. Hence, model predictions for amino acids were generated using E-AIM, using the UNIFAC model with Peng et al. parameterization (Peng et al., 2001) and Model III (Clegg et al., 1998). Even then UNIFAC predictions cannot be performed for all the amino acids examined here. In particular, the ring structures found in proline and histidine cannot be represented as subgroups in the current version of E-AIM, although these could be represented with the further parametrisations reported by Kuramochi et al. (1997b) or Gupta and Heidemann (1990)."

In addition, on P10 L28-29 we have stated: "We used the UNIFAC model with Peng et al. parameterization (Peng et al. 2001), typically run in E-AIM in the Model III mode (Clegg et al. 1998)."

Referee Comment: P10, l. 22: "except for L-valine"; According to Fig. 8, L-Threonine behaves similar to L-valine even though it contains a hydroxyl group instead of a methyl group. So it seems that L-valine is not an exception or not the only one. Also, the UNIFAC prediction for glycine is missing in Fig. 8a.
Response: We have added the UNIFAC prediction for glycine to Fig. 8a. We have also amended Page 10 line 20 "On a MFS scale, the hygroscopic response of these compounds is similar except for L-threonine which is less hygroscopic, an observation that is not expected given the additional hydrophilicity of the hydroxyl substituent."

Referee Comment: P10, l. 30: "is fitted to molality experimental data"; molality of what? The last part of that sentence needs to be rephrased as well.
Response: We have amended P10 L30 to read: "The model (equation 27 in Dutcher et al. 2013) is fitted to experimental data for solute molality as a function of water activity, in order to determine the adjustable model parameter. The model predicts solute activities and concentrations across all water activities, by combining short-range adsorption isotherm and long-range Debye-Huckel expressions. The isotherm model results in improvement in MFS predictions when compared to UNIFAC. However, the notable difference in accuracy between the two models is not overly surprising: the isotherm based model of Dutcher et al. 2013 has an adjustable parameter (Table S0.2), while UNIFAC is a fully predictive model."

Referee Comment: P11, l. 13: Statement needs to be revised given the above clarification about specific UNIFAC parameterisations for aqueous solutions of amino acids.
Response: On P11 L15, we have removed: "This is a consequence of the current reliance of the UNIFAC parameterisation on the data of Chan et al. (2005)."

Referee Comment: P11, l. 15: "This is a consequence of the current reliance of the UNIFAC parameterisation on the data of Chan et al. (2005)." This statement is incorrect, because the UNIFAC models used by the authors do in fact not contain the modified parameters by Chan et al. (2005); rather, they are based on Hansen et al. (1991) and Peng et al. (2001) parameters for the amino acids. Also, as is clearly shown in Chan et al. (2005), their modified UNIFAC parameterisation yields similar results to the Peng et al. version in many cases and the Peng et al. parameterisation is in reasonable agreement with their own experimental data (e.g. for threonine). Therefore, the discrepancies between the new CK-EDB data and the UNIFAC model curves shown

indicate clear discrepancies among different experimental data sets, as is discussed by the authors in the first paragraph of page 11.
Response: On P11 L15, we have removed "This is a consequence of the current reliance of the UNIFAC parameterisation on the data of Chan et al. (2005)."

Referee Comment: P12, l. 27: "Molecular structures presented in Fig. 10 are the open chain form, which must be used during modelling using UNIFAC."; Why "must"? AIOMFAC also allows you to use the cyclic structure of sugars in aqueous solution, e.g. glucopyranose instead of glucose, if desired.
Response: Cyclic sugar structures do not appear to be available on AIOMFAC-web. Amended P11 L27 to read 'Molecular structures presented in Fig. 10 are the open chain form, which must be used during modelling using AIOMFAC-web.'

Referee Comment: P12, l. 10: and Fig. 11 & 12: replace the compound class labelled "organic acids" by a more appropriate label, e.g. "dicarboxylic acids", since amino acids are also organic acids but not part of that class.
Response: Labels in Figures 11 and 12 have been amended from organic acids to dicarboxylic acids as suggested.

Referee Comment: P12, l. 32: Statement is incorrect, see comment to P11, l. 15.
Response: We have removed the statement: 'this is due to earlier experimental measurements by Chan et al. (2005) which have been used to parametrise UNIFAC'

Referee Comment: P13, first paragraph. With respect to the applicability of the determined component-kappa values from binary data with a simple mixing rule for a complex mixture's total hygroscopicity parameter kappa, I suggest the authors consider in this section that it remains rather uncertain whether the kappa values determined based on binary water + amino acid data apply in multicomponent mixtures of relevance for atmospheric aerosol. This is because the substantial hygroscopicity exhibited by many of the amino acids, due to their zwitterionic nature in aqueous solution, may be affected substantially by the presence of inorganic acids and dissolved salts in aerosol mixtures, altering the partial water uptake contribution by the amino acids in a non-linear manner. This may motivate further experimental investigations for organic-inorganic mixtures with the CK-EDB and other setups.
Response: We agree with the referee's comment and will indeed soon progress to measurements of the hygroscopic response of mixtures.

Referee Comment: Table 1: State the temperature (range) for the measurements. Also the caption text and table header concerning SMILES needs revision.
Response: We have added the temperature of the measurements to caption to read: "Table 1. Experimentally determined κ values at $a_w = 0.95$ for all compounds studied at 293.15 K, presented alongside κ values calculated using UManSysProp and the smile string used for this calculation." We have changed 'smile string' to 'SMILES String'
Referee Comment: Fig. 1: Lower panel, at around 0.9 water activity, the red triangles-up and black triangles-down symbols suggest a larger scatter in experimental data than the binned data and error bars account for. It is unclear why if it is assumed that the different drying rates have similar measurement uncertainty? A brief discussion may be useful.
Response: Each dataset has an associated uncertainty on water activity depending on the RH at which the evaporation occurs (Rovelli et al. 2016). The higher the RH in the gas phase, the slower the evaporation, and there is consequently a greater density of measured data points. This is why the dataset at the higher RH has a higher weighting in the overall averaged data.

Referee Comment: Fig. 2: state the UNIFAC parameterisation used, if AIOMFAC-web was used, then stating that would be sufficiently specific.

Response: AIOMFAC-web was used and this has been stated in the caption on appropriate figures: "UNIFAC predictions using AIOMFAC-web."

Referee Comment: Fig. 6: the y-axis label "n(water)/n(solute)" would be better written as in Fig. 7 or perhaps in abbreviated form, such as nw/ns.
Response: This has been amended to match that in Figure 7.

Referee Comment: Figs. 8 and 9: The UNIFAC (Peng et al. parameterisation) model curve for Glycine is missing.
Response: The UNIFAC prediction for Glycine has been added in Figures 8 and 9.

Referee Comment: Fig. 9: Comparing this figure to Fig. 1 of Chan et al. (2005), it is clear that many experimental data points from Na et al. are missing, as well as bulk data by Kuramochi et al. (1997) to higher MFS/lower aw than shown and data by Ninni and Mereilles (2001) in Fig. 9b. Including all these measurements in Fig. 9 will provide a better comparison for the discussion concerning the substantial discrepancies found among the experimental data sets and in comparison to model predictions.

Response: As suggested, more data points from Na et al. have been added in Figure 9(a) and (b). It should be noted that in Na et al. the parametrisation of the hygroscopicity data for glycine does not accurately reproduce the experimental data presented in their manuscript. Thus these points in Figure 9(a) were determined by reading a number of points from the graph and a curve with the following formula fit to them MFS = 0.65967 + 0.5305 a_w -1.1458 a_w^2, and this equation was used to generate additional points now plotted on Figure 9a). All available data from Ninni and Mereilles (2001) and Kuramochi et al. (1997) have now been included in both Figure 9(a) and (b).

Referee Comment: Supplementary Information: It would be useful to briefly state at the end of the main text what information is provided in the SI.
Response: This statement has been added on P13 L4-5: 'The supplementary information provides tabulated hygroscopicity data for all compounds measured in this study, it also details compound purities, density and refractive index parametrisations for all compounds.'

Referee Comment: SI, Table S0: the page numbers for different systems are listed, but the pages in the SI were not numbered. Also, the AIOMFAC subgroups stated for the dicarboxylic acids with CHn groups should be revised, see general comment. The "CHn(OH)" groups stated for citric acid, tartaric acid and other compounds should be stated with OH preferentially in superscript (e.g. CH2[OH] for a CH2 subgroup bonded to an OH group, which is specified separately) to avoid confusion about the number of OH groups present in the molecular structure (see also Table 3 of Zuend et al., 2011).
Response: Supporting Information pages have now been numbered, groups in Table S0 have been labelled according to the suggestions above; an example for tartaric acid is $(COOH)_2$ $(OH)_2$ $(CH)_2$ $^{(OH)}$.

Referee Comment: SI, Fig. S8.1: Check the caption text and symbols in the figure. I do not see any coloured curves for data at different temperatures stated in the caption.
Response: S8.1. This caption has been altered to remove any reference to temperature dependent data. This will be reported in a subsequent paper. 'Hygroscopicity of L-Valine, (Sigma Aldrich, Purity ≥ 98 %), at 293.15 K Open symbols, these CK-EDB experiments; black filled circles, literature data (Kuramochi et al.); solid black line, UNIFAC model (293.15 K).'

Referee Comment: SI, S26 and S27: For aqueous PEG mixtures, much improved interaction parameters have been determined for a PEG-specific version of AIOMFAC, but these are not yet included in AIOMFAC web (see also Hodas et al., 2016).
Response: We are grateful to the referee for highlighting this and will provide a further comparison when the refined parameters are available in AIOMFAC.

Response to Anonymous Referee #2 on "Influence of Organic Compound Functionality on Aerosol Hygroscopicity: Dicarboxylic Acids, Alkyl-Substituents, Sugars and Amino Acids"

Aleksandra Marsh[1], Rachael E. H. Miles[1], Grazia Rovelli[1], Alexander G. Cowling[1], Lucy Nandy[2], Cari S. Dutcher[2] and Jonathan. P Reid[1]
[1] School of Chemistry, University of Bristol, Bristol, BS8 1TS, UK
[2] Department of Mechanical Engineering, University of Minnesota, 111 Church Street SE, Minneapolis, MN 55455, USA

Correspondence to: Jonathan. P. Reid j.p.reid@bristol.ac.uk

The authors would like to thank the referee for their generally positive comments on the quality of the manuscript. We respond to the specific comments made by the referee below and identify the changes we have to the manuscript.

Referee Comment: *Page 1 line 12 "The dual micro dispenser set up allows for sequential trapping of probe and sample droplets for accurate determination of droplet water activities from 0.45 to > 0.99." This sentence is not entirely correct. The CK-EDB is based on kinetic measurements and it does have the advantage of fast measurements that reduce evaporation of volatile materials.*

Response: In prior publications we have provided considerable data that confirm the validity of the technique for a wide range of inorganic and organic systems. See particularly:

Rovelli, G., Miles, R. E. H., Reid, J. P., & Clegg, S. L. (2016). Hygroscopic Properties of Aminium Sulphate Aerosols. Atmospheric Chemistry and Physics Discussions. https://doi.org/10.5194/acp-2016-959

Rovelli, G., Miles, R. E. H., Reid, J. P., & Clegg, S. L. (2016). Accurate Measurements of Aerosol Hygroscopic Growth Over a Wide Range in Relative Humidity. The Journal of Physical Chemistry A, 120, 4376−4388. https://doi.org/10.1021/acs.jpca.6b04194

Davies, J. F., Haddrell, A. E., Rickards, A. M. J., & Reid, J. P. (2013). Simultaneous Analysis of the Equilibrium Hygroscopicity and Water Transport Kinetics of Liquid Aerosol. Analytical Chemistry, 85, 5819–5826. https://doi.org/dx.doi.org/10.1021/ac4005502

The referee is correct in suggesting that the measurements are in essence kinetic, however we still consider that our statement is accurate. Compared with the timescale of internal dynamics within the droplet (diffusional mixing, heat transport), the evaporative process may actually be considered to be sufficiently slow that the droplet adopts a uniform composition, a particular water activity and, consequently, the equilibrium vapour pressure for the solution composition at that moment in time. Indeed, based on the expression for the mass flux, equation (5), it is the water activity in the droplet that is the determining quantity and it is this that is measured.

Referee Comment: *However, the fast measurements would also potentially lead to non-equilibrium measurements, especially for some organics at low RH. The authors seem to admit a potential shortcoming of the technique on page 11, line 23, "For many compounds, measurements unimpeded by kinetic limitations have not been possible below 80 % RH, and consequently data presented below 80 % do not average to a consistent series of points". More evidence to demonstrate that the measurements presented in this paper are equilibrium measurements would be needed.*

Response: We have responded in detail to this comment in our response to referee #1. In brief, we have clearly shown in our earlier publications that equilibrium hygroscopicity curves can be retrieved with high accuracy. We reproduce below Figure 5 from Rovelli et al. (2016) as an example, comparing hygroscopicity measurements of inorganic salts taken using the CK-EDB with equilibrium thermodynamic model predictions,

all of which are in very good agreement. For some organic components that lead to viscous droplets on drying, departure from equilibrium behaviour with varying water content is clearly apparent from the measurements. We show in our response to referee #1 (and discuss further below) that the hygroscopicity measurement remains extremely accurate unless the viscosity increases above 0.1 Pa s. We have included the data for such systems in this manuscript to be entirely transparent and to demonstrate when the approach does not work, as well as showing when it does.

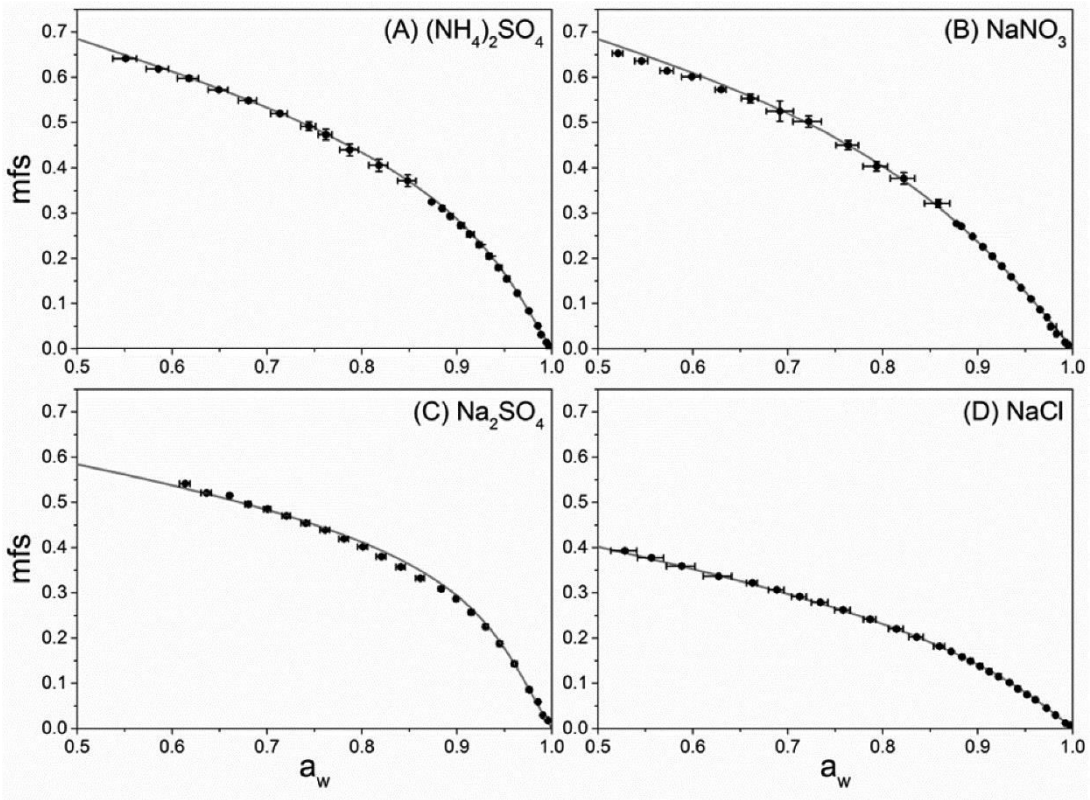

Measured mfs vs *a*w plots for $(NH_4)_2SO4$, $NaNO_3$, Na_2SO_4, and NaCl (panels A–D). Symbols: filled circles, experimental data; solid lines, calculation from the E-AIM model. Note: error bars are smaller than the data point when not shown.

Referee Comment: Page 1 line 15: This significance of this sentence is not clear. New data agree better with the UNIFAC predictions than the old data, from which UNIFAC parameters were derived, do. Are the UNIFAC parameters/predictions useful or not?

Response: The reproducibility of our measurement is much better than that of Peng et al. and, thus, our method is much better equipped to help refine the UNIFAC model parameters than the work of Peng et al.

Referee Comment: Page 1 line 22 - The authors should discuss the agreement between the measured hygroscopicities and UNIFAC predictions on sugars/alcohols.

Response: The level of agreement between the measurements and predictions for the sugars/alcohols is highly system dependent and no general statements can be made. Instead, we have added the phrase: "and show variable levels of agreement with predictions" to the end of line 22.

Referee Comment: Page 8, line 25: "In addition, the short timescale of the measurement ensures that evaporation of the semi-volatile components, such as these dicarboxylic acids, is avoided". Has this been verified or is this merely an assumption? Did they experimentally verify this with some other semi-volatile solutes? Can they really say that evaporation is avoided? In reality, there must be a range of vapor pressure

that evaporation is "negligible" but appreciable at larger values.

Response: As a first indicator, it is clear that the evaporation of water (with a gradient in vapour pressure of >100 Pa from the droplet surface to infinite distance at ~80 % RH) occurs in a timescale of ~ 10 s. Thus, components less than 1 Pa can be expected to take >1000 s to evaporate. More precisely, we can estimate the lower limit in vapour pressure that the CK-EDB is sensitive to in a 10 s period, equivalent to the hygroscopicity measurement timescale. The uncertainty in radius in a CK-EDB measurement is ± 100 nm. Then, assuming a droplet size change from 10.1 to 10 μm in the measurement period of 10 s due to volatilisation, we can infer the vapour pressure of the volatile component, p_i (Pa) would be 0.43 Pa, using the Maxwell equation:

$$\frac{dr^2}{dt} = -\frac{2M_i D_i}{RT\rho}\, p_i \qquad (1.0)$$

r is radius (m), t is time (s), M_i is molecular weight (kg mol^{-1}, taken here as 100 g mol^{-1}), D_i is the gas phase diffusion constant (~1×10^{-5} m^2 s^{-1}) , R is the ideal gas constant, T is the temperature (K) and ρ is the droplet solution density (kg mol^{-1}, taken here as 1.46 g cm^{-3}). This is considerably more volatile than any of the species that we investigate in this study; for example the vapour pressure of malonic acid (one of the most volatile species in this study) is 10^{-4} Pa. Thus, during the timescale of the measurement only water is lost from the droplet.

Referee Comment: Page 10, line 1 - "In summary, UNIFAC predictions agree well with measurements for simple unbranched dicarboxylic acids with the exception of pimelic acid," Is there any explanation why the UNIFAC cannot predict the hygroscopicity of pimelic acid? Can the authors provide suggestions to make improve the predictions of UNIFAC?

Response: We can only comment that pimelic acid was not included in the original compounds used to parametrise the UNIFAC groups for the dicarboxylic acids.

Referee Comment: Page 10, line 30 - "The model (equation 27 in Dutcher et al. 2013) is fitted to molality experimental data with respect to water activity for finding the parameter value, which results in a significant improvement in the MFS than UNIFAC." Why does the multilayer adsorption isotherm based model from Dutcher et al. (2013) give a better prediction beyond the use of an adjustable parameter?

Response: We agree that this was not clear. The sentences now read (P10 L30): "The model (equation 27 in Dutcher et al. 2013) is fitted to experimental data for solute molality as a function of water activity, in order to determine the adjustable model parameter. The model predicts solute activities and concentrations across all water activities, by combining short-range adsorption isotherm and long-range Debye-Huckel expressions. The isotherm model results in improvement in MFS predictions when compared to UNIFAC. However, the notable difference in accuracy between the two models is not overly surprising: the isotherm based model of Dutcher et al. 2013 has an adjustable parameter (Table S0.2), while UNIFAC is a fully predictive model."

Referee Comment: Page 10 line 20. From Figure 8a, it seems L-threonine, rather than L-valine, deviates from the other three compounds most.
Response: We agree with the reviewer and have amended the sentence Page 10 line 20 "On a MFS scale, the hygroscopic response of these compounds is similar except for L-threonine which is less hygroscopic, an observation that is not expected given the additional hydrophilicity of the hydroxyl substituent.*"*

Referee Comment: Page 11 line 6: Is there any other possible explanation for the discrepancy between measured and literature (Chan et al., 2005) data on those amino acids? Can they rule out the possibility of mass transfer effects or evaporation of solute? They show that their data are consistent with Na et al. (1995), which are compromised by evaporation of solute since they made EDB measurements in vacuum. Furthermore, Chan et al. also made measurements of these amino acids to lower RH to determine the mfs of solid of unity. The assertion that Chan et al. were wrong, which is possible, need to be accompanied by the discussions on

how that would affect the mfs of the dried particles. Would the new data provided here yield unreasonable mfs of the dried particles?

Response: Volatilisation is not a concern for the amino acid measurements on the timescale of our measurement: once solvated in water, amino acids become zwitterionic and behave more like inorganic salts. In addition, in our previous response we have shown that volatilisation is insufficient to give any appreciable change in composition during the measurement time frame for any component with a vapour pressure less than 1 Pa. At a MFS as low as 0.0075, the pH of an aqueous solution of glycine is high enough for nearly 100 % of the solution to contain zwitterionic amino acid species (Kuramochi et al. (1997)). To further confirm this, we show below measurements made using the aerosol optical tweezers technique for an aqueous glycine droplet, suspended at variable RH's for thousands of seconds. Even over such prolonged periods, once water was removed following a step in RH from 75 % to 55 %, there was minimal observed volatilisation. For example, over a period of 1000 s, the size decreases from 3227 to 3218 nm (between times of 5000 and 6000 s). Thus, over a 10 s measurement time in our CK-EDB measurements, volatilisation can be ignored. By contrast, the data taken by Chan et al. (2005) require much longer confinement of droplets in the EDB (10 – 20 hours) (Chan et al., 2005).

Further, our CK-EDB measurements reach a sufficiently high enough RH to *overlap* with all bulk data available from Kuramochi et al. (1997) and Ninni and Mereilles (2001), which both show very good agreement. Instead, we believe that the discrepancy between our data and that of Chan et al. arises because of the extrapolation required to reconcile their first aerosol phase measurement (at the highest water activity) with the bulk data.

Based on these two facts, our data are not compromised by volatilisation and overlap with bulk data where available. By contrast, neither of these two concerns can be ignored when considering the data of Chan et al. We must stress that there are challenges associated with these measurements, particularly in reaching a high enough water activity to overlap and compare with bulk data, a challenge which our technique is able to address.

Chan, M. N., Choi, M. Y., Ng, N. L., and Chan, C. K.: Hygroscopicity of Water-Soluble Organic Compounds in Atmospheric Aerosols, Environ. Sci. Technol., 39, 1555-1562, 2005.

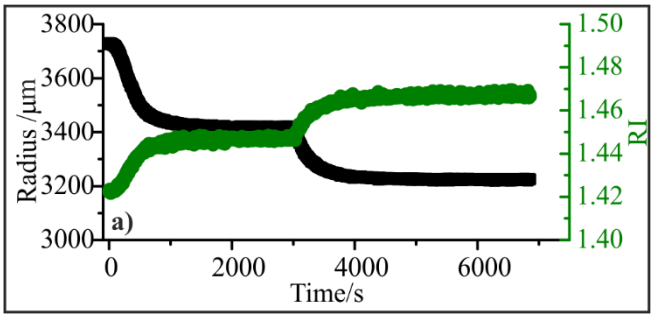

Glycine hygroscopicity experiment a) Radius vs time and RI vs time.

Referee Comment: Page 11 line 23: It is unclear why kinetic limitations will not affect the hygroscopicity measurements of sugars and alcohols in this study by saying "as established by the RH of the gas phase the droplet is drying in". Elaborate please.

Response: We have added the following discussion and Figures to the SI, "The kinetic modelling framework used in the analysis of the droplet evaporation events is valid only in the absence of a bulk-kinetic limitation on near surface composition, i.e. the particle must be assumed to be homogeneous in composition. Such a limitation was obvious for hygroscopicity measurements of trehalose, galactose and sorbitol at RH's lower than 80 %. To ensure the measurements are not compromised by bulk diffusion, we consider two important factors.

Firstly, the impact of viscosity on the hygroscopicity retrievals becomes very obvious when we consider the consistency and uncertainty in the raw hygroscopic growth curves determined from different droplets

evaporating into differing RHs. Droplets drying into different RHs reach different compositions at different times, and will retain different amounts of water because of different drying rates. This leads to an artificially low MFS at a particular RH which then slowly returns to the equilibrium curve overtime. Thus, an inconsistency is apparent between retrieved hygroscopic growth curves (or MFS vs a_w) when drying into different RHs. An example of this is shown in Figure S39.1, where we report unbinned hygroscopicity data for alanine (a non-viscous amino acid) and trehalose (viscous at RHs lower than 80%). It is clear here that the different portions of the hygroscopic curves retrieved from measurements at different RHs are consistent for alanine but not for trehalose. A further easy way to identify this retention of water in a particle that is not fully equilibrated is simply to measure the much longer time-dependence in size once the initial evaporation of water has stopped. In droplets that have reached a bulk diffusion limitation, the existence of a kinetic limitation is apparent in a steadily decreasing size as water continues to leave over a timescale longer than 10 s.

Fig S39.1 a) Unbinned hygroscopicity data for the compound alanine. b) Unbinned hygroscopicity data for the compound trehalose. At 50 % RH trehalose has a viscosity of 3.8 x 10^5 Pa.s (Song et al. 2016).

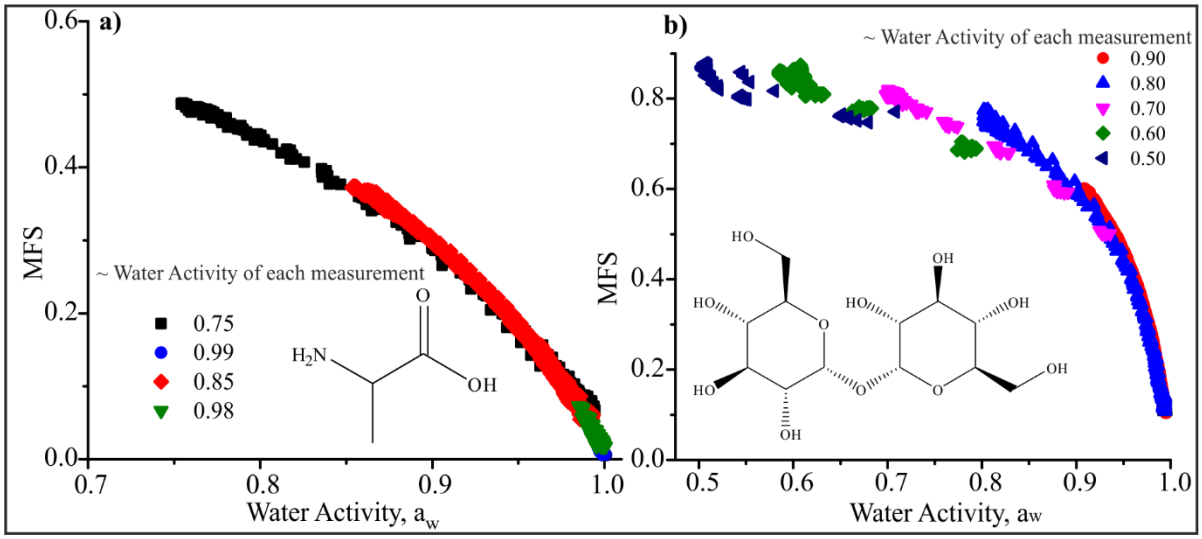

Secondly, we can determine the expected conditions under which we might expect problems to arise in retrieving hygroscopic growth curves from an evaporation measurement. Considering again trehalose at 80 % RH, an aqueous-trehalose droplet has a viscosity of 0.5 Pa.s, increasing to 3.8×10^5 Pa.s at 50 % RH (Song et al. 2016). Therefore, as the RH of the gas phase for the evaporation measurement is lowered, we can expect the increasing viscosity/decreasing diffusivity to become increasingly important. By contrast, for aqueous-carboxylic acid droplets, the viscosity never gets above 1 Pa s even at the driest RHs considered here (Song et al. 2016).

With these known dependencies of viscosity on water activity, we can estimate the timescale for diffusional mixing within a droplet, assuming that this provides an estimate of the timescale for an evaporating droplet to form a homogeneous mixture. This timescale must be considerably shorter than the evaporation timescale for our hygroscopicity estimations to be valid. First, the Stokes-Einstein equation is used to estimate the diffusion constant of water at varying viscosity (varying RH).

$$D = \frac{k_B T}{6\pi r_{mol} \eta} \qquad (1.1)$$

D is the diffusion constant, k_B is the Boltzmann constant, T is temperature, r_{mol} is the molecular radius of water (taken as 1.375 Å) and η is the viscosity. It should be noted that equation (1.1) is likely to provide a significant underestimate of the diffusion constant due to the failure of the Stokes-Einstein equation. At a viscosity of 100 Pa s, the diffusion constant for water in sucrose is already more than one order of magnitude larger than estimated from the viscosity (Power et al. 2013). However, using diffusion constants estimated from (1.1) will provide an upper limit on the diffusional mixing timescale. The timescale for diffusional mixing, τ, is then estimated using the expression

$$\tau = \frac{a^2}{\pi^2 D} \qquad (1.2)$$

where a is the droplet radius (set as 10 microns in this calculation).

We compare the diffusional mixing timescales for aqueous droplets of trehalose, NaCl, $NaNO_3$ and glutaric acid in the newly added supplemental Figure S39.2 (and repeated below). Given that we have been able to report accurate hygroscopic growth curves for $NaNO_3$ down to 50 % RH (see Rovelli et al. 2016 and the response to referee 2), it is clear that a final viscosity at 50 % of ~ 0.1 Pa.s (Baldelli et al.) is insufficient to impede accurate measurement of the hygroscopicity. Indeed, this suggests that water transport in any aerosol droplet that maintains a viscosity lower than 0.1 Pa.s during drying should remain sufficiently fast to avoid a bulk diffusion limitation, permitting accurate hygrosocpicity measurements. As an example of the diacarboyxlic acids considered in this study, glutaric acid has a considerably lower viscosity at 50 % RH of ~ 0.01 Pa.s (Song et al. 2016), indicative of what we might expect for all such similar systems. By contrast, aqueous-trehalose droplets cross the 0.1 Pa.s viscosity threshold at a water activity of ~0.85 (Song et al. 2016), commensurate with the deviation and increased scatter in the hygroscopicity measurements reported above for this compound.

Again, we must reiterate that the true diffusion constants are generally found to be much larger than values estimated from the Stokes-Einstein equation. A droplet with a viscosity of 0.1 Pa s takes ~0.3 s to mix by diffusion based on our analysis here, but this is an upper limit on the timescale.

Based on the two considerations above and to indicate clearly the water activity ranges over which we consider the hygroscopicity measurements to be valid for trehalose (S30), galactose (S31) and sorbitol (S29), we have added a dashed line to indicate where the data appear to become kinetically limited. We have added the following words to the captions of these Figures: "Data taken at RHs lower than indicated by the dashed black line show increased error in hygroscopicity retrieval due to the imposition of a kinetic limitation on water transport."

Fig S39.2 a) Viscosity of Trehalose, NaCl, NaNO3 and Glutaric Acid as a function of RH. b) Estimated diffusion constant as a function of RH. c) Timescale for diffusional mixing at the RH shown on x-axis. Dashed green line represents 1 second timescale for diffusional mixing.

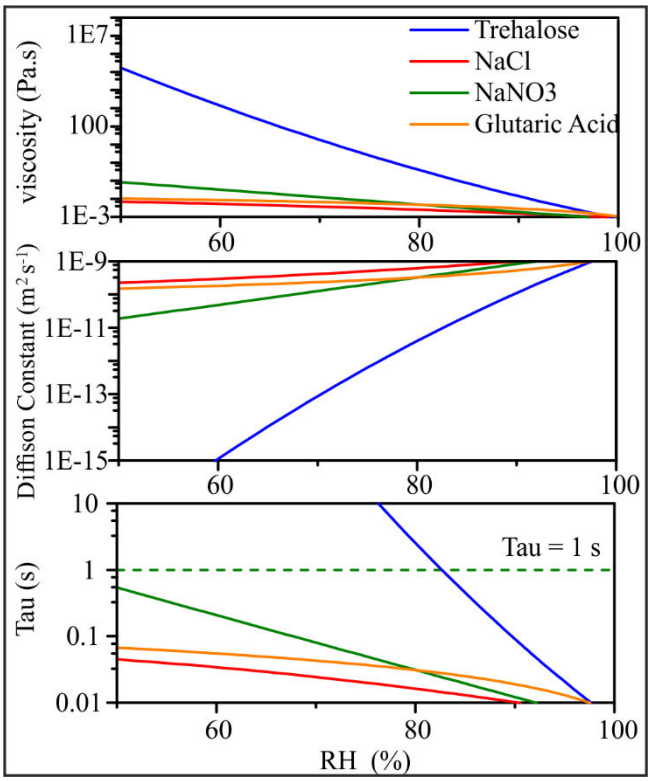

A. Baldelli, R. M. Power, R. E. H. Miles, J. P. Reid and R. Vehring *Effect of crystallization kinetics on the properties of spray dried microparticles,* Aerosol Science and Technology, 2016, 50:7, 693-704, DOI:10.1080/02786826.2016.1177163

R. M. Power, S. H. Simpson, J. P. Reid and A. J. Hudson, *The transition from liquid to solid-like behaviour in ultrahigh viscosity aerosol particles,* Chemical Science, 2013, 4 , 2597, DOI: 10.1039/c3sc50682g
Y. Chul Song, A. E. Haddrell, B. R. Bzdek, J. P. Reid, T. Bannan, D. O. Topping,, C. Percival, and C. Cai *Measurements and Predictions of Binary Component Aerosol Particle Viscosity* J. Phys. Chem. A 2016, 120, 8123−8137, DOI: 10.1021/acs.jpca.6b07835"

Referee Comment: Page 11 line 26: Would the C4-polyol be described as "long chain"? Would sorbitol be classified as sugar?

Response: We have removed 'long chain' in the description of erythritol. Sorbitol and erythritol are best described as polyols (sugar alcohols) and they have now been correctly labelled in the amended text Page 11 line 26: "Equilibrium hygroscopicity curves for the two sugars galactose and xylose, and two sugar alcohols (polyols) erythritol and sorbitol, are shown in Fig. 10."

Referee Comment: Page 12 line 25: The authors discussed on the over-estimation of kappa parameter. However, it seems the UManSysProp model can over-estimate as well as under-estimate the kappa (Figure 12b).

Response: We agree with the referees comment and have expanded this sentence to indicate that the parameter can be underestimated. We have added on P12 line 25 "Further, UManSysProp predictions can also lead to an underestimation of κ for a limited number of compounds, including valine, histidine, and glutaric and methyl succinic acid."

Referee Comment: The authors seem to be sending very mixed messages on the reliability of simple parameterized models/equations for predicting hygroscopicity. On one hand, they criticized the limitation of UNIFAC in predicting hygroscopicity of branched acids. On the other hand, they promoted the use of κ values and O:C and N:C ratios based on Figure 11(b) and 12 (a), which do show discrepancies between model predictions and experimental results in κ. When plotted in the form of mfs hygroscopic data, some of these differences are not much smaller than those between the measurements of the branched DCAs and the UNIFAC predictions based on parameterization of simpler acids. Furthermore, the comparison of data and model Kappa parameters are evaluated at 95% but the comparison of UNIFAC related results are in mfs as a function of RH. How would the results look like if Kappa values are evaluated at lower RH? Finally, are these predictive tools considering these very general and smooth relationships really much less computationally expensive than current group contribution methods? κ was calculated by isotherms that require an adjustable parameters. Overall, the comments made by the authors on the use of UNIFAC, Kappa/isotherm models, and more elaborated models such as AIOMFAC and UManSysProp appear not to be unbiased. Elaboration is needed.

Response: The main purpose of this manuscript is to provide an evaluation of the current thermodynamic models for predicting the hygroscopic response of aerosols. Models such as AIOMFAC, UNIFAC, E-AIM and UManSysProp will always be the preferred choice when a full and accurate representation of the equilibrium response is required (e.g. over a wide range in RH as the referee suggests). However, simple parametrisations such as κ are finding very widespread use in providing an albeit limited characterisation of the hygroscopic response – a single parameter is easier to report and measure than a full hygroscopicity curve. We are not aware of anywhere in the paper where we make a value judgement on the relative merits of these two approaches: both methods have the strengths and uses in different domains and are used to provide the appropriate level of information required in any application. Given that the κ treatment is increasingly used, we felt it was of importance to try and connect the more detailed thermodynamic models with the much more simplistic approach. We hope we have achieved this in the revised manuscript.

Influence of Organic Compound Functionality on Aerosol Hygroscopicity: Dicarboxylic Acids, Alkyl-Substituents, Sugars and Amino Acids

Aleksandra Marsh[1], Rachael E. H. Miles[1], Grazia Rovelli[1], Alexander G. Cowling[1], Lucy Nandy[2], Cari S. Dutcher[2] and Jonathan. P Reid[1]

[1] School of Chemistry, University of Bristol, Bristol, BS8 1TS, UK
[2] Department of Mechanical Engineering, University of Minnesota, 111 Church Street SE, Minneapolis, MN 55455, USA

Correspondence to: Jonathan. P. Reid j.p.reid@bristol.ac.uk

Abstract. Hygroscopicity data for 36 organic compounds including amino acids, organic acids, alcohols and sugars is determined using a Comparative Kinetics Electrodynamic Balance (CK-EDB). The CK-EDB employs an electric field to trap charged aqueous droplets in a temperature and relative humidity (RH) controlled chamber. The dual micro dispenser set up allows for sequential trapping of probe and sample droplets for accurate determination of droplet water activities from 0.45 to > 0.99. Here, we validate and benchmark the CK-EDB for the homologous series of straight chain dicarboxylic acids (oxalic – pimelic) with measurements in better agreement with UNIversal quasichemical Functional group Activity Coefficients (UNIFAC) predictions than the original data used to parametrise UNIFAC. Further, a series of increasingly complex organic compounds, with subtle changes to molecular structure and branching, are used to rigorously assess the accuracy of predictions by UNIFAC, which does not explicitly account for molecular structure. We show that the changes in hygroscopicity that result from increased branching and chain length are poorly represented by UNIFAC, with UNIFAC under-predicting hygroscopicity. Similarly, amino acid hygroscopicity is under-predicted by UNIFAC predictions, a consequence of the original data used in the parametrisation of the molecular subgroups. New hygroscopicity data are also reported for a selection of alcohols and sugars and show variable levels of agreement with predictions.

Formatted: Highlight

1. Introduction

The hygroscopicity of an aerosol can be defined as the capacity of an aerosol particle to absorb water and quantifies the equilibrium partitioning of water between the gas and condensed phases (Krieger et al., 2012). Aerosol hygroscopic growth impacts directly on the radiative balance of the atmosphere, with the size and refractive index of aerosol particles influencing their light scattering and absorption cross-sections (Ravishankara et al., 2015;Moise et al., 2015). Similarly, the hygroscopic response of aerosol impacts on the transport of chemical components in the environment and on atmospheric chemical composition through heterogeneous chemistry and cloud chemistry with implications for air quality (Akimoto, 2003;Farmer et al., 2015;Hallquist et al., 2009). The activation of cloud condensation nuclei (CCN) to form cloud droplets is governed by

hygroscopic response as well as aerosol size distribution, leading to the indirect effect of aerosols on climate (Farmer et al., 2015;Lohmann and Feichter, 2005). Furthermore, hygroscopic growth on inhalation can influence the depth of penetration of aerosol into the respiratory system, with consequences for the impact of ambient aerosol and particulate matter on rates of morbidity and mortality (Haddrell et al., 2015;Pöschl and Shiraiwa, 2015). Thus, an improved characterisation and quantification of the hygroscopic response of ambient aerosol is important for more accurate predictions of the radiative forcing of aerosol, their impact on air quality and their consequences for human health.

Atmospheric aerosol are composed of a plethora of inorganic and organic species from a diverse range of biogenic and anthropogenic sources including inorganic salts, sulphates, nitrates, metals and organic compounds, such as acids, alcohols, amino acids and sugars (Baltensperger, 2016;Seinfeld and Pankow, 2003;Zhang et al., 2015). Organic species can dominate ambient fine aerosol mass (particles < 1μm in diameter) and have varying degrees of oxidation, molecular mass, hygroscopicity and volatility (Jimenez et al., 2009;McNeill, 2015). Further, the composition of ambient aerosol is constantly changing due to heterogeneous reaction chemistry (Hallquist et al., 2009;Jimenez et al., 2009;Pandis et al., 1995;Ziemann and Atkinson, 2012), varying relative humidity (RH) and temperature (Farmer et al., 2015), and photochemistry (Jacob, 2000;George et al., 2015).

The equilibrium response of an aerosol to changes in ambient RH is described by the Köhler equation, which is a product of the solution water activity (the solute term) and a correction for surface curvature (the Kelvin term) (Wex et al., 2008). The solute term, representing the dependence of the equilibrium water activity on the composition of the solution of inorganic and organic compounds, can be determined from thermodynamic models that represent in detail the non-ideal interactions between the ionic and neutral species within the solution. Based on parameterisations from experimental data, these models include the Aerosol Inorganic/Organic Mixtures Functional groups Activity Coefficients (AIOMFAC) (Zuend et al., 2008;Zuend et al., 2011), the Extended Aerosol Inorganic Model (Wexler and Clegg, 2002;Clegg et al., 1998), and UManSysProp (Topping et al., 2016) which allow calculation of the activity coefficients that characterise the non-ideality of the aqueous solutions. The key challenges in generating accurate predictions include capturing accurately the non-ideality of solutions, particularly under very dry conditions/high solute concentrations (Dutcher et al., 2013;Nandy et al., 2016;Ohm et al., 2015), ion-neutral interactions in mixed inorganics/organics (Zuend et al., 2008;Zuend et al., 2011;Losey et al., 2016), the acidity and basicity of solutes (Rindelaub et al., 2016), liquid-liquid phase separation (Zuend and Seinfeld, 2012), solubility (Pajunoja et al., 2015) and the co-condensation of semi-volatile organic compounds (SVOC) with increase in water fraction (Topping et al., 2013). To treat the organic component, AIOMFAC, E-AIM and UManSysProp use the UNIversal quasichemical Functional group Activity Coefficients (UNIFAC) method developed by Fredenslund et al. (Fredenslund et al., 1975). In this approach, molecules are divided into characteristic molecular subgroups and the activity coefficients derived from group contributions with limited consideration for molecular structure. AIOMFAC-web implements several improved parameters which are detailed by Zuend et al. (2011).

Formatted: Highlight
Deleted: no
Formatted: Highlight
Deleted: (Zuend et al., 2011)

In UManSysProp, compounds are specified using the Simplified Molecular Input Line Entry System (SMILES) which are then converted to UNIFAC groups within the programme. Using these approaches, Petters et al. have shown that the CCN activity of organic compounds can be modelled using group contribution methods (Petters et al., 2016).

Despite their accuracy, the use of group contribution methods to predict the water uptake for a larger number of organic components in ambient aerosol is too computationally expensive for inclusion in regional chemical transport and climate models. Reduced parameter models are instead required to represent the thermodynamic properties of ambient organic aerosols. κ-Köhler theory characterises the solute component of hygroscopic growth by a single parameter κ applicable in the limit of dilute aqueous solution aerosol (Kreidenweis et al., 2008;Petters and Kreidenweis, 2007). It must be assumed that the compounds are fully soluble and the aerosol does not undergo phase separation. The value of κ spans from a value close to 0 for un-hygroscopic/hydrophobic components to a value around 1 for the most hygroscopic inorganic salts (Kreidenweis et al., 2008;Petters and Kreidenweis, 2007). Values are typically determined from sub-saturated hygroscopic growth measurements and reported at the highest accessible RH (Pajunoja et al., 2015). The value of κ can also be inferred from measurements of the critical supersaturation required for CCN activation, a measurement in a super-saturated regime (Carrico et al., 2008). Further, κ values reported at different RHs can vary significantly and can also differ substantially from measurements in the supersaturated regime, (Hodas et al., 2016). Despite the inherent approximations, reported values of κ provide a way of linking the hygroscopicity of complex ambient aerosol with empirical measurements of chemical functionality such as the level of oxidation, often reported as the ratio O:C from aerosol mass spectrometry measurements (Jimenez et al., 2009;R. Y.-W. Chang et al., 2010). Possible correlations of κ with chemical composition (particularly O:C) have been extensively explored and reviewed (Rickards et al., 2013;Suda et al., 2014).

Formatted: Highlight

Although many ambient measurements of κ have been made, there remains a necessity to rigorously address some of the challenges in quantifying aerosol hygroscopicity through controlled laboratory measurements on well-characterised aerosol of known composition. Dicarboxylic acids from $C_1 - C_7$ have been studied extensively in the literature and have been used as the basis for providing revisions of UNIFAC for typical organic components found in the atmosphere (Peng et al., 2001). Further, previous laboratory studies have examined correlations of κ with composition, and have focussed on identifying the influence of certain key functional groups on κ. For example, Suda *et al.* (2014) have studied the systematic impact on κ of hydroxyl, carboxyl, peroxy, nitro and alkene groups of varying carbon chains lengths ($C_1 - C_{25}$) (Suda et al., 2014). However, there remain many gaps in hygroscopicity data for a number of compound classes, including; highly branched dicarboxylic acids, multifunctional compounds (including ring containing species), amino acids, organo-sulphates and nitro compounds.

We report here a systematic study of the hygroscopicity of a large number of organic compounds (listed in Table 1.) of varying functionality, solubility and molecular weight. This work benefits from the application of a novel electrodynamic balance (EDB) method that offers significant advantages over both alternative single particle techniques and ensemble experimental

setups (Rovelli et al., 2016;Davies et al., 2013). Measurements can be made at high water activities (approaching values very close to 1) with a very accurate comparative kinetics method for determining the gas phase RH. The timescale for the measurement to record the whole growth curve is <10 s, sufficiently fast that the growth curves of organic species with vapour pressures of >1 Pa can be measured without significant volatilisation of the organic species. A temperature regulated chamber allows for stable and prolonged temperature control of the trapping region in the range -25°C – +50°C. The use of piezo-electric droplet-on-demand dispensers allows for the use of small sample volumes, allowing measurements on expensive (small amounts) of test compounds or the use of even filter collected samples. Measurements are made on droplets spanning the radius range from 4 – 30 µm, avoiding the additional complexity of correcting the hygroscopic growth measurement for the surface curvature term and providing an unambiguous measurement of the solute term (Rovelli et al., 2016).

More specifically, we will present hygroscopic data for 36 organic compounds from 4 distinct compound classes. A series of 17 dicarboxylic acids, with subtle differences to molecular branching and chain length, are used to examine the impact of structural isomerisation on water uptake. Measurements are also presented for a series of amino acids; despite their extensive release from biogenic sources, their hygroscopic properties have yet to be fully characterised (Chan et al., 2005). Although the UNIFAC model predicts water uptake of simple structures reasonably well, we will show that increasing molecular complexity and inclusion of nitrogen containing groups leads to considerably poorer prediction of hygroscopicity. Following an introduction to the methods and materials in Sect. 2, we will present the results for these different compound classes in Sect. 3.

2. Methods and Materials

Hygroscopicity studies are presented with measurements from a comparative kinetics technique applied in an EDB instrument, (referred to as the comparative kinetics EDB, CK-EDB, below) with electrodes in a concentric cylindrical arrangement. The full experimental details for the CK-EDB have been discussed extensively in previous publications and will only be briefly reviewed here (Rovelli et al., 2016;Davies et al., 2013), along with a discussion of the treatments used for parameterising solution density and refractive index (Cai et al., 2016). Purity and supplier for all compounds is presented in the supplementary information. Further, all measurements presented in this work are taken at 293.15 K. All solutions are prepared using HPLC grade water (VWR Chemicals).

2.1 The Comparative Kinetics Electrodynamic Balance

The CK-EDB can be used to probe the hygroscopic growth of aerosol particles from low to high water activities (<0.45 to >0.99) with a greater accuracy (<±0.2 % error in water activity at water activities > 0.8 and ±1 % error in water activity at water activities < 0.8) than can be achieved in conventional approaches (Rovelli et al., 2016). The CK-EDB employs an electric field to trap a charged dilute aqueous droplet starting at a water activity > 0.99. The droplet evaporates towards an equilibrium

Formatted: Highlight

Formatted: Highlight

Formatted: Highlight

composition set by the RH of the surrounding gas flow; the RH is determined accurately from an independent measurement of the evaporation profile of a probe droplet of known hygroscopic response (either a pure water droplet or an aqueous sodium chloride solution droplet). The time-dependence in size and composition of the sample droplet (typically over a period of ~10 s) is then used to infer the hygroscopic equilibrium growth curve over the full range in water activities experienced by the droplet during evaporation. The reader is referred to Rovelli et al. (2016) and Davies et al. (2013) for a full description of the method and the analysis.

A pulse voltage is consecutively applied to two droplet dispensers (MicroFab MJ-ABP-01, orifice size 30 μm) to sequentially generate probe and sample droplets of known starting solute concentration. The droplets are charged by an induction electrode and are trapped within the electric field of the cylindrical electrodes within 100 ms of generation. Thermally regulated water channels through the electrodes and chamber body allow the temperature to be carefully controlled (-25°C – +50°C) by a refrigerated circulator (F32-ME, Julabo) using a mixture of polyethylene glycol and water. Humidified nitrogen gas flows vertically through the cylindrical electrodes and allows control of the gas phase RH of the chamber (total flow 200 mL min^{-1} equivalent to a gas velocity of 3 cm s^{-1}). Evaporating droplets are illuminated with a 532 nm laser (Laser Quantum Ventus CW laser) and the elastic scattered light is collected using a CCD camera over a range of angles near a scattering angle of 45°. The droplet radius (r) is first estimated using the geometric optics approximation (error <±1 % for droplets > 10 μm) and the angular separation of fringes in the phase function ($\Delta\varphi$, radians) (Glantschnig and Chen, 1981),

$$r = \frac{\lambda}{\Delta\varphi}\left(cos\frac{\varphi}{2} + \frac{nsin\frac{\varphi}{2}}{\sqrt{1+n^2-2ncos\frac{\varphi}{2}}}\right)^{-1} \quad (1)$$

where n is the refractive index of the droplet, λ is the incident laser wavelength and φ is the median observation angle. Initially, during data collection n is assumed to be that of water. However, this assumption is corrected in subsequent data processing for the change in n during evaporation; the compositional dependencies of density and n are described below.

2.2. Molar Refraction: Refractive Index and Density Treatments

Solutes in aerosol droplets can reach supersaturated concentrations as water evaporates. Thus, to represent the solution density and refractive index, bulk measurements are insufficient and must be extrapolated to account for the full compositional range, i.e. the entire range in mass fraction of solute, MFS or ϕ_s, from 0 to 1. We have recently provided a comprehensive assessment of the parameterisations that can be used to predict the density and refractive index of supersaturated organic solutions, and we summarise below the recommendations of this study relevant to their application in this work (Cai et al., 2016).

Aqueous solutions of an organic solute are prepared up to the solubility limit of the compound, and the density and refractive index are measured using a vibrating capillary density meter (Mettler Toledo Densito, accuracy ± 0.001 $g.cm^{-3}$) and a

refractometer (Misco Palm Abbe, accuracy ±0.0001 at 589 nm), respectively. If the solubility of the organic solute allows measurements above an MFS of ~0.4, a third order polynomial in $\phi_s^{0.5}$ is fit to the bulk solution density values (where ϕ_s is the MFS). If bulk measurements are limited by solubility to an upper limit in MFS <0.4, an ideal mixing treatment is applied to the bulk density values to allow the estimation of the density of the solute, ρ_s, constraining the bulk data to the equation:

$$\frac{1}{\rho_{em}(1-\phi_s)} = \frac{\phi_s}{(1-\phi_s)\rho_s} + \frac{1}{\rho_w} \quad (2)$$

where ρ_{em} is the mass density of the mixture and ρ_w the density of water. These two approaches assume that the density of the pure organic solute (ρ_s) is not known; under the conditions of aqueous solution aerosol measurements, the density of the solute corresponds to that of the pure sub-cooled melt with most pure organic compounds instead existing in a crystalline form at room temperature. Further details of the density measurements and parameterisations for all systems studied are provided in the Supplementary Information Section.

Formatted: Highlight

Once the dependence of solution density on MFS is established, a fit of the bulk solution refractive indices is constrained to follow the molar refraction mixing rule (Liu and Daum, 2008):

$$R_e = \left(\frac{n^2-1}{n^2+2}\right)\left(\frac{M_e}{\rho}\right) \quad (3)$$

where n is the refractive index of the mixture, M_e the effective molecular weight and R_e is the molar refraction of the mixture. This allows the estimation of the molar refraction of the pure organic solute, again as a sub-cooled melt. In subsequent use, the molar refraction can be calculated for solutions of any composition,

$$R_e = (1-x_s)R_w + x_s R_s \quad (4)$$

and the value of n for the solution determined by solving for n from equation (3). Pure component refractive indices, determined using the molar refraction mixing rule are presented in the Supplementary Information Sections alongside parametrisations of aqueous solution densities and sub-cooled pure component melt densities. Values of aqueous density and refractive index as a function of compound mass fraction are available in the supplementary information in Cai et al. (2016). Further in SI Fig S37.1 we consider the impact of uncertainties in density and refractive index treatments to the measured hygroscopicity, for all compounds shown, the error envelope on hygroscopicity is smaller than the size of the points.

2.3. Extraction of Hygroscopicity properties

During the evaporation of an aqueous droplet, the mass flux (I) of water can be estimated at each recorded time step from the change in size and the associated density for the known composition of the droplet at that time, starting with a generated droplet of known solution composition. At each time step, the loss in mass is associated solely with loss of water, allowing a calculation of the new MFS and, thus, new values of n and density. The new value of n allows a refinement of the estimated radius, with

Deleted: a component *i* (in this, case

Deleted:)

full details (Davies et al., 2012). The mass flux can then be used to determine the gradient in water partial pressure in the gas phase using an analytical treatment (Kulmala et al., 1993), with

$$I = -4\,Sh\,\pi\,r(RH - a_w)\left(\frac{RT_\infty}{M\beta_M D\rho^0(T_\infty)A} + \frac{a_w L^2 M}{R\beta_T K T_\infty^2}\right)^{-1} \quad (5)$$

which accounts for the limiting influence of heat transport, due to latent heat lost, on the mass flux. In this equation, the gradient in water partial pressure is the difference between the RH and a_w, the instantaneous water activity at the droplet surface. The RH is determined from the probe droplet measurements, as described previously (Rovelli et al., 2016). In this study, the probe droplets are trapped in exactly the same position within the gas flow as the sample droplets which allows the measurement of the RH in situ. The probe droplets are either pure water (for the RH range 80 – 99 %) or aqueous NaCl (for the RH range 50 – 80 %). All quantities in this equation are known apart from a_w and this can be estimated for every time-step by rearranging the equation to solve for a_w. Sh is the Sherwood number, accounting for the enhancement in evaporation rate due to the moving gas flow over the droplet, and r is droplet radius, measured experimentally. R is the ideal gas constant, T_∞ is the ambient temperature, M is the molecular mass of water, D is the binary diffusion coefficient of water in nitrogen and $\rho^0$is the saturation vapour pressure. A is a correction factor for Stefan flow, K is thermal conductivity and L is the latent heat of vaporization of water at T_∞. Finally β_M and β_T represent the Fuchs-Suttugin correction factors for mass and heat flux, respectively.

It is imperative that the evaporative cooling be accounted for as this suppresses the apparent vapour pressure at any instant, particularly at early time when the mass flux is larger. Indeed, equation (5) explicitly accounts for the latent heat lost from the droplet. At very early times and when evaporating into low RH, the temperature suppression can be sufficient (>3 K) so as to reduce the accuracy of approximations made when deriving equation 5. Under these circumstances, when the temperature suppression is larger than this limit, we do not infer equilibrium water activities, but instead only retrieve the equilibrium hygroscopic growth when the temperature suppression is smaller than 3 K. This procedure has been discussed and verified in detail in our earlier work, and the reader is referred to Rovelli et al. (2016) for further details.

The time-dependent data can also be used to estimate sub-saturated values of κ from (Petters and Kreidenweis, 2007)

$$GF = \left(1 + \kappa\frac{a_w}{1-a_w}\right)^{\frac{1}{3}} \quad (6)$$

where GF represents the radius growth factor which is a ratio between the wet droplet radius and dry particle radius. The dry size is estimated from the known starting size of the solution droplet and the starting concentration (MFS) of solutes. Time-dependencies in radius for a number of compounds with different κ values are shown in Fig. 1(a), illustrating how the CK-EDB experiment can discriminate between compounds of different κ during evaporation. For increasingly hygroscopic aerosol, there is a trend to a final equilibrated size that is larger and the temporal dependence of radius shows a shape that is characterised by less rapid loss of water. A caveat must be noted, however: the profiles do also depend on starting size, solute

Formatted: Highlight
Formatted: Highlight
Formatted: Highlight
Formatted: Highlight
Formatted: Highlight

concentration and the exact RH of the chamber, factors which are all explicitly accounted for in the full quantitative analysis. Values of κ for all compounds studied are reported at $a_w = 0.95$ in Table 1. It should be recognised that the apparent value of κ varies with the RH at which it is reported (Rickards et al., 2013).

During a typical experiment, measurements of sample and probe droplets are taken sequentially at several steady RHs, typically 50, 60, 70 and 80 % using an aqueous NaCl probe droplet and 80 and 90 % with a water probe droplet. Furthermore, at each measured RH, 10 sample and probe droplets are taken to ensure measurement reproducibility. Final hygroscopicity data is averaged (binned in small steps in RH) and presented as a function of MFS against water activity; full hygroscopicity curves are typically the result of measurements from between 30 – 80 droplets. It must be noted that kappa, κ, values are calculated using all data points before the binning process. In Fig. 1(b) we show typical time-dependencies in radius for a series of aqueous-glycine droplets evaporating into four different RHs. The final hygroscopicity curve for glycine is shown in Fig. 1(c): the large orange points represent data which have been averaged (binned in a_w steps) from 100's of data points measured from ~50 droplets.

3. Results and Discussion

Graphical and tabulated hygroscopicity curves for all 36 compounds studied, UNIFAC predictions, density parametrisations, refractive index values and compound purities are available as Supporting Information. Here, we summarise and compare the behaviour observed for the different classes of chemical compounds studied and consider the trends observed in the value of the parameter κ.

3.1. Hygroscopic Response of Dicarboxylic Acids of Varying Complexity

Structurally similar organic acids were chosen to examine the relationship between the hygroscopicity of binary component aerosol and the degree of carbon-chain branching, chain length and O:C ratio; some of the compounds chosen are identified in Fig. 2(a) and (b). All experimental hygroscopicity data are compared with thermodynamic predictions from the UNIFAC model to assess whether compound hygroscopicity is accurately represented. All calculations for dicarboxylic acids were performed using the AIOMFAC-web model.

As a benchmark test, we consider the homologous series of dicarboxylic acids, $HOOC(CH_2)_nCOOH$, from oxalic to pimelic acid (i.e. with n=0 to 5) in Fig. 2(a). The UNIFAC model predictions mostly agree closely with experimental observations at moderate to high water activity with some deviation at lower water activity although pimelic acid is an exception with experimental data deviating significantly from the model prediction. In Fig. 2(b) we compare data from a series of compounds with a malonic acid backbone, but with varying alkyl substituents (methyl, dimethyl and diethyl). The trend towards decreasing hygroscopicity with increasing hydrophobicity (increasing number and length of alkyl substituents) on a mass basis is clear,

recognised from observing that there is less water associated with the solution at constant water activity as the molecular weight increases. In addition, the UNIFAC predictions become less accurate as the added substituent becomes larger. The approach used here is particularly valuable for low solubility organic compounds as dilute solutions at high water activity provide the starting point for the measurement. For example, the dry particle size must be measured using a Hygroscopic Tandem Differential Mobility Analyser (HTDMA), necessarily setting a lower limit on the concentration of solutes use when atomising solutions to form aerosol. In addition, the short timescale of the measurement ensures that evaporation of the semi-volatile components, such as these dicarboxylic acids, is avoided.

We compare the measurements reported here with previous data (Peng et al., 2001) in Fig. 3(a)-(d) and Fig S38.1(a)-(d) for the straight chain dicarboxylic acids for which comparison can be made, oxalic, malonic, succinic and glutaric acid. The comparisons made in Fig. 3(a)-(d) act as a form of method validation, extending our previous work; bulk and EDB measurements (Peng et al., 2001) are presented alongside our CK-EDB data and UNIFAC predictions, with good agreement for all systems. Further to this, Fig S38.1(a)-(d) show the dependence on water activity of the difference in MFS (ΔMFS) between the current experimental data or the previously published data (Peng et al., 2001) and UNIFAC predictions, allowing a quantitative comparison of the different experimental techniques. For these four straight chain dicarboxylic acids, the average deviations, ΔMFS, between UNIFAC predictions and our CK-EDB data (a_w range 0.5 – 1) and the data of Peng et al. (2001) (up to ~0.9) are 0.017 ± 0.017 and -0.0037 ± 0.065. Note that although our data corresponds to a small systematic shift from the UNIFAC model predictions, the spread of data about this mean offset is considerably less than in the previous study and extends to much higher water activity. The differences are summarised in Fig. 4, where the grey shaded area represents the standard deviation from UNIFAC for our measurements of the straight chain carboxylic acids (Fig 3.) and these data are plotted alongside all ΔMFS values for all 13 branched dicarboxylic acids studied. Nearly all branched acids deviate more from the UNIFAC predictions than is observed for the straight chain dicarboxylic acids. This confirms our previous observation that the thermodynamic model predictions become increasingly unreliable as branching increases.

To further illustrate this trend in failure to capture the hygroscopicity reliably, we compare a sequence of dicarboxylic acids with carbon backbone length from 3-6 and with a methyl substituent attached in Fig. 5(a). All systems are poorly reproduced by the UNIFAC predictions with a value of ΔMFS that is larger than the limit set by straight chain dicarboxylic acids, highlighting the lack of availability in branched chain experimental data to constrain the model. Interestingly, we compare the equilibrium hygroscopic response of a sequence of branched chain dicarboxylic acids in Fig. 5(b) with compounds selected to have the same O:C ratio of 0.57. It is striking that the equilibrium response curves are so similar for these compounds; this is captured by the similarity in their κ values of 0.065, 0.054, 0.066, 0.064 and 0.060 for diethylmalonic acid, 2,2-dimethyl glutaric acid, 3,3-dimethyl glutaric acid, 3-methyl adipic acid and pimelic acid, respectively. UNIFAC predictions are only possible for two distinct formulaic units with the measurements indicating that these compounds have a higher degree of hygroscopicity than is captured by the model.

Deleted: , ~~a consequence of representing all CH, CH_2, and CH_3 substituents by CH_x (Zuend et al., 2008).~~

Formatted: Strikethrough

Hygroscopicity can also be represented as a function of the number of moles of water per mole of solute, shown in Fig. 6(a) for straight chain dicarboxylic acids. This is particularly informative for compounds with similar κ values (similar hygroscopicity), shown in Fig. 6(b)-(c), because the differences in moles of solvating water molecules per mole of solute molecule, should be indicative of molecular structure. For the homologous series of straight chain dicarboxylic acids, a higher water activity is required to achieve the same molar balance of water and solute, Fig. 6(a). For the more hydrophobic branched dicarboxylic acids, an even larger water activity is required, although the curves are notably similar for these compounds which all have the same O:C ratio, Fig. 6(b). Figure 7 compares the experimental number of moles of water per number moles of solute compared with that predicted by UNIFAC for the four compounds with the largest deviation in ΔMFS presented in Fig. 4. Rovelli et al. (2016) presented a similar comparison of experimental data and model predictions for inorganic salts, showing remarkable agreement between experimental values and model predictions with all points for all inorganic compounds falling within the ±0.002 uncertainty envelope in a_w, with this uncertainty envelope shown. However, there is a significant deviation from model predictions for the case of the branched dicarboxylic acids presented.

In summary, UNIFAC predictions agree well with measurements for simple unbranched dicarboxylic acids with the exception of pimelic acid, although there is an increasing degree of deviation with decreasing water activity. However, as the level of molecular complexity increases through the addition of single or multiple alkyl branches, there is increasing disparity between UNIFAC predictions and measurements.

3.2. Hygroscopic Response of Amino Acids

A selection of amino acids were chosen for their biological relevance and to represent a wide range of structures and O:C ratios. Nitrogen containing compounds are prevalent in the atmosphere; amino acids contribute to this class of compounds due to their biological origin (Matsumoto and Uematsu, 2005;Barbaro et al., 2015). Recent studies have shown that nitrogen containing compounds react to form brown carbon species, which absorb solar radiation in the UV and visible region. Absorption by brown carbon in cloud droplets leads to water evaporation and cloud dispersion counteracting the aerosol indirect effect (Laskin et al., 2015). Despite their importance as nitrogen containing compounds in the atmosphere, the hygroscopic properties of amino acids are yet to be fully characterised (Chan et al., 2005). Amino acids form zwitterions in solution, which supresses their vapour pressure and presents challenges in representing them with current thermodynamic models with most models not allowing the inclusion of nitrogen amine containing groups (e.g. AIOMFAC-web). AIOMFAC-web only allows for the inclusion of organonitrate and peroxy acyl nitrate sub groups. Hence , thermodynamic model predictions for amino acids were generated using E-AIM, using the UNIFAC model with Peng et al. parameterization (Peng et al., 2001) and Model III. (Clegg et al., 1998). Even then UNIFAC predictions cannot be performed for all the amino acids examined here. In particular, the ring structures found in proline and histidine cannot be represented as subgroups in the current

Deleted: UNIFAC predictions cannot be performed for all amino acids examined here; in particular, the ring structures found in proline and histidine, cannot be represented as subgroups in the current version of UNIFACAIOMFAC-web. T

Deleted: .

version of E-AIM, although these could be represented with the further parametrisations reported by(Kuramochi et al., 1997b) or (Gupta and Heidemann, 1990).

The equilibrium hygroscopic responses for glycine, DL-alanine, L-valine and L-threonine are shown in Fig. 8(a). These four compounds all contain a similar glycine subunit, but include additional methyl, ethyl and hydroxyl groups. On a MFS scale, the hygroscopic response of these compounds is similar except for L-threonine which is less hygroscopic, an observation that is not expected given the additional hydrophilicity of the hydroxyl substituent. In a similar comparison to that considered in Fig. 5(b), compounds of the same O:C are compared in Fig. 8(b) with equilibrium relationships shown for L-lysine, L-histidine and L-arginine. Lysine (κ, 0.219) is more hygroscopic than histidine (κ, 0.188) and arginine (κ, 0.147), illustrating that compounds with the same O:C can have very different hygroscopic responses, contrary to the observations for dicarboxylic acids. For improved predictions of the amino acids measured, the multilayer adsorption isotherm based model from Dutcher et al. (2013) that includes arbitrary number of adsorbed monolayers is used in Fig. 8c) and d) to fit to the CK-EDB data. The model uses a power law relationship for aqueous solutions to determine adsorption energy parameter, C of water molecules with a solute by adjusting a single parameter shown in Table S0.2. The model (equation 27 in Dutcher et al. (2013)) is fitted to experimental data for solute molality as a function of water activity, in order to determine the adjustable model parameter. The model predicts solute activities and concentrations across all water activities, by combining short-range adsorption isotherm and long-range Debye-Huckel expressions. The isotherm model results in improvement in MFS predictions when compared to UNIFAC. However, the notable difference in accuracy between the two models is not overly surprising: the isotherm based model of Dutcher et al. 2013 has an adjustable parameter (Table S0.2), while UNIFAC is a fully predictive model.

Figure 9(a) and (b) show comparisons between CK-EDB with available literature data for the hygroscopicity of both glycine and alanine. For glycine (Fig. 9 (a and b)) at high water activity there is good agreement between our CK-EDB data and bulk literature data (Ninni and Meirelles, 2001;Kuramochi et al., 1997a). Further, in Fig. 9 (b) CK-EDB data for alanine agrees with Kuramochi *et al.* (1997). However, there is relatively poor agreement across the entire water activity range between CK-EDB data points from this study for both glycine and alanine with literature data (Chan et al., 2005). The discrepancy arises from the method used by Chan et al. (2005) to identify the *'reference state'* to which all growth measurements are compared. For example, for certain systems Chan et al. (2005) have been required to extrapolate from bulk measurements to the highest RH of the droplet measurements. A similar approach is used by Peng et al. (2001) with dicarboxylic acid measurements presented in Fig. 3. However, the bulk data points in this case have sufficient overlap between bulk and aerosol phase measurements to require very little or no extrapolation.

Formatted: Highlight

Deleted: valine

Deleted: hydrophobicity

Formatted: Highlight

Deleted: ethyl

Formatted: Highlight

Deleted: The model (equation 27 in Dutcher et al. 2013) is fitted to molality experimental data with respect to water activity for finding the parameter value, which results in a significant improvement in the MFS than UNIFAC. However, the notable difference in accuracy between the two models is not surprising: the isotherm based model of Dutcher et al. 2013 has an adjustable parameter (Table S0.2), while UNIFAC is a fully predictive model

Furthermore, the general trends show that the amino acids are much more hygroscopic than is currently predicted using UNIFAC; indeed, when considering all 10 amino acids included in the SI, all are more hygroscopic than their model predictions suggest (except asparagine). Increased hygroscopicity compared with dicarboxylic acids with similar O:C ratios could be due to the zwitterionic nature of amino acids with their behaviour more similar to that of a salt than an organic species.

Deleted: This is a consequence of the current reliance of the UNIFAC parameterisation on the data of Chan et al. (2005).

3.3. Sugars and Alcohols

When retrieving hygroscopic growth curves from the comparative kinetic measurements presented here, it is of critical importance that there is no kinetic impairment to the evaporation of water. For many of the sugars we now consider, it is well established that the diffusion constant of water is strongly dependent on water activity, diminishing by many orders of magnitude and leading to slow diffusion limited release of water under dry conditions (Rickards et al., 2015). Thus, we present data that have been carefully assessed as independent of drying rate, as established by the RH of the gas phase the droplet is drying in. For trehalose, galactose and sorbitol, measurements unimpeded by kinetic limitations have not been possible below 80 % RH, and consequently data presented below 80 % do not average to a consistent series of points.

Deleted: many

Deleted: compounds

Equilibrium hygroscopicity curves for the two sugars galactose and xylose, and two sugar alcohols (polyols) erythritol and sorbitol, are shown in Fig. 10. Molecular structures presented in Fig. 10 are the open chain form, which must be used during modelling using AIOMFAC-web. These have been selected to illustrate the comparable degree of hygroscopic growth for these compounds, all of which have the same O:C ratio of 1, even though they are subtly different in molecular structure and weight. Indeed, their experimental κ values are similar (galactose, 0.134; sorbitol 0.165; erythritol 0.255) and their hygroscopic properties are reasonably well represented by AIOMFAC-web.

Deleted: three

Deleted: , sorbitol

Deleted: he

Deleted: long chain

Deleted: alcohol

Deleted: UNIFAC

Deleted:

3.4. Trends in κ with O:C Ratio and Molecular Structure

In order to efficiently represent the hygroscopic growth of aerosols in large scale models, it is crucially important that models of low complexity are used to represent aerosol of broad ranging source and chemical complexity. Correlations of the value of the parameter κ with surrogate measures of ambient aerosol composition such as O:C have been considered (Duplissy et al., 2011;Massoli et al., 2010). We consider the trends arising from the results presented here in the variation in κ with degree of substitution and functional group identity. In Fig. 11(a), we compare the values of κ for the homologous series of dicarboxylic acids and their branched derivatives. Clearly, both increased chain length and increased branching lead to greater hydrophobicity and lower hygroscopicity. Overall trends in hygroscopicity, as represented by the dependence of MFS on water activity, can be fit to the power law model from Dutcher et al. 2013 (Table S0.1) and we show the upper and lower bounds for compounds from each class (amino acids, organic acids, sugars and alcohols) in Fig. 11(b). This clearly illustrates that the amino acids are more hygroscopic than the majority of the other compounds studied.

Further, we consider in Fig. 12(a) the variation in κ with O:C ratio for all of the compounds examined here. The variation in κ with O:C ratio for the organic acids, sugars and alcohols is well-described (within the uncertainties) by the parametrisation provided by Rickards *et al.* (2013). However, the trend for the sequence of amino acid compounds shows that they are considerably more hygroscopic than comparable dicarboxylic acids with the same or similar O:C ratios. For example succinic acid and glycine have the same O:C ratio of 1 but with experimental κ values of 0.198, and 0.671 respectively. This illustrates the additional complexity in representing hygroscopicities with a simple single parameter model when multi-functional compounds are present, likely to be typical of the composition of atmospheric aerosol. Compounds with the same O:C ratio can have κ values that span from very low hygroscopicity (less than 0.05) to very high hygroscopicity (approaching 0.4), as is seen for compounds with an O:C around 0.6. Fig. 12(b) shows the correlation between κ values determined in this study and calculated κ values from UManSysProp (Topping et al., 2016) using the hygroscopic growth factors [organic systems] model with density calculated using (Girolami, 1994). During the calculations the particle was assumed to have a dry diameter of 1000 nm and surface tension of 72 mNm^{-1}. Although there is a reasonably clear correlation between experimentally determined κ values and calculated κ, it is also clear that the value can be over-estimated by as much as a factor of 2. Further, UManSysProp predictions can also lead to an underestimation of κ for a limited number of compounds, including valine, histidine, and glutaric and methyl succinic acid.

The supplementary information provides tabulated hygroscopicity data for all compounds measured in this study, it also details compound purities, density and refractive index parametrisations for all compounds.

4. Conclusions

In conclusion we have presented equilibrium hygroscopicity data and density and refractive index parametrisations for 36 organic compounds of varying functionality, molecular weight and O:C ratio. Of these compounds straight chain dicarboxylic acids ($C_2 - C_5$) were found to be in better agreement with UNIFAC than the initial data used to parametrise UNIFAC (Peng et al., 2001). Equilibrium hygroscopicity curves of increasingly branched dicarboxylic acids are not well predicted by UNIFAC. Additionally amino acid thermodynamic model predictions are not in agreement with experimental observations. The discernible differences in hygroscopicity for different compound classes shown in both hygroscopicity curves in Fig. 13(b) and κ values in Fig. 12(a) offers the potential for future modelling methods to be built on relationships between compound classes and O:C and N:C ratios. Predictive tools considering these very general and smooth relationships would be much less computationally expensive than current group contribution methods and thus could be incorporated into climate models.

Deleted: , this is due to earlier experimental measurements by Chan *et al.* (2005) which have been used to parametrise UNIFAC

Acknowledgements

REHM and JPR acknowledge support from the Natural Environment Research Council through grant NE/N006801/1. AM acknowledges the EPSRC for support through DTA funding. GR acknowledges the Italian Ministry of Education for the award

of a PhD studentship. CSD and LN acknowledge support from the National Science Foundation through Grant Number 1554936. Young Chul Song from the University of Bristol is acknowledged for CK-EDB measurement for the compound Erythritol, data used in this work.

References

Akimoto, H.: Global Air Quality and Pollution, Science, 302, 1716-1719, doi:10.1126/science.1092666, 2003.

Baltensperger, U.: Spiers Memorial Lecture Introductory lecture: chemistry in the urban atmosphere, Farad. Discuss., 189, 9-29, doi:10.1039/C6FD00065G, 2016.

Barbaro, E., Zangrando, R., Vecchiato, M., Piazza, R., Cairns, W. R. L., Capodaglio, G., Barbante, C., and Gambaro, A.: Free amino acids in Antarctic aerosol: potential markers for the evolution and fate of marine aerosol, Atmos. Chem. Phys., 15, 5457-5469, doi:10.5194/acp-15-5457-2015, 2015.

Cai, C., Miles, R. E. H., Cotterell, M. I., Marsh, A., Rovelli, G., Rickards, A. M. J., Zhang, Y.-h., and Reid, J. P.: Comparison of Methods for Predicting the Compositional Dependence of the Density and Refractive Index of Organic–Aqueous Aerosols, J. Phys. Chem. A, 120, 6604-6617, doi:10.1021/acs.jpca.6b05986, 2016.

Carrico, C. M., Petters, M. D., Kreidenweis, S. M., Collett, J. L., Engling, G., and Malm, W. C.: Aerosol hygroscopicity and cloud droplet activation of extracts of filters from biomass burning experiments, J Geophys Res Atmos, 113, doi:10.1029/2007JD009274, 2008.

Chan, M. N., Choi, M. Y., Ng, N. L., and Chan, C. K.: Hygroscopicity of Water-Soluble Organic Compounds in Atmospheric Aerosols, Environ. Sci. Technol., 39, 1555-1562, doi:10.1021/es049584l, 2005.

Clegg, S. L., Brimblecombe, P., and Wexler, A. S.: Thermodynamic Model of the System H+−NH4+−SO42-−NO3-−H2O at Tropospheric Temperatures, J. Phys. Chem. A, 102, 2137-2154, doi:10.1021/jp973042r, 1998.

Davies, J. F., Haddrell, A. E., and Reid, J. P.: Time-Resolved Measurements of the Evaporation of Volatile Components from Single Aerosol Droplets, Aerosol Sci Tech, 46, 666-677, doi:10.1080/02786826.2011.652750, 2012.

Davies, J. F., Haddrell, A. E., Rickards, A. M. J., and Reid, J. P.: Simultaneous Analysis of the Equilibrium Hygroscopicity and Water Transport Kinetics of Liquid Aerosol, Anal. Chem., 85, 5819-5826, doi:10.1012/ac4005502, 2013.

Duplissy, J., DeCarlo, P. F., Dommen, J., Alfarra, M. R., Metzger, A., Barmpadimos, I., Prevot, A. S. H., Weingartner, E., Tritscher, T., Gysel, M., Aiken, A. C., Jimenez, J. L., Canagaratna, M. R., Worsnop, D. R., Collins, D. R., Tomlinson, J., and Baltensperger, U.: Relating hygroscopicity and composition of organic aerosol particulate matter, Atmos. Chem. Phys., 11, 1155-1165, doi:10.5194/acp-11-1155-2011, 2011.

Dutcher, C. S., Ge, X., Wexler, A. S., and Clegg, S. L.: An Isotherm-Based Thermodynamic Model of Multicomponent Aqueous Solutions, Applicable Over the Entire Concentration Range, J. Phys. Chem. A, 117, 3198-3213, doi:10.1021/jp310860p, 2013.

Farmer, D. K., Cappa, C. D., and Kreidenweis, S. M.: Atmospheric Processes and Their Controlling Influence on Cloud Condensation Nuclei Activity, Chem. Rev., 115, 4199-4217, doi:10.1021/cr5006292, 2015.

Fredenslund, A., Jones, R. L., and Prausnitz, J. M.: Group-contribution estimation of activity coefficients in nonideal liquid mixtures, AIChE Journal, 21, 1086-1099, doi:10.1002/aic.690210607, 1975.

George, C., Ammann, M., D'Anna, B., Donaldson, D. J., and Nizkorodov, S. A.: Heterogeneous Photochemistry in the Atmosphere, Chem. Rev., 115, 4218-4258, doi:10.1021/cr500648z, 2015.

Girolami, G. S.: A Simple "Back of the Envelope" Method for Estimating the Densities and Molecular Volumes of Liquids and Solids, Journal of Chemical Education, 71, 962-964, doi:10.1021/ed071p962, 1994.

Glantschnig, W. J., and Chen, S.-H.: Light scattering from water droplets in the geometrical optics approximation, Appl. Opt., 20, 2499-2509, doi:10.1364/AO.20.002499, 1981.

Gupta, R. B., and Heidemann, R. A.: Solubility Models for Amino-Acids and Antibiotics, Aiche Journal, 36, 333-341, DOI 10.1002/aic.690360303, 1990.

Haddrell, A. E., Davies, J. F., and Reid, J. P.: Dynamics of Particle Size on Inhalation of Environmental Aerosol and Impact on Deposition Fraction, Environ. Sci. Technol., 49, 14512-14521, doi:10.1021/acs.est.5b01930, 2015.

Hallquist, M., Wenger, J. C., Baltensperger, U., Rudich, Y., Simpson, D., Claeys, M., Dommen, J., Donahue, N. M., George, C., Goldstein, A. H., Hamilton, J. F., Herrmann, H., Hoffmann, T., Iinuma, Y., Jang, M., Jenkin, M. E., Jimenez, J. L., Kiendler-

Scharr, A., Maenhaut, W., McFiggans, G., Mentel, T. F., Monod, A., Prévôt, A. S. H., Seinfeld, J. H., Surratt, J. D., Szmigielski, R., and Wildt, J.: The formation, properties and impact of secondary organic aerosol: current and emerging issues, Atmos. Chem. Phys., 9, 5155-5236, doi:10.5194/acp-9-5155-2009, 2009.

Hodas, N., Zuend, A., Schilling, K., Berkemeier, T., Shiraiwa, M., Flagan, R. C., and Seinfeld, J. H.: Discontinuities in hygroscopic growth below and above water saturation for laboratory surrogates of oligomers in organic atmospheric aerosols, Atmos Chem Phys, 16, 12767-12792, 10.5194/acp-16-12767-2016, 2016.

Hori, M., Ohta, S., Murao, N., and Yamagata, S.: Activation capability ofwater soluble organic substances as CCN, J. Aerosol Sci., 34, 419-448, doi:10.1016/S0021-8502(02)00190-8, 2003.

Huff-Hartz, K. E. H., Tischuk, J. E., Chan, M. N., Chan, C. K., Donahue, M. N., and Pandis, S. N.: Cloud condensation nuclei activation of limited solubility organic aerosol, Atmos. Environ., 40, 605-617, doi:10.1016/j.atmosenv.2005.09.076, 2006.

Jacob, D. J.: Heterogeneous chemistry and tropospheric ozone, Atmos. Environ., 34, 2131-2159, doi:10.1016/S1352-2310(99)00462-8, 2000.

Jimenez, J. L., Canagaratna, M. R., Donahue, N. M., Prevot, A. S. H., Zhang, Q., Kroll, J. H., DeCarlo, P. F., Allan, J. D., Coe, H., Ng, N. L., Aiken, A. C., Docherty, K. S., Ulbrich, I. M., Grieshop, A. P., Robinson, A. L., Duplissy, J., Smith, J. D., Wilson, K. R., Lanz, V. A., Hueglin, C., Sun, Y. L., Tian, J., Laaksonen, A., Raatikainen, T., Rautiainen, J., Vaattovaara, P., Ehn, M., Kulmala, M., Tomlinson, J. M., Collins, D. R., Cubison, M. J., E., Dunlea, J., Huffman, J. A., Onasch, T. B., Alfarra, M. R., Williams, P. I., Bower, K., Kondo, Y., Schneider, J., Drewnick, F., Borrmann, S., Weimer, S., Demerjian, K., Salcedo, D., Cottrell, L., Griffin, R., Takami, A., Miyoshi, T., Hatakeyama, S., Shimono, A., Sun, J. Y., Zhang, Y. M., Dzepina, K., Kimmel, J. R., Sueper, D., Jayne, J. T., Herndon, S. C., Trimborn, A. M., Williams, L. R., Wood, E. C., Middlebrook, A. M., Kolb, C. E., Baltensperger, U., and Worsnop, D. R.: Evolution of Organic Aerosols in the Atmosphere, Science, 326, 1525-1529, doi:10.1126/science.1180353, 2009.

Koehler, K. A., Kreidenweis, S. M., DeMott, P. J., Prenni, A. J., Carrico, C. M., Ervens, B., and Feingold, G.: Water activity and activation diameters from hygroscopicity data – Part II: Application to organic species, Atmos. Chem. Phys., 6, 795-809, doi:10.5194/acp-6-795-2006, 2006.

Kreidenweis, S. M., Petters, M. D., and DeMott, P. J.: Single-parameter estimates of aerosol water content, Environ. Res. Lett., 3, doi:10.1088/1748-9326/3/3/035002, 2008.

Krieger, U. K., Marcollia, C., and Reid, J. P.: Exploring the complexity of aerosol particle properties and processes using single particle techniques, Chem. Soc. Rev., 41, 6631-6662, doi:10.1039/c2cs35082c, 2012.

Kulmala, M., Vesala, T., and Wagner, P.: An Analytical Expression For the Rate of Binary Condensational Particle Growth, Proc. R. Soc. London. A, 441, 689-605, 1993.

Kumar, P. P., Broekhuizen, K., and Abbatt, J. P. D.: Organic acids as cloud condensation nuclei: Laboratory studies of highly soluble and insoluble species, Atmos. Chem. Phys., 3, 509-520, doi:10.5194/acp-3-509-2003, 2003.

Kuramochi, H., Noritomi, H., Hoshino, D., and Nagahama, K.: Measurements of Vapor Pressures of Aqueous Amino Acid Solutions and Determination of Activity Coefficients of Amino Acids, J. Chem. Eng. Data, 42, 470-474, doi:S0021-9568(96)00113-6, 1997a.

Kuramochi, H., Noritomi, H., Hoshino, D., and Nagahama, K.: Representation of activity coefficients of fundamental biochemicals in water by the UNIFAC model, Fluid Phase Equilibria, 130, 117-132, doi.org/10.1016/S0378-3812(96)03209-8, 1997b.

Laskin, A., Laskin, J., and Nizkorodov, S. A.: Chemistry of Atmospheric Brown Carbon, Chem. Rev., 115, 4335-4382, doi:10.1021/cr5006167, 2015.

Liu, Y., and Daum, P. H.: Relationship of refractive index to mass density and self-consistency of mixing rules for multicomponent mixtures like ambient aerosols, J Aerosol Sci, 39, 974-986, doi:10.1016/j.jaerosci.2008.06.006, 2008.

Lohmann, U., and Feichter, J.: Global indirect aerosol effects: a review, Atmos. Chem. Phys. , 5, 715-737, doi:1680-7324/acp/2005-5-715, 2005.

Losey, D. J., Parker, R. G., and Freedman, M. A.: pH Dependence of Liquid–Liquid Phase Separation in Organic Aerosol, J. Phys. Chem. Lett., 7, 3861-3865, doi:10.1021/acs.jpclett.6b01621, 2016.

Massoli, P., Lambe, A. T., Ahern, A. T., Williams, L. R., Ehn, M., Mikkila, J., Canagaratna, M. R., Brune, W. H., Onasch, T. B., Jayne, J. T., Petaja, T., Kulmala, M., Laaksonen, A., Kolb, C. E., Davidovits, P., and Worsnop, D. R.: Relationship between aerosol oxidation level and hygroscopic properties of laboratory generated secondary organic aerosol (SOA) particles, Geophys. Res. Lett., 37, 5, doi:10.1029/2010gl045258, 2010.

Matsumoto, K., and Uematsu, M.: Free amino acids in marine aerosols over the western North Pacific Ocean, Atmos. Environ., 39, 2163-2170, doi:10.1016/j.atmosenv.2004.12.022, 2005.
McNeill, V. F.: Aqueous Organic Chemistry in the Atmosphere: Sources and Chemical Processing of Organic Aerosols, Environ. Sci. Technol., 49, 1237-1244, doi:10.1021/es5043707, 2015.
Moise, T., Flores, J. M., and Rudich, Y.: Optical Properties of Secondary Organic Aerosols and Their Changes by Chemical Processes, Chem. Rev., 115, 4400-4439, doi:10.1021/cr5005259, 2015.
Nandy, L., Ohm, P. B., and Dutcher, C. S.: Isotherm-Based Thermodynamic Models for Solute Activities of Organic Acids with Consideration of Partial Dissociation, J. Phys. Chem. A, 120, 4147−4154, doi: 10.1021/acs.jpca.6b01904, 2016.
Ninni, L., and Meirelles, A. J. A.: Water Activity, pH and Density of Aqueous Amino Acids Solutions, Biotechnol. Prog., 17, 703−711, doi:10.1021/bp0100427, 2001.
Ohm, P. B., Asato, C., Wexler, A. S., and Dutcher, C. S.: Isotherm-Based Thermodynamic Model for Electrolyte and Nonelectrolyte Solutions Incorporating Long- and Short-Range Electrostatic Interactions, The Journal of Physical Chemistry A, 119, 3244-3252, doi:10.1021/jp512646k, 2015.
Pajunoja, A., Lambe, A. T., Hakala, J., Rastak, N., Cummings, M. J., Brogan, J. F., Hao, L., Paramonov, M., Hong, J., Prisle, N. L., Malila, J., Romakkaniemi, S., Lehtinen, K. E. J., Laaksonen, A., Kulmala, M., Massoli, P., Onasch, T. B., Donahue, N. M., Riipinen, I., Davidovits, P., Worsnop, D. R., Petäjä, T., and Virtanen, A.: Adsorptive uptake of water by semisolid secondary organic aerosols, Geophys. Res. Lett., 42, 3063-3068, doi:10.1002/2015GL063142, 2015.
Pandis, S. N., Wexler, A. S., and Seinfeld, J. H.: Dynamics of Tropospheric Aerosols, J. Phys. Chem., 99, 9646-9659, doi:10.1021/j100024a003, 1995.
Peng, C., Chan, M. N., and Chan, C. K.: The Hygroscopic Properties of Dicarboxylic and Multifunctional Acids, Environ. Sci. Technol., 35, doi:10.1021/es0107531, 2001.
Petters, M. D., and Kreidenweis, S. M.: A single parameter representation of hygroscopic growth and cloud condensation nucleus activity, Atmos. Chem. Phys., 7, 1961-1971, doi:10.5194/acp-7-1961-2007, 2007.
Petters, M. D., Kreidenweis, S. M., and Ziemann, P. J.: Prediction of cloud condensation nuclei activity for organic compounds using functional group contribution methods, Geosci. Model Dev, 9, 111–124, doi:10.5194/gmd-9-111-2016, 2016.
Pöschl, U., and Shiraiwa, M.: Multiphase Chemistry at the Atmosphere–Biosphere Interface Influencing Climate and Public Health in the Anthropocene, Chem. Rev., 115, 4440-4475, doi:10.1021/cr500487s, 2015.
R. Y.-W. Chang, Slowik, J. G., Shantz, N. C., Vlasenko, A., Liggio, J., Sjostedt, S. J., Leaitch, W. R., and Abbatt, J. P. D.: The hygroscopicity parameter (κ) of ambient organic aerosol at a field site, Atmos. Chem. Phys., 10, 5047-5064, doi:10.5194/acp-10-5047-2010, 2010.
Ravishankara, A. R., Rudich, Y., and Wuebbles, D. J.: Physical Chemistry of Climate Metrics, Chem. Rev., 115, 3682-3703, doi:10.1021/acs.chemrev.5b00010, 2015.
Rickards, A. M. J., Miles, R. E. H., Davies, J. F., Marshall, F. H., and Reid, J. P.: Measurements of the Sensitivity of Aerosol Hygroscopicity and the κ, J. Phys. Chem. A, 117, 14120−14131, doi:10.1021/jp407991n |, 2013.
Rickards, A. M. J., Song, Y.-C., Miles, R. E. H., Preston, T. C., and Reid, J. P.: Variabilities and uncertainties in characterising water transport kinetics in glassy and ultraviscous aerosol, Phys Chem Chem Phys, 17, 10059-10073, doi:10.1039/C4CP05383D, 2015.
Rindelaub, J. D., Craig, R. L., Nandy, L., Bondy, A. L., Dutcher, C. S., Shepson, P. B., and Ault, A. P.: Direct Measurement of pH in Individual Particles via Raman Microspectroscopy and Variation in Acidity with Relative Humidity, J. Phys. Chem. A, 120, 911-917, doi:10.1021/acs.jpca.5b12699, 2016.
Rovelli, G., Miles, R. E. H., Reid, J. P., and Clegg, S. L.: Accurate Measurements of Aerosol Hygroscopic Growth over a Wide Range in Relative Humidity, J. Phys. Chem. A, 120, 4376−4388, doi:10.1021/acs.jpca.6b04194, 2016.
Seinfeld, J. H., and Pankow, J. F.: Organic Atmospheric Particulate Matter, Annu. Rev. Phys. Chem., 54, 121-140, doi:10.1146/annurev.physchem.54.011002.103756, 2003.
Suda, S. R., Petters, M. D., Yeh, G. K., Strollo, C., Matsunaga, A., Faulhaber, A., Ziemann, P. J., Prenni, A. J., Carrico, C. M., Sullivan, R. C., and Kreidenweis, S. M.: Influence of Functional Groups on Organic Aerosol Cloud Condensation Nucleus Activity, Environ. Sci. Technol., 48, 10182-10190, doi:10.1021/es502147y, 2014.
Topping, D., Connolly, P., and McFiggans, G.: Cloud droplet number enhanced by co-condensation of organic vapours, Nature Geosci, 6, 443-446, doi:10.1038/ngeo1809, 2013.

Topping, D., Barley, M., Bane, M. K., Higham, N., Aumont, B., Dingle, N., and McFiggans, G.: UManSysProp v1.0: an online and open-source facility for molecular property prediction and atmospheric aerosol calculations, Geosci. Model Dev., 9, 899-914, doi:10.5194/gmd-9-899-2016, 2016.

Wex, H., Stratmann, F., Topping, D., and McFiggans, G.: The Kelvin versus the Raoult Term in the Kohler Equation, J. Atmos. Sci., 65, 4004-4016, doi:10.1175/2008jas2720.1, 2008.

Wexler, A. S., and Clegg, S. L.: Atmospheric aerosol models for systems including the ions H+, NH4+, Na+, SO42−, NO3−, Cl−, Br−, and H2O, J Geophys Res Atmos, 107, ACH 14-11-ACH 14-14, doi:10.1029/2001JD000451, 2002.

Zhang, R., Wang, G., Guo, S., Zamora, M. L., Ying, Q., Lin, Y., Wang, W., Hu, M., and Wang, Y.: Formation of Urban Fine Particulate Matter, Chem. Rev., 115, 3803-3855, doi:10.1021/acs.chemrev.5b00067, 2015.

Ziemann, P. J., and Atkinson, R.: Kinetics, products, and mechanisms of secondary organic aerosol formation, Chem. Soc. Rev., 41, 6582-6605, doi:10.1039/C2CS35122F, 2012.

Zuend, A., Marcolli, C., Luo, B. P., and Peter, T.: A thermodynamic model of mixed organic-inorganic aerosols to predict activity coefficients, Atmos. Chem. Phys., 8, 4559-4593, doi:10.5194/acp-8-4559-2008, 2008.

Zuend, A., Marcolli, C., Booth, A. M., Lienhard, D. M., Soonsin, V., Krieger, U. K., Topping, D. O., McFiggans, G., Peter, T., and Seinfeld, J. H.: New and extended parameterization of the thermodynamic model AIOMFAC: calculation of activity coefficients for organic-inorganic mixtures containing carboxyl, hydroxyl, carbonyl, ether, ester, alkenyl, alkyl, and aromatic functional groups, Atmos. Chem. Phys., 11, 9155-9206, doi:10.5194/acp-11-9155-2011, 2011.

Zuend, A., and Seinfeld, J. H.: Modeling the gas-particle partitioning of secondary organic aerosol: the importance of liquid-liquid phase separation, Atmos. Chem. Phys., 12, 3857-3882, doi:10.5194/acp-12-3857-2012, 2012.

Tables.

Table 1. Experimentally determined κ values at a_w = 0.95 for all compounds studied at 293.15 K, presented alongside κ values calculated using UManSysProp and the smile string used for this calculation.

Compound	Average Experimental κ Value (a_w= 0.95)	Standard Deviation in κ (±)	UManSysProp Calculated κ (a_w= 0.95)	SMILES String
		Amino Acids		
DL-Alanine	0.357	0.010	0.402	O=C(O)C(N)C
L-Asparagine	0.187	0.017	0.337	O=C(N)C[C@H](N)C(=O)O
L-Aspartic Acid	-	-	0.332	O=C(O)CC(N)C(=O)O
L-Arginine	0.147	0.005	0.267	NC(CCCNC(N)=N)C(O)=O
Glycine	0.671	0.013	0.621	C(C(=O)O)N
L-Histidine	0.188	0.003	0.052	O=C([C@H](CC1=CNC=N1)N)O
L-Lysine	0.219	0.007	0.250	C(CCN)CC(C(=O)O)N
L-Proline	0.272	0.005	0.273	OC(=O)C1CCCN1
L-Threonine	0.235	0.001	0.307	C[C@H]([C@@H](C(=O)O)N)O
L-Valine	0.253	0.003	0.136	CC(C)[C@@H](C(=O)O)N
		Carboxylic Acids		
Oxalic Acid	0.409	0.005	0.488	C(=O)(C(=O)O)O
Malonic Acid	0.281	0.003	0.362	O=C(O)CC(=O)O
Succinic Acid	0.198	0.011	0.252	C(CC(=O)O)C(=O)O
Methyl Malonic acid	0.234	0.006	0.252	CC(C(=O)O)C(=O)O
Glutaric Acid	0.144	0.005	0.139	C(CC(=O)O)CC(=O)O
Methyl Succinic Acid	0.160	0.003	0.138	CC(CC(=O)O)C(=O)O
Dimethyl Malonic Acid	0.149	0.002	0.150	CC(C)(C(=O)O)C(=O)O
Adipic Acid	0.101	0.004	0.055	C(CCC(=O)O)CC(=O)O
2-Methyl Glutaric Acid	0.102	0.005	0.055	CC(CCC(=O)O)C(=O)O
3-Methyl Glutaric Acid	0.103	0.006	0.055	CC(CC(=O)O)CC(=O)O
2,2 -Dimethyl Succinic Acid	0.116	0.009	0.061	CC(C)(CC(=O)O)C(=O)O
2,3-Dimethyl Succinic acid	0.130	0.002	0.054	CC(C(C)C(=O)O)C(=O)O
Pimelic Acid	0.060	0.003	0.030	OC(=O)CCCCCC(=O)O

Deleted: Smile

Deleted: ,

Deleted: ,

Deleted: –

Deleted: –

2,2-Dimethyl Glutaric Acid	0.054	0.002	0.032	CC(C)(CCC(=O)O)C(=O)O
3-Methyl Adipic Acid	0.064	0.002	0.030	CC(CCC(=O)O)CC(=O)O
3,3-Dimethyl Glutaric Acid	0.066	0.003	0.032	CC(C)(CC(=O)O)CC(=O)O
Diethyl Malonic Acid	0.065	0.001	0.032	CCC(CC)(C(=O)O)C(=O)O
Citric Acid	0.189	0.002	0.192	OC(=O)CC(O)(C(=O)O)CC(=O)O
Tartaric Acid	0.27	0.006	0.308	O=C(O)C(O)C(O)C(=O)O
Sorbitol	0.165	0.003	0.303	OC([C@H](O)[C@@H](O)[C@H](O)CO)CO
D-(+)-Trehalose Dihydrate	0.088	0.001	0.151	C([C@@H]1[C@H]([C@@H]([C@H](O1)O[C@@H]2[C@@H]([C@H]([C@@H]([C@H](O2)CO))O)O)O)O)O)O
Galactose	0.134	0.004	0.246	O[C@H]1[C@@H](O)[CH](O[C@H](O)[C@@H]1O)O
Xylose	-	-		
PEG4	0.154	0.004		
PEG3	0.151	0.003		
Erythritol	0.255	0.006	0.380	OC[C@@H](O)[C@@H](O)CO

Table 2. κ values available in the literature for dicarboxylic acids.

Compound	Literature κ
Oxalic acid	0.504 ± 0.044(Rickards et al., 2013)
Malonic acid	0.44 ± 0.16 (Koehler et al., 2006) 0.227 ± 0.028 (Kumar et al., 2003) 0.292 ± 0.011(Rickards et al., 2013)
Succinic acid	0.231 ± 0.065 (Hori et al., 2003) 0.216 ± 0.20(Rickards et al., 2013)
Glutaric acid	0.20 ± 0.08 (Koehler et al., 2006) 0.088 (Huff-Hartz et al., 2006) 0.168 ± 0.30 (Rickards et al., 2013)
Adipic acid	0.096 0.102 ± 0.009 (Kumar et al., 2003) (Rickards et al., 2013)

Deleted: ,

Figures.

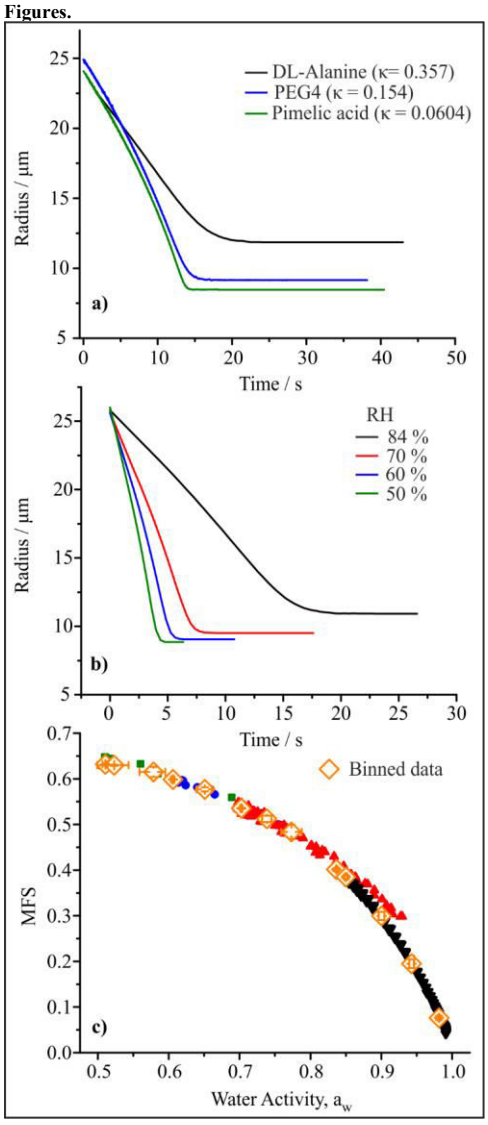
DL-Alanine (κ= 0.357)
PEG4 (κ = 0.154)
Pimelic acid (κ = 0.0604)
Radius / µm
Time / s
a)
RH
84 %
70 %
60 %
50 %
Radius / µm
Time / s
b)
Binned data
MFS
Water Activity, a_w
c)

Fig. 1. (a) Examples of the time-dependent evaporation of aqueous droplets containing compounds with varying κ value evaporating into similar RHs (~82 %). (b) The time-dependence of the radii of droplets of aqueous glycine evaporating into different RHs. (c) Equilibrium hygroscopicity curve for glycine, with binned data points (large open orange diamonds) estimate across the four different experiments at four RHs shown in (b).

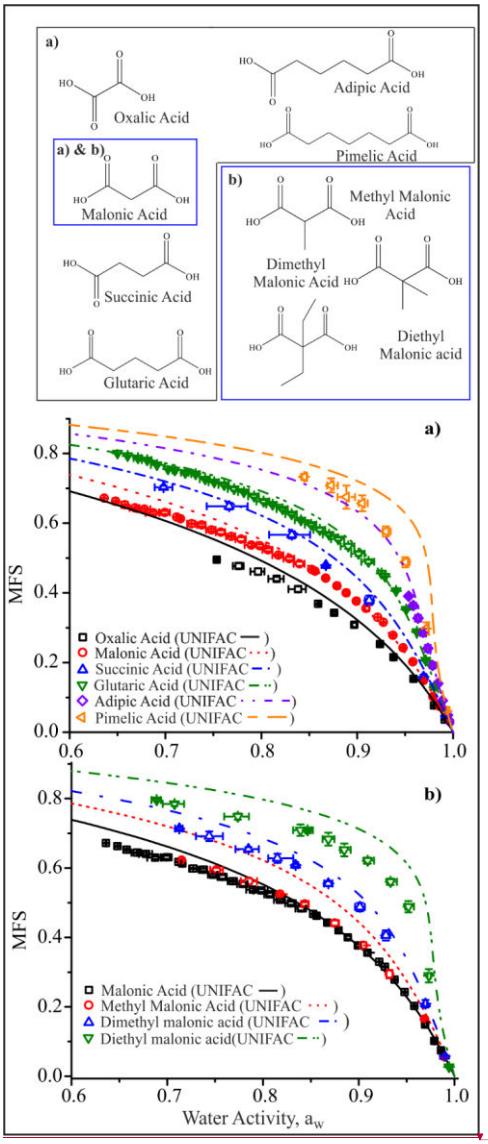
a)
Oxalic Acid
Adipic Acid
Pimelic Acid
a) & b)
Malonic Acid
b)
Methyl Malonic Acid
Dimethyl Malonic Acid
Diethyl Malonic acid
Succinic Acid
Glutaric Acid
a)
MFS
Oxalic Acid (UNIFAC)
Malonic Acid (UNIFAC)
Succinic Acid (UNIFAC)
Glutaric Acid (UNIFAC)
Adipic Acid (UNIFAC)
Pimelic Acid (UNIFAC)
b)
MFS
Malonic Acid (UNIFAC)
Methyl Malonic Acid (UNIFAC)
Dimethyl malonic acid (UNIFAC)
Diethyl malonic acid(UNIFAC)
Water Activity, a_w

Deleted:

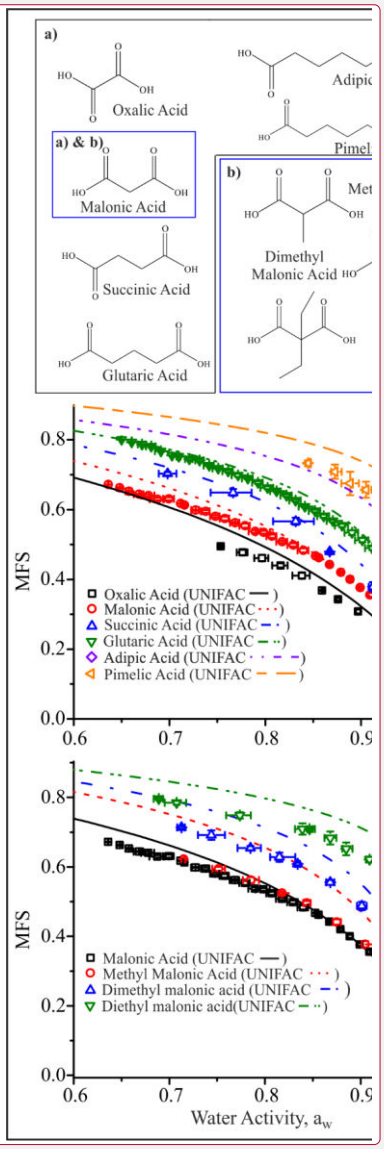
a)
Oxalic Acid
Adipic
Pimel
a) & b)
Malonic Acid
b)
Met
Dimethyl Malonic Acid
Succinic Acid
Glutaric Acid
MFS
Oxalic Acid (UNIFAC)
Malonic Acid (UNIFAC)
Succinic Acid (UNIFAC)
Glutaric Acid (UNIFAC)
Adipic Acid (UNIFAC)
Pimelic Acid (UNIFAC)
MFS
Malonic Acid (UNIFAC)
Methyl Malonic Acid (UNIFAC)
Dimethyl malonic acid (UNIFAC)
Diethyl malonic acid(UNIFAC)
Water Activity, a_w

Fig. 2. Equilibrium hygroscopic growth curves are shown in (a) for the homologous series of straight chain dicarboxylic acids and in (b) for dicarboxylic acids with a malonic acid backbone and increasing methyl substitution. UNIFAC prediction using AIOMFAC-web.

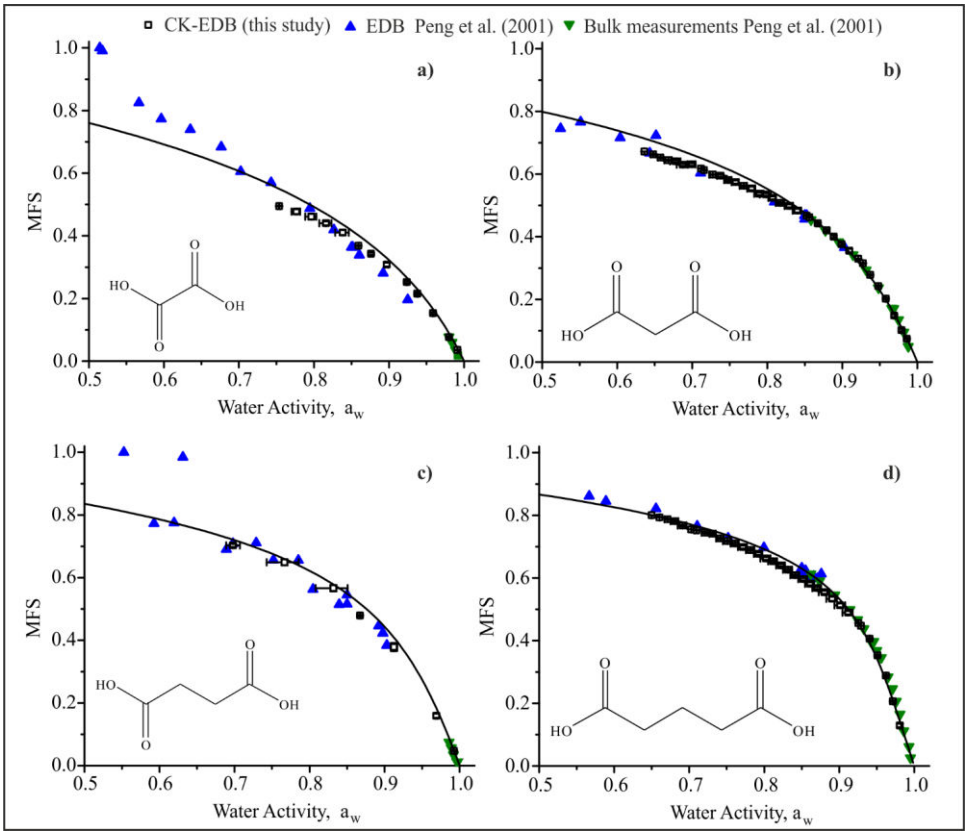

Fig. 3. Hygroscopicity of dicarboxylic acid droplets measured with the CK-EDB (black open squares) compared with the EDB data of Peng *et al.* (2001) (blue up triangles) and bulk measurements (green down triangles) for (a) oxalic acid, (b) malonic acid, (c) succinic acid and (d) glutaric acid. UNIFAC predictions are shown for all compounds (solid black line). UNIFAC prediction using AIOMFAC-web.

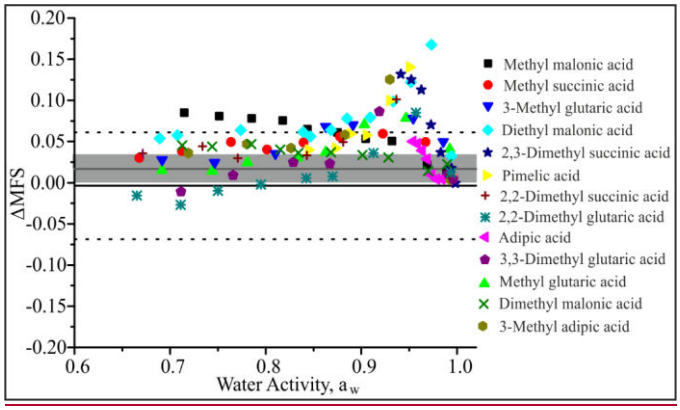

Deleted:

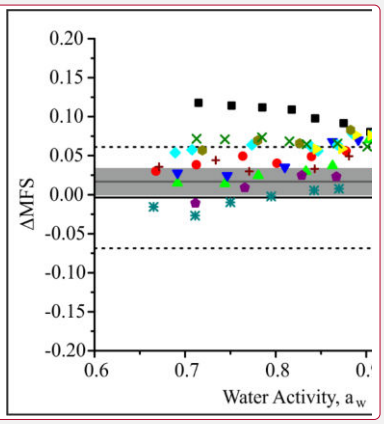

Fig. 4. The difference between the mass fraction of solute from UNIFAC predictions and the CK-EDB data from this study (ΔMFS) for all 13 branched dicarboxylic acids studied. The average in ΔMFS for the 4 dicarboxylic acids in Fig. 3 (CK-EDB data, this study) across the whole water activity range is represented with a grey shaded area, the average represented by the dark grey line. Additionally, the average ΔMFS (black solid line) and standard deviation (black dashed lines) derived from the Peng et al. (2001) data also shown in Fig. 3.

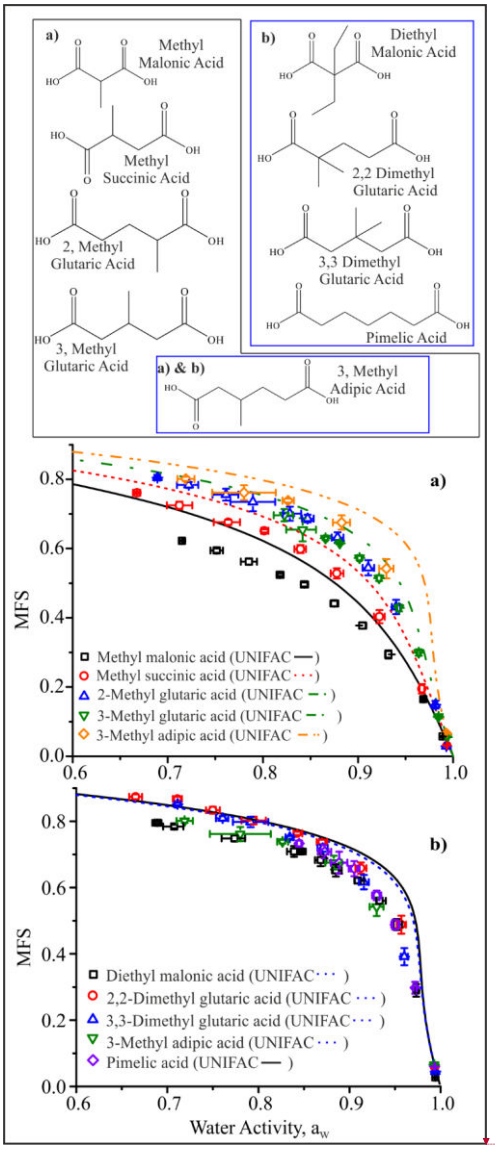
a)
Methyl Malonic Acid
Methyl Succinic Acid
2, Methyl Glutaric Acid
3, Methyl Glutaric Acid
b)
Diethyl Malonic Acid
2,2 Dimethyl Glutaric Acid
3,3 Dimethyl Glutaric Acid
Pimelic Acid
a) & b)
3, Methyl Adipic Acid
a)
MFS
Methyl malonic acid (UNIFAC —)
Methyl succinic acid (UNIFAC ···)
2-Methyl glutaric acid (UNIFAC – ·)
3-Methyl glutaric acid (UNIFAC – ·)
3-Methyl adipic acid (UNIFAC – ··)
b)
MFS
Diethyl malonic acid (UNIFAC ···)
2,2-Dimethyl glutaric acid (UNIFAC ···)
3,3-Dimethyl glutaric acid (UNIFAC ···)
3-Methyl adipic acid (UNIFAC ···)
Pimelic acid (UNIFAC —)
Water Activity, a_w

Deleted:

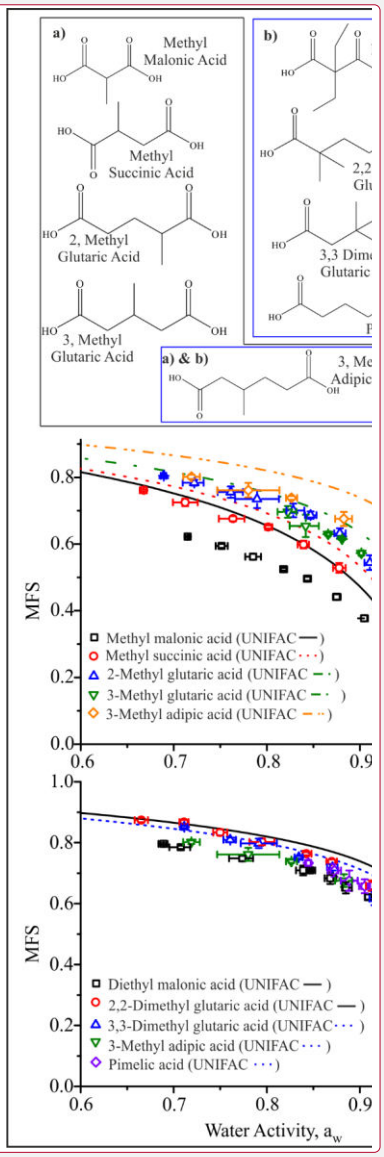
a)
Methyl Malonic Acid
Methyl Succinic Acid
2, Methyl Glutaric Acid
3, Methyl Glutaric Acid
a) & b)
MFS
Methyl malonic acid (UNIFAC —)
Methyl succinic acid (UNIFAC ···)
2-Methyl glutaric acid (UNIFAC – ·)
3-Methyl glutaric acid (UNIFAC – ·)
3-Methyl adipic acid (UNIFAC – ··)
MFS
Diethyl malonic acid (UNIFAC —)
2,2-Dimethyl glutaric acid (UNIFAC —)
3,3-Dimethyl glutaric acid (UNIFAC ···)
3-Methyl adipic acid (UNIFAC ···)
Pimelic acid (UNIFAC ···)
Water Activity, a_w

Figure 5. Equilibrium hygroscopicity curves for a series of branched dicarboxylic acids are shown in a). In (b) CK-EDB hygroscopicity curves for a series of dicarboxylic acids with the same O:C ratio of 0.57. UNIFAC prediction using AIOMFAC-web. In b) the AIOMFAC-web prediction for 3-methyl adipic acid, $[(CH_3)(CH)(CH_2)_3(COOH)_2]$, 3,3-dimethylglutaric acid, $[(CH_3)_2(C)(CH_2)_2(COOH)_2]$, 2,2-dimethylglutaric acid, $[(CH_3)_2(C)(CH_2)_2(COOH)_2]$ is represented by the blue dashed line. Note that the equilibrium curves for the first 4 compounds are in such close agreement and indistinguishable on this scale that only one curve is shown for clarity. The prediction for pimelic acid $[(CH_2)_5(COOH)_2]$ is shown as a black solid line.

Formatted: Subscript
Formatted: Subscript
Formatted: Subscript
Formatted: Subscript
Formatted: Subscript
Formatted: Subscript
Formatted: Subscript
Formatted: Subscript
Formatted: Subscript
Formatted: Subscript
Formatted: Subscript
Formatted: Subscript
Formatted: Subscript
Formatted: Subscript
Formatted: Subscript
Formatted: Subscript

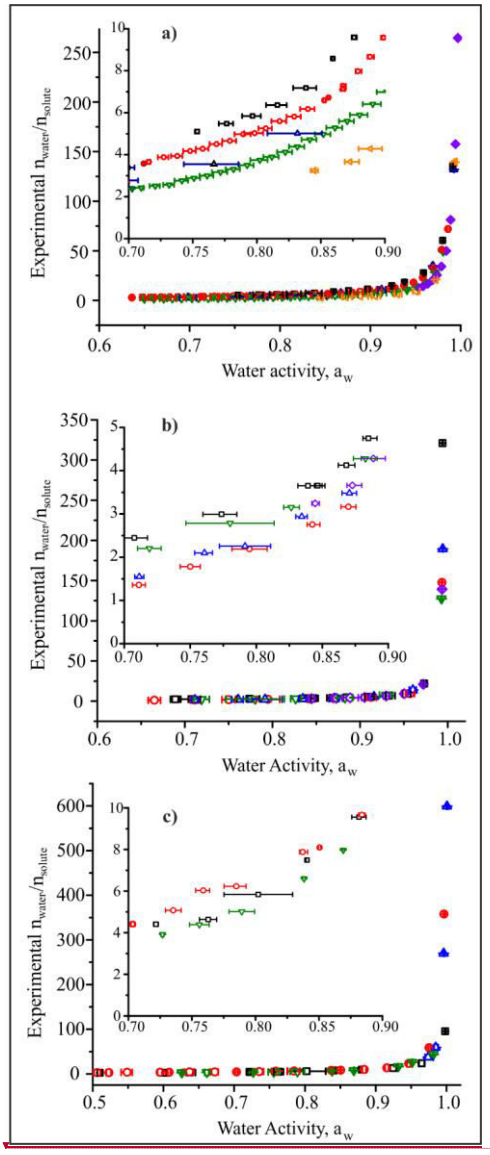
a)
b)
c)
Experimental n_{water}/n_{solute}
Water activity, a_w
Water Activity, a_w

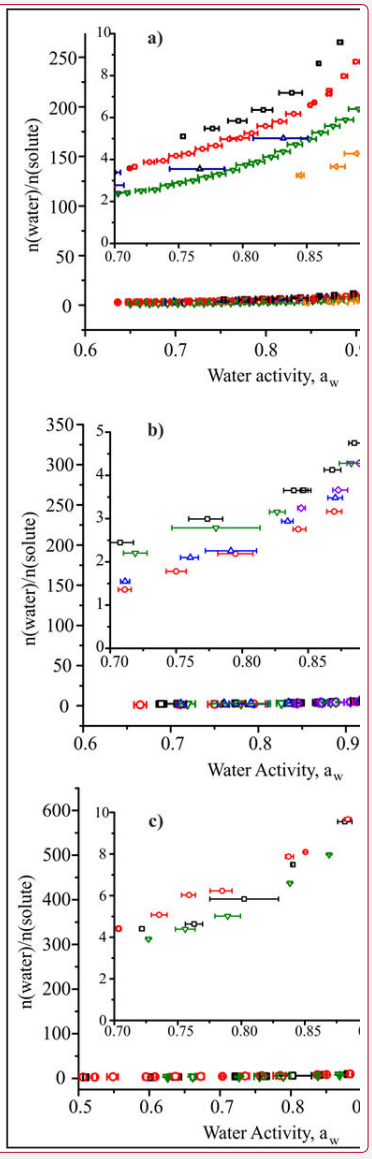
a)
b)
c)
n(water)/n(solute)
Water activity, a_w
Water Activity, a_w

Deleted:

Figure 6. Moles of water, per mole of solute for (a) for straight chain dicarboxylic acids for oxalic (black squares), malonic acid (red circles), succinic acid (blue up triangles), glutaric acid (green down triangles), adipic acid (violet diamonds) and pimelic acid (orange left triangles). In (b) for diethylmalonic acid (black squares), 2,2-dimethyl glutaric acid (red circles), 3,3-dimethyl glutaric acid (blue triangles), 3-methyl adipic acid (pink down triangles) and pimelic acid (green diamonds). And in (c) for galactose (black squares), sorbitol (red circles), xylose (blue down triangles) and erythritol (green down triangles).

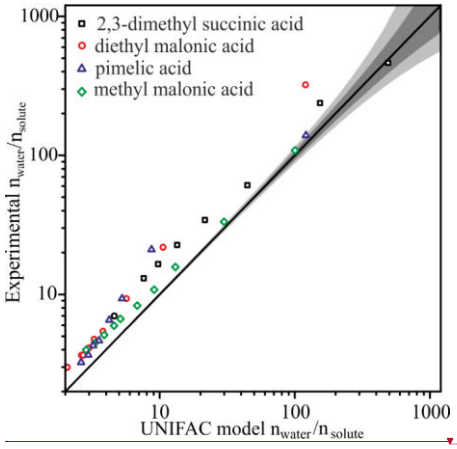

Deleted:

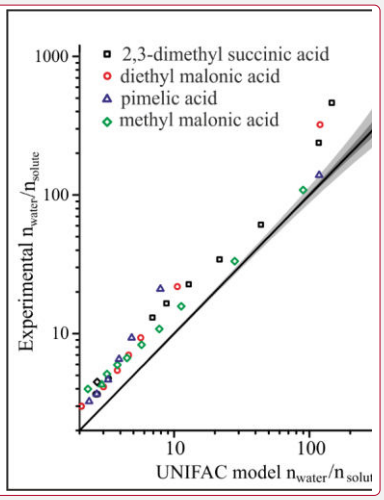

Figure 7. Comparison of the experimentally determined number of moles of water per mole of solute and the value predicted from UNIFAC for the four dicarboxylic acids with the largest deviation from UNIFAC. Shaded regions correspond to error in aw of ±0.001 (dark shaded grey regions) and ±0.002 (light shaded grey regions).

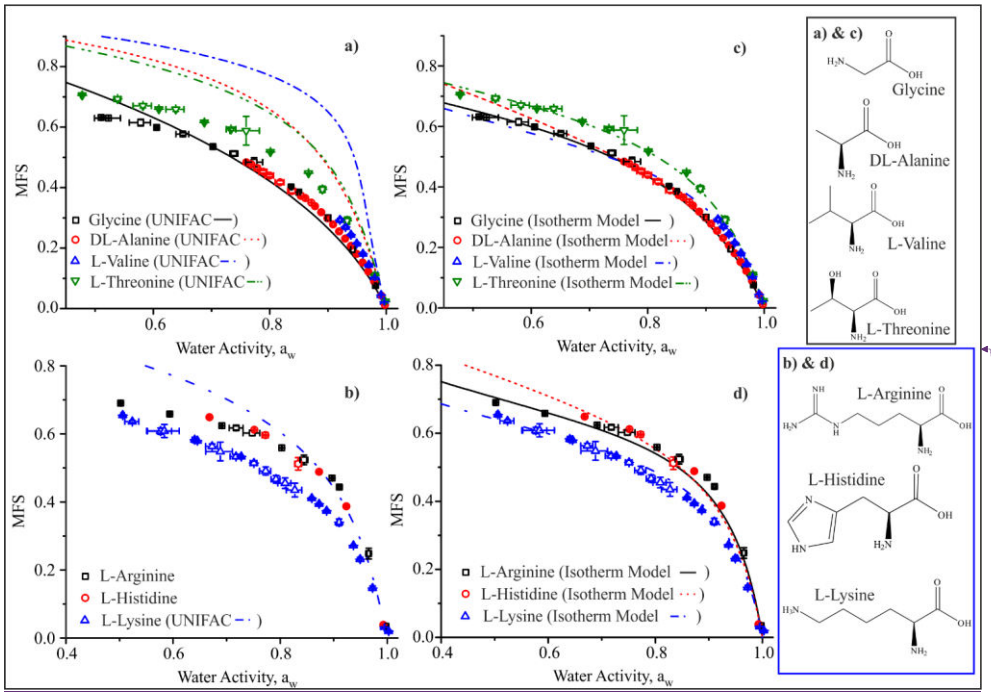

Figure 8. Equilibrium hygroscopicity curves in (a) for structurally similar amino acids with different substituents alongside UNIFAC predictions. In (b) equilibrium hygroscopicity curves of amino acids with the same O:C ratio (0.33) with UNIFAC predictions generated using E-AIM model III. In c) and d) the same amino acids as a) and b) respectively and are presented alongside thermodynamic predictions using the isotherm model discussed in Dutcher et al. (2013) with coefficients available in Table S0.2.

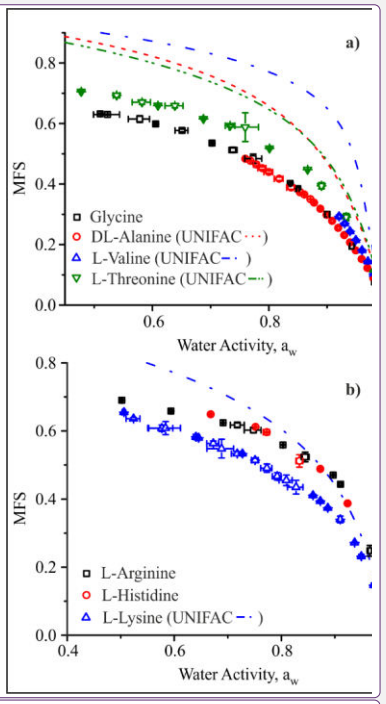

Deleted:

Formatted: Normal, Left

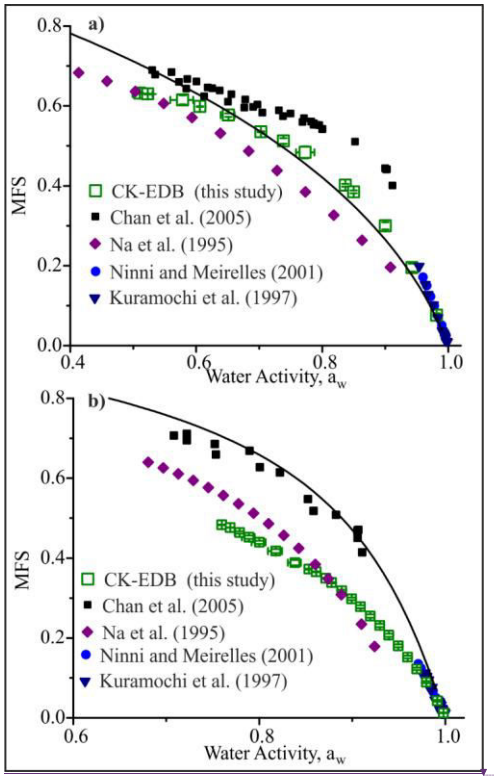

Figure 9. Equilibrium hygroscopicity data for (a) glycine and (b) alanine. The solid black line is the UNIFAC model prediction for alanine and glycine, generated using E-AIM Model III.

Deleted:

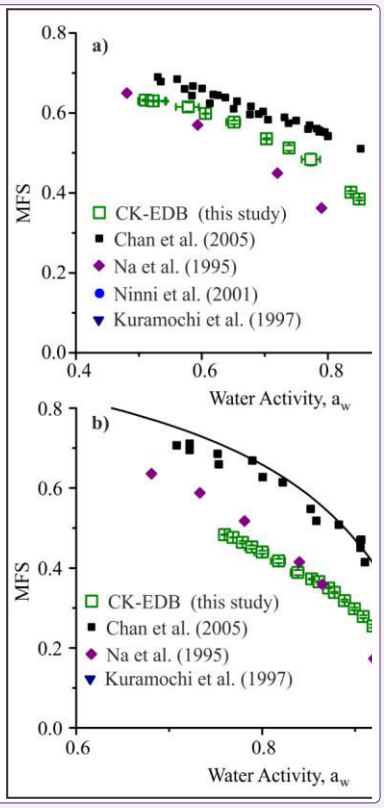

Deleted: is also shown (solid black line).

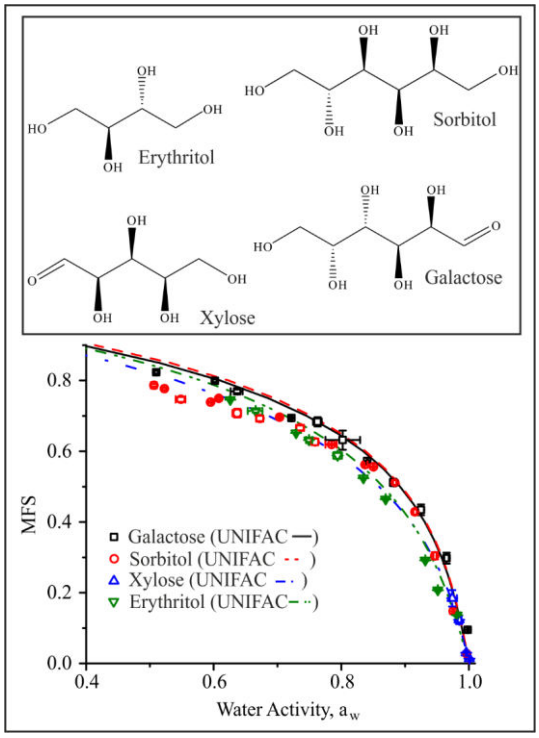

Figure 10. Equilibrium hygroscopicity curves for sugars and alcohols with the same O:C ratio of 1. UNIFAC prediction using AIOMFAC-web.

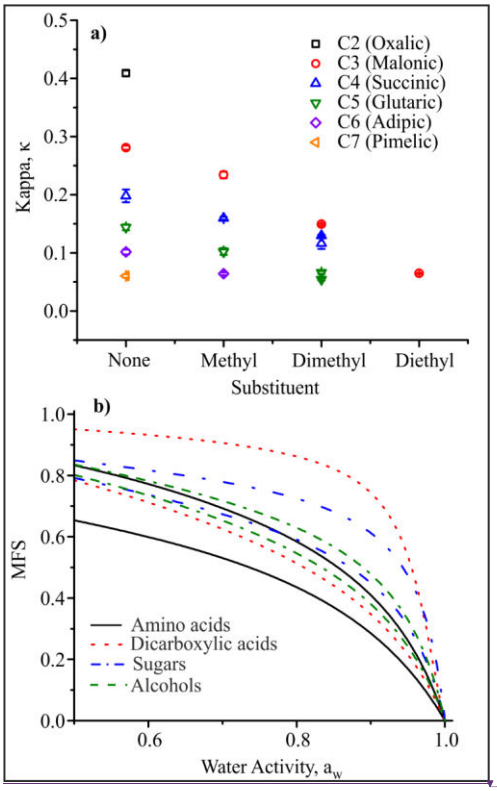

Deleted:

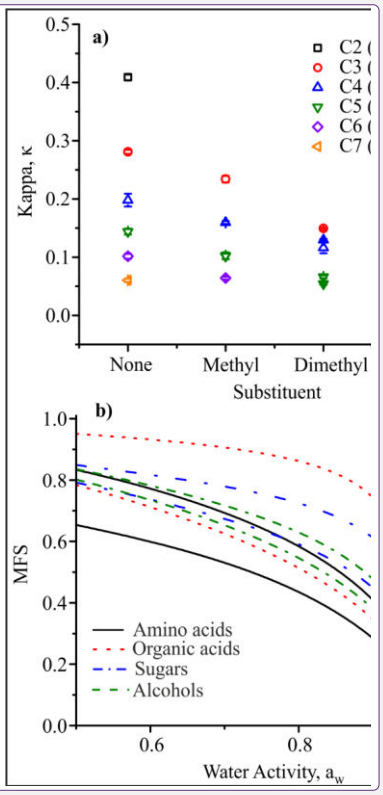

Figure 11. In a) κ values at a water activity of 0.95 are plotted as a function of increasing length of substituent and carbon backbone. In (b) generalised equilibrium hygroscopicity curves are presented as a function of compound class. Upper and lower hygroscopicity limits for each compound class have been fitted using the isotherm model discussed in Dutcher et al. (2013) (coefficients available in Table S0.1).

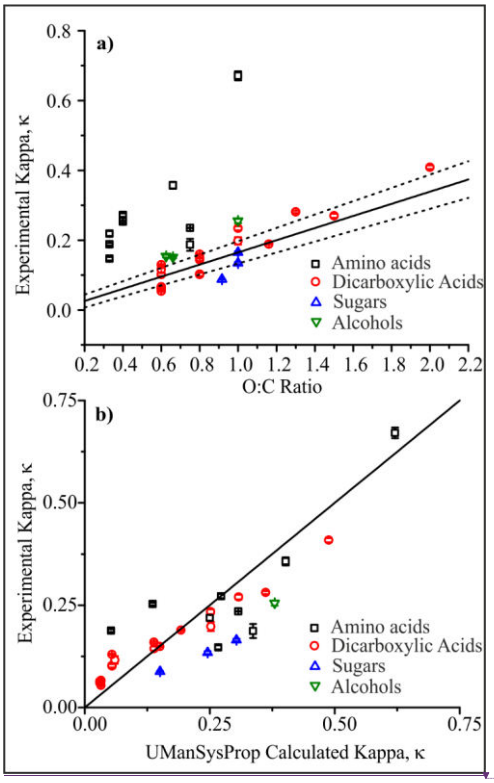

Deleted:

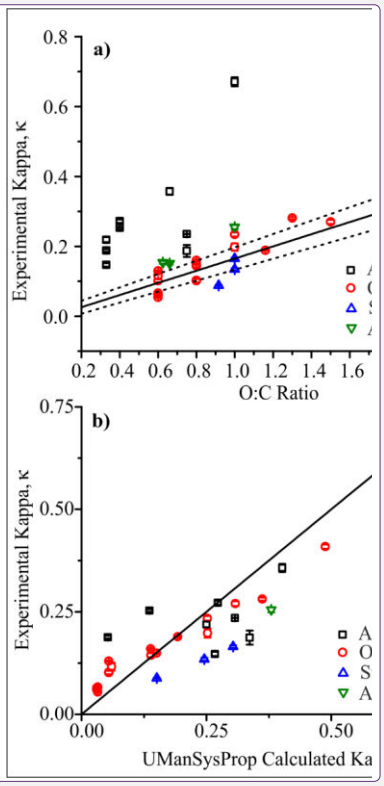

Figure 12. All values of κ for all compound classes presented as a plot of (a) κ vs O:C ratio and (b) as a correlation plot between calculated κ and experimental κ. Errors are indicated but are smaller than some points. In (a) the black solid line overlaid of the form κ = (0.174 ± 0.017)×O:C – (0.009 ± 0.015), the parametrisation of Rickards *et al.* (2013),with the black dashed lines showing the upper and lower limits of this parametrisation. In (b) the line represents y=x.

Influence of Organic Compound Functionality on Aerosol Hygroscopicity: Dicarboxylic Acids, Alkyl-Substituents, Sugars and Amino Acids

Aleksandra Marsh[1], Rachael E. H. Miles[1], Grazia Rovelli[1], Alexander G. Cowling[1], Lucy Nandy[2], Cari S. Dutcher[2] and Jonathan. P Reid[1]

[1] School of Chemistry, University of Bristol, Bristol, BS8 1TS, UK
[2] Department of Mechanical Engineering, University of Minnesota, 111 Church Street SE, Minneapolis, MN 55455, USA

Correspondence to: Jonathan. P. Reid j.p.reid@bristol.ac.uk

Table S0 Parameters required for thermodynamic model predictions (* available from a predefined list). And contents of supplement by page and S number.

Compound	Molar Mass / g.mol $^{-1}$	UNIFAC Structure	Page and S No
DL- Alanine	89.09	CH_3 COOH $CHNH_2$	P3 S1
L-Asparagine	132.12	COOH CH_2 $CONH_2$	P38 S36
L-Aspartic Acid	133.10	CH_2 $(COOH)_2$ $CHNH_2$	P37 S35
L-Arginine	174.2	-	P4 S2
Glycine	75.06	COOH $CHNH_2$	P5 S3
L-Histidine	155.15	-	P6 S4
L-Lysine	146.19	COOH $CHNH_2$ $(CH_2)_3$ CH_2NH_2	P7 S5
L-Proline	115.13	-	P8 S6
L-Threonine	119.12	OH CH_3 CH COOH $CHNH_2$	P9 S7
L-Valine	117.15	$(CH_3)_2$ CH COOH $CHNH_2$	P10 S8
Oxalic Acid*	90.03	$(COOH)_2$	P13 S11
Malonic Acid*	104.062	$(COOH)_2CH_2$	P14 S12
Succinic Acid*	118.09	$(COOH)_2$ $(CH_2)_2$	P15 S13
Methyl Malonic acid		$(CH_3)(CH)(COOH)_2$	P19 S17
Glutaric Acid*	132.116	$(COOH)_2$ $(CH_2)_3$	P16 S14
Methyl Succinic Acid*		$(CH_3)(CH_2)(CH)(COOH)_2$	P20 S18
Dimethyl Malonic Acid		$(CH_3)_2(C)(COOH)_2$	P36 S34
Adipic Acid*	146.14	$(COOH)_2$ $(CH_2)_4$	P17 S15
2-Methyl Glutaric Acid*		$(CH_3)(CH_2)_2(CH)(COOH)_2$	P24 S22
3-Methyl Glutaric Acid*		$(CH_3)(CH_2)_2(CH)(COOH)_2$	P26 S24
2,2-Dimethyl Succinic Acid*		$(CH_3)_2(CH_2)(C)(COOH)_2$	P23 S21
2,3-Dimethyl Succinic acid		$(CH_3)_2(CH)_2(COOH)_2$	P35 S33
Pimelic Acid	160.17	$(COOH)_2$ $(CH_2)_5$	P18 S16
2,2-Dimethyl Glutaric Acid		$(CH_3)_2(CH_2)_2(C)(COOH)_2$	P22 S20
3-Methyl Adipic Acid		$(CH3)_1(CH2)_3(CH)(COOH)_2$	P25 S23
3,3-Dimethyl Glutaric Acid		$(CH_3)_2(CH_2)_2(C)(COOH)_2$	P27 S25
Diethyl Malonic Acid		$(CH3)_2(CH2)_2(C)(COOH)_2$	P21 S19
Citric Acid*	192.12	$(COOH)_3$ $(CH_2)_2$ $C^{(OH)}$	P11 S9
Tartaric Acid	150.09	$(COOH)_2$ $(OH)_2$ $(CH)_2$ $^{(OH)}$	P12 S10
Sorbitol	182.17	$(CH_2^{[alc]})_2(CH_1^{(OH)})_4$ $(OH)_6$	P31 S29
D-(+)-Trehalose Dihydrate	378.33	(CH) $(CH_2^{[OH]})_8(CHO^{[ether]})_2$ $(OH)_8$	P32 S30

Deleted: 1*…H_3 1*…OOH 1*
Deleted: 1*…OOH 1*…H_2 1*
Deleted: 1*…H_2 2*…$COOH)_2$ 1*
Deleted: -
Deleted: 1*…OOH 1*…HNH_2 3*…CH_2 …3 1*
Deleted: 1*…H 1*…H_3 1*…H 1*…OOH 1*
Deleted: 2*…$CH_3)_2$ 1*…H 1*…OOH 1*
Deleted: 2*
Formatted
Deleted: 2*…$COOH)_2$ 1*CH_n
Deleted: 2*
Formatted
Deleted: 2*CH_n
Formatted
Formatted
Deleted: 2*
Formatted
Deleted: 3*CH_n
Formatted
Formatted
Formatted
Deleted: 2*…$COOH)_2$ 4*CHn
Formatted
Formatted
Formatted
Formatted
Formatted
Deleted: 2*
Formatted
Deleted: 5*CH_n
Deleted: ¶
Formatted
Formatted
Formatted
Formatted
Formatted
Deleted: 3*
Formatted
Deleted: 2*…$CH_2)_2$ 1*…H_n
Formatted
Deleted: 2*
Formatted
Deleted: 2*…$OH)_2$ 2*…$CH)_{2\,n}$
Formatted
Deleted: 6*…CH_n
Formatted
Deleted: 6*
Formatted
Deleted: 8*CH_n(OH) 8*OH 1*CH_n 3*CH_nO
Formatted

Galactose	180.16	$CHO(CH_1^{(OH)})_4CH_2^{(alc)}(OH)_5$	P33	S31
Xylose	150.13	$(CH_2(OH))_3CH_2^{(alc)}CHO(OH)_4$	P34	S32

PEG4	194.23	$(OH)_2(CH_2O)_3(CH_2)_3(CH_2^{(OH)})_2$	P29	S27
PEG3	150.17	$(OH)_2(CH_2)_2(CH_2O)_3(CH_2^{(OH)})_2$	P28	S26
Erythritol	122.12	$(CH^{(OH)})_2(CH_2^{(OH)})_2(OH)_4$	P30	S28

Table S0.1 Fitted parameters for upper and lower MFS vs water activity of compounds in each class, amino and organic acids, sugars and alcohols, as shown in Figure 11b) in the manuscript. The power law coefficient P is used to calculate energy parameter C for the first to $(n-1)$th layers, hence $C_i = (i/n)^P$, where i is the layer number and n is the total number of hydration layers, here $n = 8$ for all compounds except glycine ($n = 3$) and 2,2-dimethyl glutaric acid ($n = 16$). MSE is a normalized mean-square error, equal to $\left(\frac{1}{n_p}\right)\sum_{i=1}^{n_p}((m_{model,i} - m_{data,i})/(m_{model,i}))^2$, where n_p is the number of data points.

Solute	*P*	MSE
Amino acid Upper (Glycine)	-1.934	0.00321
Amino acid Lower (Asparagine)	-0.171	0.04151
Organic acid Upper (Malonic acid)	-0.212	0.00819
Organic acid Lower (2,2 dimethyl glutaric acid)	0.206	0.08315
Sugar Upper (Sorbitol)	-0.522	0.01025
Sugar Lower (Trehalose)	-0.870	0.01687
Alcohol Upper (Erythritol)	-0.238	0.01311
Alcohol Lower (PEG4)	-1.180	0.16205

Table S0.2 Fitted parameters for nine amino acids. The power law coefficient P is used to calculate energy parameter C for the first to $(n-1)$th layers, hence $C_i = (i/n)^P$, where i is the layer number and n is the total number of hydration layers, here $n = 8$ for all compounds except glycine ($n = 3$) and threonine ($n = 5$). MSE is a normalized mean-square error, equal to $\left(\frac{1}{n_p}\right)\sum_{i=1}^{n_p}((m_{model,i} - m_{data,i})/(m_{model,i}))^2$, where n_p is the number of data points. (Parameter for L-aspartic acid could not be determined due to data range available.)

Solute	*P*	MSE
Alanine	-0.356	0.00051
Asparagine	-0.171	0.04151
Arginine	-0.993	0.04039
Glycine	-1.934	0.00321
Histidine	-0.502	0.02211
Lysine	-1.225	0.00667
Proline	-0.619	0.03764
Threonine	-0.960	0.20107
Valine	-0.892	0.00397

S1 DL-Alanine Hygroscopicity

Deleted: 1*
Deleted: 4*
Deleted: 1*
Formatted: Superscript
Formatted: Superscript
Deleted: 5*
Formatted: Subscript
Deleted: 3*
Deleted: 1*
Formatted: Superscript
Deleted: 1*
Deleted: 4*
Formatted: Subscript
Deleted: 2*
Deleted: 3*
Deleted: 3*
Deleted: 2*
Formatted: Subscript
Formatted: Superscript
Formatted: Subscript
Deleted: 2*
Deleted: 2*
Deleted: 2*
Deleted: 2*
Formatted: Superscript
Formatted: Subscript
Deleted: 2*
Formatted: Superscript
Formatted: Subscript
Deleted: 2*
Deleted: 4*
Deleted:
Formatted: Superscript

Fig. S1.1: Hygroscopicity of DL-Alanine (Sigma Aldrich, Purity 99 %) at 293.15 K.

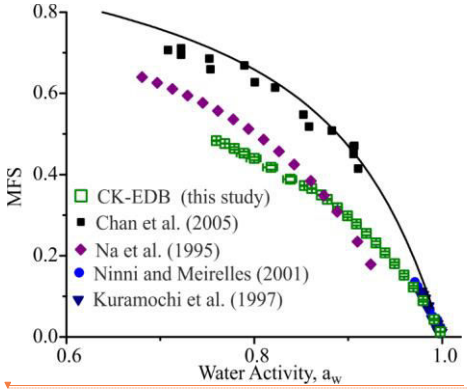

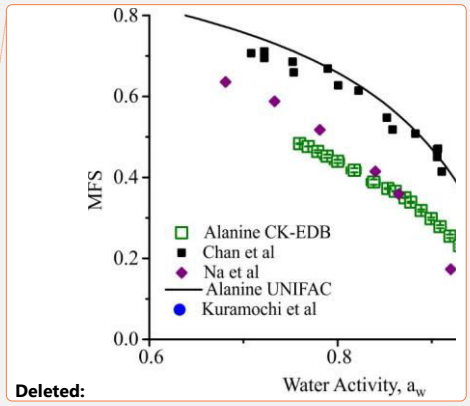

Deleted:

Table S1.1: Pure component refractive index (n_{melt}) is determined using molar refraction, assuming ideal mixing for calculation of the melt density (ρ_{melt}), from bulk data available in Cai et al. (2016). The variation of density as a function of the root of solute mass fraction ($MFS^{1/2}$ =x) is represented by polynomial fit parameters. *Upper* and *lower* refer to 95 % confidence limits for fits to experimental data, (Section 2.2 in manuscript).

			Polynomial fit ($\rho_{sol} = a + b_1x + b_2x^2 + b_3x^3$)			
	n_{melt}	ρ_{melt}/ g.cm^{-3}	a	b_1	b_2	b_3
Best	1.6205	1.4961	999	94.14	-66.93	466.48
Upper	1.6222	1.5042	999	97.38	-76.61	480.88
Lower	1.6188	1.4881	999	90.98	-57.61	452.44

Table S1.2: Tabulated experimental data points shown in **Fig S1.1.**

a_w	error a_w (+ve)	error a_w (-ve)	MFS	error MFS
0.75966	0.00182	0.00228	0.48336	8.66E-04
0.76866	1.02E-03	0.00128	0.47642	3.48E-04
0.77876	0.00413	0.00519	0.46428	0.00314
0.78887	0.00613	0.00771	0.45228	0.00412
0.80001	0.00674	0.00847	0.43959	0.00395
0.81774	0.00674	8.47E-03	0.41748	0.00512
0.83836	6.17E-03	7.75E-03	0.38848	6.39E-03
0.85334	0.00473	3.00E-03	0.37246	0.00116
0.86108	0.00116	7.54E-04	0.3655	8.92E-04
0.87144	6.02E-04	4.18E-04	0.34973	5.50E-04
0.87774	0.00139	9.81E-04	0.3386	0.00165
0.88866	0.00217	0.00153	0.31805	0.00274
0.89931	2.66E-03	1.92E-03	0.2981	0.00333
0.9087	0.00257	0.00183	0.27841	0.00381
0.91923	0.00256	0.00191	0.25483	0.00426
0.92957	0.00248	0.00181	0.23142	0.00416
0.93936	0.00243	0.00179	0.20672	0.00392
0.94936	0.00206	1.54E-03	0.18027	0.00361
0.9595	1.95E-03	1.43E-03	0.15211	0.00347
0.96935	1.49E-03	1.11E-03	0.12252	0.003
0.97954	0.00127	9.28E-04	0.08929	0.00254
0.99143	6.34E-04	7.22E-04	0.04259	0.00238

S2 L-Arginine Hygroscopicity

Fig S2.1: Hygroscopicity of L-Arginine, (Acros Organics, Purity > 98 %), at 293.15 K. Open squares, these experiments.

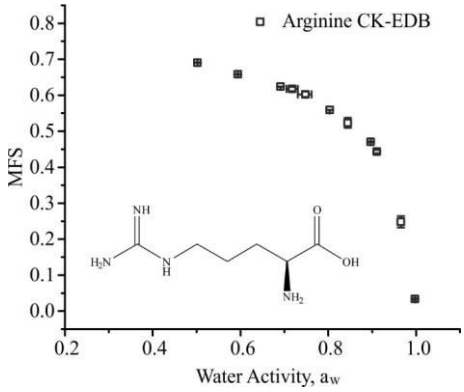

Table S2.1: Pure component refractive index (n_{melt}) is determined using molar refraction, assuming ideal mixing for calculation of the melt density (ρ_{melt}), from bulk data available in Cai et al. (2016). The variation of density as a function of the root of solute mass fraction (MFS $^{1/2}$ =x) is represented by polynomial fit parameters. *Upper* and *lower* refer to 95 % confidence limits for fits to experimental data, (Section 2.2 in manuscript).

			Polynomial fit ($\rho_{sol} = a + b_1x + b_2x^2 + b_3x^3$)			
	n_{melt}	ρ_{melt}/ g.cm^{-3}	a	b_1	b_2	b_3
Best	1.637	1.3995	998.6	59.85	28.54	310.48
Upper	1.6382	1.4045	998.6	61.44	24.47	317.9
Lower	1.6358	1.3945	998.6	58.28	32.51	303.13

Table S2.2: Tabulated experimental data points shown in **Fig S2.1.**

a_w	error a_w (+ve)	error a_w (-ve)	MFS	error MFS
0.50205	0.00177	0.0021	0.69041	0.00113
0.59399	0.00171	0.00206	0.65822	0.00115
0.69132	0.00127	0.00157	0.62391	1.74E-04
0.71788	0.01297	0.01296	0.61768	0.00607
0.74796	0.0139	0.01716	0.6026	0.00755
0.80315	7.87E-04	0.001	0.55889	4.50E-04
0.84439	0.00739	0.00741	0.52351	0.014
0.89694	0.00128	0.00112	0.47038	0.00138
0.91074	0.00174	0.00175	0.44361	0.00473
0.96538	0.00317	0.00317	0.24814	0.01569
0.99761	5.53E-04	5.28E-04	0.03416	0.00266

S3 Glycine Hygroscopicity

Fig S3.1: Hygroscopicity of Glycine, (Santa Cruz Biotech LTD), at 293.15 K. Solid line standard UNIFAC prediction.

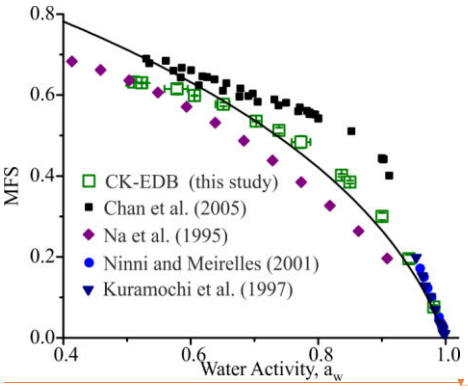

Table S3.1: Pure component refractive index (n_{melt}) is determined using molar refraction, assuming ideal mixing for calculation of the melt density (ρ_{melt}), from bulk data available in Cai et al. (2016). The variation of density as a function of the root of solute mass fraction (MFS $^{1/2}$ =x) is represented by polynomial fit parameters. *Upper* and *lower* refer to 95 % confidence limits for fits to experimental data, (Section 2.2 in manuscript).

			Polynomial fit ($\rho_{sol} = a + b_1x + b_2x^2 + b_3x^3$)			
	n_{melt}	ρ_{melt}/ $g.cm^{-3}$	a	b_1	b_2	b_3
Best	1.6634	1.6905	999.47	186.75	-363.66	860.4
Upper	1.6654	1.7006	999.47	192.41	-382.69	883.61
Lower	1.6613	1.6805	999.47	181.22	-345.14	837.67

Table S3.2: Tabulated experimental data points shown in **Fig S3.1.**

a_w	error a_w (+ve)	error a_w (-ve)	MFS	error MFS
0.51061	0.00328	0.00389	0.63189	0.00159
0.52315	0.0204	0.02421	0.62993	0.00129
0.57855	0.01673	0.01985	0.61512	0.01113
0.60598	0.00228	0.00276	0.59862	6.15E-04
0.65105	0.00995	0.01205	0.57691	0.00441
0.70256	0.00157	0.00195	0.53551	0.00146
0.73844	0.0068	0.00678	0.51233	0.00686
0.77309	0.01453	0.01453	0.48382	0.01515
0.83663	0.0021	0.00115	0.4015	0.00347
0.84998	0.00206	0.00204	0.38496	0.00336
0.90029	0.00391	0.00391	0.29984	0.00906
0.94266	0.00341	0.00339	0.19519	0.00966
0.98152	0.00147	0.00147	0.07624	0.00455

Deleted:

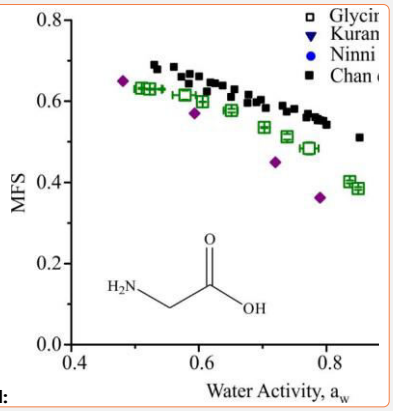

Deleted: ¶
¶

S4 Histidine Hygroscopicity

Fig S4.1: Hygroscopicity of L-Histidine, (VWR Chemicals), open symbols, these CC-EDB experiments.

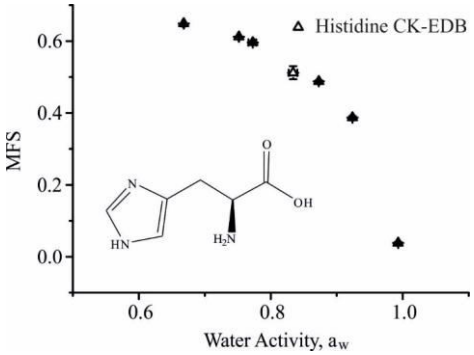

Table S4.1: Pure component refractive index (n_{melt}) is determined using molar refraction, assuming ideal mixing for calculation of the melt density (ρ_{melt}), from bulk data available in Cai et al. (2016). The variation of density as a function of the root of solute mass fraction (MFS $^{1/2}$ =x) is represented by polynomial fit parameters. *Upper* and *lower* refer to 95 % confidence limits for fits to experimental data, (Section 2.2 in manuscript).

			Polynomial fit ($\rho_{sol} = a + b_1x + b_2x^2 + b_3x^3$)			
	n_{melt}	ρ_{melt}/ $g.cm^{-3}$	a	b_1	b_2	b_3
Best	1.6892	1.5378	998.9	111.5	-119.61	542.86
Upper	1.6914	1.5462	998.9	115.17	-130.97	558.8
Lower	1.6871	1.5296	998.9	107.98	-108.77	527.49

Table S4.2: Tabulated experimental data points shown in **Fig S4.1.**

a_w	error a_w (+ve)	error a_w (-ve)	MFS	error MFS
		293.15 K		
0.66801	0.00175	0.00214	0.64888	5.85836E-4
0.75174	0.00105	0.00131	0.61182	3.82887E-4
0.77265	0.00527	0.00661	0.59614	0.00177
0.83375	0.0064	0.00643	0.51198	0.01825
0.87281	0.00111	0.00101	0.48826	0.0027
0.9239	8.9548E-4	9.46372E-4	0.38721	0.00439
0.99296	6.37951E-4	6.3374E-4	0.03829	0.00295

S5 L-Lysine Hygroscopicity

Fig S5.1: Hygroscopicity of L-Lysine, (Sigma Aldrich, Purity ≥ 98 %), at 293.15 K. Open squares, these experiments; solid line, UNIFAC model.

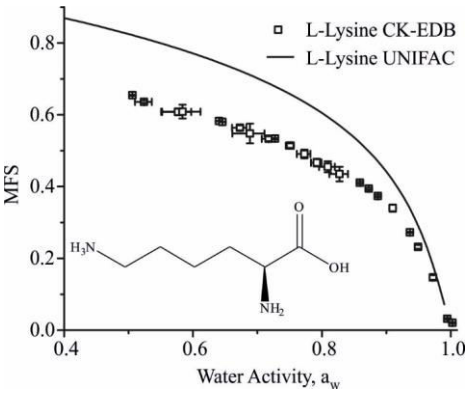

Table S5.1: Pure component refractive index (n_{melt}) determined using molar refraction where the melt density (ρ_{melt}), is determined using a polynomial fit of density to the square root of MFS ($MFS^{1/2}$ =x). Bulk values used are available in Cai et al. (2016). *Upper* and *lower* refer to 95 % confidence limits for fits to experimental data.

			Polynomial fit ($\rho_{sol} = a + b_1x + b_2x^2 + b_3x^3$)			
	n_{melt}	ρ_{melt}/ $g.cm^{-3}$	a	b_1	b_2	b_3
Best	1.5586	1.2362	998.2	-15.22	309.14	-56.02
Upper	1.5614	1.2418	998.2	-4.29	271.92	-23.99
Lower	1.5558	1.2306	998.2	-25.93	346.35	-88.05

Table S5.2: Tabulated experimental data points shown in **Fig S5.1.**

a_w	error a_w (+ve)	error a_w (-ve)	MFS	error MFS
0.50605	0.00267	0.00316	0.65479	0.00157
0.52404	0.01187	0.01406	0.63621	0.00337
0.57666	0.02059	0.02439	0.60815	0.00948
0.58372	0.02793	0.03308	0.60867	0.01931
0.64049	0.00405	0.00494	0.58275	4.04084E-4
0.64559	0.00205	0.00251	0.57997	4.926E-4
0.67292	0.00999	0.0122	0.56365	0.00675
0.68839	0.0225	0.02735	0.54807	0.02742
0.71755	0.00885	0.01092	0.53328	0.00647
0.72732	0.00179	0.00223	0.53359	0.00179
0.75098	0.0056	0.00696	0.51408	0.00626
0.77291	0.00939	0.01164	0.49095	0.01194
0.79224	0.00736	0.00909	0.46681	0.01099
0.80926	0.01092	0.01352	0.45505	0.01535
0.82751	0.01292	0.01604	0.43489	0.02026
0.85916	0.00152	0.00197	0.41093	0.00309
0.87288	0.00143	0.00143	0.39407	0.00288
0.88688	0.00151	0.00151	0.3739	0.00294
0.90999	0.00294	0.00337	0.33998	0.00983
0.93683	3.20551E-4	3.24824E-4	0.27222	0.00154
0.94931	0.00162	0.00162	0.23179	0.00544
0.97255	0.00147	0.00147	0.14683	0.00623
0.99465	4.49456E-4	4.50168E-4	0.03174	0.0021
1.00277	0.00113	0.00149	0.02039	0.00198

S6 L-Proline Hygroscopicity

Figure S6.1: Hygroscopicity of L-Proline, (Acros Organics, Purity + 99 %), at 293.15 K. Open squares, these experiments.

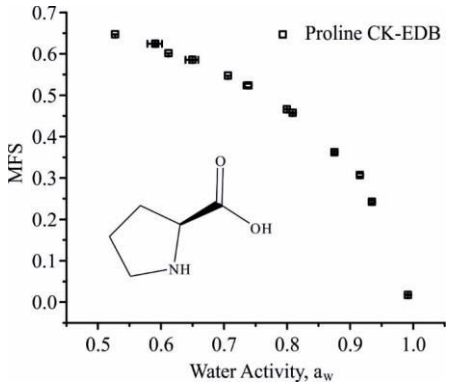

Table S6.1: Pure component refractive index (n_{melt}) is determined using molar refraction, assuming ideal mixing for calculation of the melt density (ρ_{melt}), from bulk data available in Cai et al. (2016). The variation of density as a function of the root of solute mass fraction (MFS $^{1/2}$ =x) is represented by polynomial fit parameters. *Upper* and *lower* refer to 95 % confidence limits for fits to experimental data, (Section 2.2 in manuscript).

			Polynomial fit ($\rho_{sol} = a + b_1x + b_2x^2 + b_3x^3$)			
	n_{melt}	ρ_{melt}/ $g.cm^{-3}$	a	b_1	b_2	b_3
Best	1.5948	1.3866	999	55.7	39.01	291
Upper	1.5964	1.3945	999	58.13	32.96	302.44
Lower	1.5932	1.3788	999	53.36	44.73	279.93

Table S6.2: Tabulated experimental data points shown in **Fig S6.1.**

a_w	error a_w (+ve)	error a_w (-ve)	MFS	error MFS
0.52739	0.00183	0.00218	0.647	1.53E-04
0.59111	0.01061	0.01264	0.62414	0.00218
0.61213	0.00154	0.00186	0.6013	1.44E-04
0.64995	0.00905	0.01098	0.58549	0.00122
0.70619	9.52E-04	0.00118	0.54716	3.08E-04
0.73823	0.0057	0.00705	0.52349	0.00436
0.79982	7.99E-04	0.00101	0.46617	7.45E-04
0.80883	0.00112	0.00112	0.45742	1.45E-03
0.87515	1.30E-03	0.00103	0.36217	2.56E-03
0.91551	0.00145	0.00184	0.30701	0.00352
0.93455	9.07E-04	9.29E-04	0.24258	0.00279
0.99172	5.01E-04	5.60E-04	0.01734	0.0011

S7 L-Threonine Hygroscopicity

Fig S7.1: Hygroscopicity of L-Threonine, (Acros Organics, Purity 98 %), at 293.15 K. Open squares, these experiments; solid line, UNIFAC model.

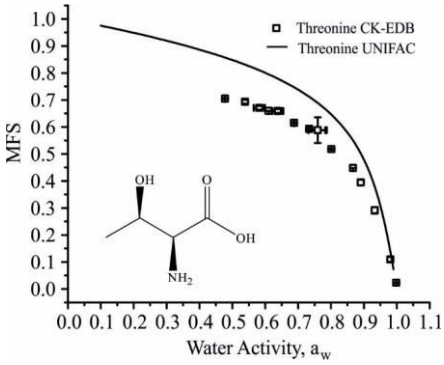

Table S7.1: Pure component refractive index (n_{melt}) is determined using molar refraction, assuming ideal mixing for calculation of the melt density (ρ_{melt}), from bulk data available in Cai et al. (2016). The variation of density as a function of the root of solute mass fraction ($MFS^{1/2}$ =x) is represented by polynomial fit parameters. *Upper* and *lower* refer to 95 % confidence limits for fits to experimental data, (Section 2.2 in manuscript).

			Polynomial fit ($\rho_{sol} = a + b_1x + b_2x^2 + b_3x^3$)			
	n_{melt}	ρ_{melt}/ $g.cm^{-3}$	a	b_1	b_2	b_3
Best	1.6185	1.4977	999.4	94.57	-68.14	468.44
Upper	1.6274	1.5403	999.4	112.31	-121.99	546.4
Lower	1.6102	1.4575	999.4	79.24	-23.63	399.69

Table S7.2: Tabulated experimental data points shown in **Fig S7.1.**

a_w	error a_w (+ve)	error a_w (-ve)	MFS	error MFS
0.47807	0.00212	0.0025	0.70511	0.00173
0.53888	0.0052	0.0062	0.69319	0.00723
0.58237	0.01442	0.01711	0.67043	0.00714
0.60978	0.00127	0.00154	0.65941	3.88E-04
0.63867	0.01393	0.01689	0.65875	0.00707
0.68779	0.00158	0.00195	0.61529	0.00161
0.73352	0.0081	0.00812	0.59255	0.0041
0.75945	0.02291	0.02781	0.58815	0.04754
0.80118	0.00157	7.31E-04	0.51778	0.00135
0.86674	7.26E-04	4.84E-04	0.44784	3.66E-04
0.89045	0.00426	0.00419	0.39429	0.0104
0.93289	0.00438	0.00418	0.29104	0.01212
0.98064	0.00213	0.00214	0.10966	0.00862
0.99865	7.16E-04	4.45E-04	0.02317	0.00125

S8 L-Valine Hygroscopicity

Figure S8.1: Hygroscopicity of L-Valine, (Sigma Aldrich, Purity ≥ 98 %), at 293.15 K (blue Open symbols, these CK-EDB experiments; black filled circles, literature data (Kuramochi *et al.*); solid black line, UNIFAC model (293.15 K).

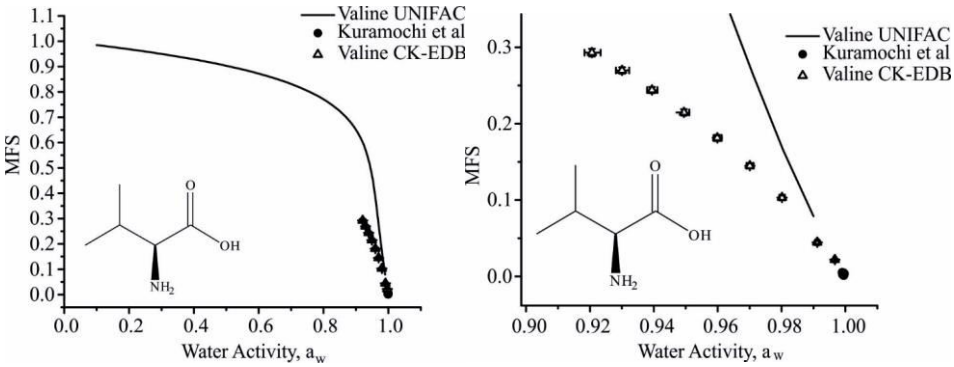

Table S8.1: Pure component refractive index (n_{melt}) is determined using molar refraction, assuming ideal mixing for calculation of the melt density (ρ_{melt}), from bulk data available in Cai et al. (2016). The variation of density as a function of the root of solute mass fraction ($MFS^{1/2}$ =x) is represented by polynomial fit parameters. *Upper* and *lower* refer to 95 % confidence limits for fits to experimental data, (Section 2.2 in manuscript).

			Polynomial fit ($\rho_{sol} = a + b_1x + b_2x^2 + b_3x^3$)			
	n_{melt}	ρ_{melt}/ $g.cm^{-3}$	a	b_1	b_2	b_3
Best	1.5791	1.2824	998.77	28.73	94.37	159.64
Upper	1.58	1.2872	998.77	29.8	92.82	164.91
Lower	1.5781	1.2776	998.77	27.71	95.81	154.45

Table S8.2: Tabulated experimental data points shown in **Fig S8.1.**

a_w	error a_w (+ve)	error a_w (-ve)	MFS	error MFS
		293.15 K		
0.92062	0.0027	0.00232	0.29295	0.00499
0.93004	2.26E-03	0.00195	0.26962	4.18E-03
0.93941	0.00173	0.00148	0.24396	0.00404
0.94943	0.00169	0.00145	0.21478	0.00403
0.9599	0.00138	0.00118	0.18125	0.00388
0.97008	0.00118	0.00101	0.14482	0.00345
0.98014	8.66E-04	7.41E-04	0.10314	2.94E-03
0.99117	5.34E-04	5.69E-04	0.04451	0.00201
0.99669	4.13E-04	4.57E-04	0.02205	8.65E-04

S9 Citric Acid Hygroscopicity

Figure S9.1: Hygroscopicity of Citric Acid, (Sigma Aldrich, Purity 99 %), at 293.15 K. Open squares, these EDB experiments; solid line, UNIFAC model.

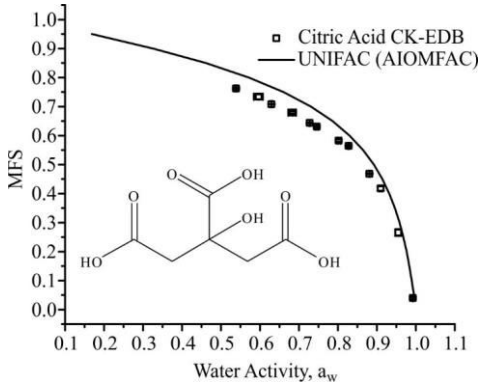

Table S9.1: Pure component refractive index (n_{melt}) determined using molar refraction where the melt density (ρ_{melt}) is determined using a polynomial fit of density to the square root of MFS ($MFS^{½} = x$). Bulk values used are available in Cai et al. (2016). *Upper* and *lower* refer to 95 % confidence limits for fits to experimental data.

			Polynomial fit ($\rho_{sol} = a + b_1x + b_2x^2 + b_3x^3$)			
	n_{melt}	ρ_{melt}/ $g.cm^{-3}$	a	b_1	b_2	b_3
Best	1.5054	1.550	998.0	25.0	253.84	273.2
Upper	1.5071	1.5565	998.0	37.88	211.13	309.49
Lower	1.5037	1.5436	998.0	12.11	296.56	236.92

Table S9.2: Tabulated experimental data points shown in **Fig S9.1.**

a_w	error a_w (+ve)	error a_w (-ve)	MFS	error MFS
0.53894	0.0024	0.00286	0.76226	0.00233
0.59688	0.01043	0.01244	0.73375	0.00875
0.62961	0.00223	0.00271	0.70793	7.62E-04
0.6837	0.00876	0.01065	0.67914	0.00409
0.72762	0.00123	0.00153	0.64368	0.00135
0.74592	0.00403	0.00404	0.63069	0.00342
0.80229	0.00504	0.0029	0.58246	0.00401
0.82734	0.00237	0.00196	0.56406	0.00314
0.88104	0.00107	0.0012	0.4682	0.00149
0.90968	0.00331	0.00327	0.41761	0.00738
0.95487	0.0028	0.00279	0.26562	0.01165
0.99255	6.21E-04	6.70E-04	0.03973	0.00355

S10 L-Tartaric Acid Hygroscopicity

Figure S10.1: Hygroscopicity of Tartaric Acid, (Sigma Aldrich, Purity ≥ 99.5 %), at 293.15 K. Open squares, these EDB experiments; solid line, UNIFAC model.

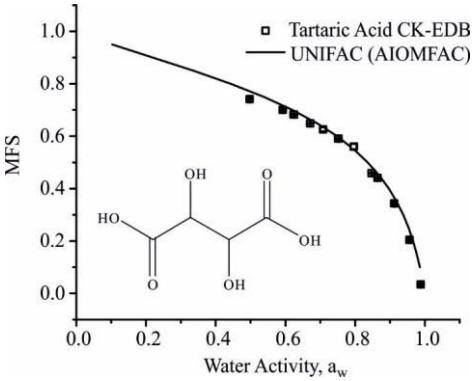

Table S10.1: Pure component refractive index (n_{melt}) determined using molar refraction where the melt density (ρ_{melt}) is determined using a polynomial fit of density to the square root of MFS ($MFS^{½} = x$). Bulk values used are available in Cai et al. (2016). *Upper* and *lower* refer to 95 % confidence limits for fits to experimental data.

			Polynomial fit ($\rho_{sol} = a + b_1x + b_2x^2 + b_3x^3$)			
	n_{melt}	ρ_{melt}/ g.cm^{-3}	a	b_1	b_2	b_3
Best	1.4992	1.6007	999	15.08	325.84	260.78
Upper	1.4996	1.6128	999	29.23	273.11	311.49
Lower	1.4936	1.5886	999	93.2	378.58	210.06

Table S10.2: Tabulated experimental data points shown in **Fig S10.1.**

a_w	error a_w (+ve)	error a_w (-ve)	MFS	error MFS
0.49764	0.00285	0.00337	0.74075	0.00145
0.59229	0.00275	0.00332	0.70005	0.00184
0.62457	0.00897	0.01082	0.68273	0.00361
0.67107	0.00165	0.00203	0.64893	7.95E-04
0.70799	0.00711	0.00826	0.6255	0.0076
0.75229	0.00853	0.01048	0.59046	0.00337
0.79666	0.00778	0.00946	0.56049	0.00992
0.84739	9.37E-04	5.51E-04	0.45906	0.00122
0.86463	0.00206	0.00206	0.44068	0.00269
0.91248	0.00302	0.00302	0.34362	0.00774
0.95599	0.00217	0.00216	0.20415	0.00789
0.98847	0.00104	0.00105	0.03363	0.00337

S11 Oxalic Acid Hygroscopicity

Deleted: ¶
¶
¶
¶
¶

Fig S11.1: Hygroscopicity of Oxalic Acid, (Sigma Aldrich, Purity 98 %), at 293.15 K. Open squares, these experiments; solid line, UNIFAC model.

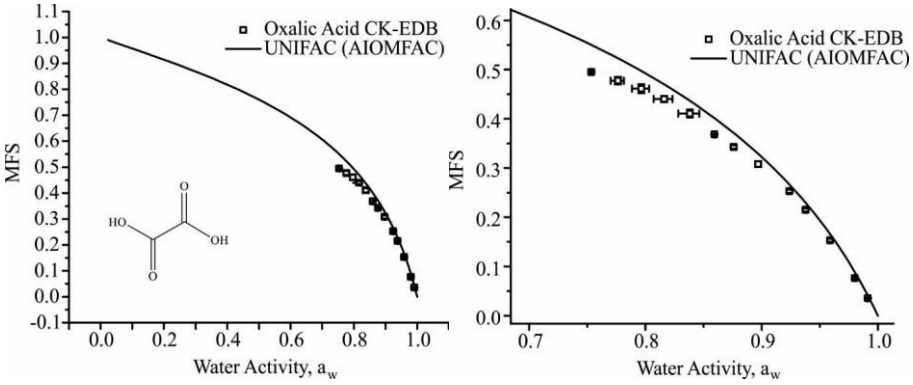

Table S11.1: Pure component refractive index (n_{melt}) is determined using molar refraction, assuming ideal mixing for calculation of the melt density (ρ_{melt}), from bulk data available in Cai et al. (2016). The variation of density as a function of the root of solute mass fraction ($MFS^{1/2}$ =x) is represented by polynomial fit parameters. *Upper* and *lower* refer to 95 % confidence limits for fits to experimental data, (Section 2.2 in manuscript).

			Polynomial fit ($\rho_{sol} = a + b_1x + b_2x^2 + b_3x^3 + b_4x^4 + b_5x^5 + b_6x^6$)						
	n_{melt}	ρ_{melt}/ $g.cm^{-3}$	a	b_1	b_2	b_3	b_4	b_5	b_6
Best	1.5167	1.7237	998.4	-14.98	636.47	-1074.2	2603.92	-2596.5	1170.54
Upper	1.5185	1.7403	998.4	-16.27	660.48	-1165.1	2811.06	-2809	1260.66
Lower	1.5149	1.7073	998.4	-13.78	613.65	-989.39	2409.96	-2397.5	1085.84

Table S11.2: Tabulated experimental data points shown in **Fig S11.1.**

a_w	error a_w (+ve)	error a_w (-ve)	MFS	error MFS
0.75352	0.00146	0.00183	0.49497	0.00148
0.77652	0.00502	0.00629	0.47731	0.0077
0.79664	0.00652	0.00817	0.46116	0.00912
0.81614	0.00716	0.00896	0.44009	0.00613
0.83841	0.00803	0.01005	0.41068	0.00808
0.85938	0.0012	7.60E-04	0.36829	0.00113
0.87602	0.00199	0.00188	0.34275	0.00355
0.89702	0.00235	0.00215	0.30804	0.00596
0.92388	8.50E-04	0.00115	0.25275	0.00331
0.93784	0.00106	0.00106	0.21515	0.00299
0.9589	8.73E-04	8.75E-04	0.15314	0.00313
0.98012	5.72E-04	5.68E-04	0.07645	0.00227
0.99129	2.93E-04	3.54E-04	0.03567	8.98E-04

S12 Malonic Acid Hygroscopicity

Figure S12.1: Hygroscopicity of Malonic Acid, (Sigma Aldrich, Purity 98 %), at 293.15 K. Open squares, these experiments; solid line, UNIFAC model.

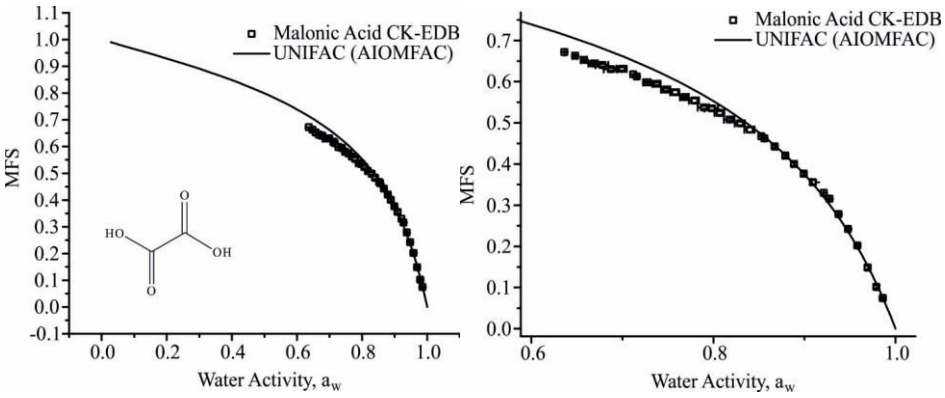

Table S12.1: Pure component refractive index determined using molar refraction where the melt density is determined using a polynomial fit of density to the square root of MFS ($MFS^{1/2}$ =x). Bulk values used are available in Cai et al. (2016). *Upper* and *lower* refer to 95 % confidence limits for fits to experimental data.

			Polynomial fit ($\rho_{sol} = a + b_1x + b_2x^2 + b_3x^3$)			
	n_{melt}	ρ_{melt}/ $g.cm^{-3}$	a	b_1	b_2	b_3
Best	1.4611	1.4558	997.2	13.47	262.36	182.76
Upper	1.4627	1.4612	997.2	20.7	235.91	207.37
Lower	1.4594	1.4504	997.2	6.24	288.82	158.15

Table S12.2: Tabulated experimental data points shown in **Fig S12.1.**

a_w	error a_w (+ve)	error a_w (-ve)	MFS	error MFS
0.63613	4.14E-04	5.04E-04	0.6718	1.62E-04
0.64803	0.00253	0.00308	0.66275	0.00161
0.65776	0.00301	0.00367	0.65273	0.00197
0.66822	0.00457	0.00558	0.64421	0.00162
0.67795	0.00624	0.00761	0.64043	0.00324
0.68747	0.00679	0.00828	0.62992	0.00337
0.6994	0.0051	0.00625	0.63085	0.00413
0.7117	4.61E-04	5.72E-04	0.6176	2.85E-04
0.71572	0.00132	0.00164	0.61275	0.00135
0.72728	0.00371	0.00458	0.59849	0.00119
0.73786	0.00398	0.0049	0.59485	0.00362
0.74792	0.00441	0.00544	0.58075	0.00309
0.75777	0.00438	0.00539	0.57442	0.00518
0.76852	0.00437	0.00539	0.56217	0.00227
0.77901	0.00483	0.00595	0.55399	0.00568
0.78948	0.00564	0.00694	0.53743	0.0039
0.79831	0.00665	0.00816	0.53501	0.00406
0.80703	0.00469	0.00576	0.52388	0.00468
0.81779	0.00517	0.00637	0.50809	0.00307
0.82931	0.00495	0.0061	0.49855	0.00449
0.83997	0.00501	0.00616	0.48341	0.0058
0.85259	0.0013	8.20E-04	0.46721	9.32E-04
0.85596	0.00112	6.98E-04	0.46233	0.00114
0.86726	0.00223	0.00146	0.44257	0.00286
0.87898	0.00278	0.00183	0.4203	0.0033
0.8885	0.00291	0.00204	0.4002	0.0044
0.89906	0.00294	0.00205	0.37643	0.00371

0.90919	0.00337	0.00233	0.35563	0.00559
0.9213	1.65E-04	2.03E-04	0.32987	3.33E-04
0.92743	2.61E-04	2.85E-04	0.31545	0.00122
0.93737	3.90E-04	4.01E-04	0.27835	0.00185
0.94793	4.69E-04	4.71E-04	0.24233	0.00205
0.95802	4.67E-04	4.69E-04	0.20227	0.00223
0.96932	0.0018	0.0011	0.14857	0.00427
0.97897	0.00144	8.79E-04	0.10171	0.00358
0.98599	0.00158	9.62E-04	0.07431	0.00205

S13 Succinic Acid Hygroscopicity

Fig S13.1: Hygroscopicity of Succinic Acid, (Sigma Aldrich, Purity 99 %), at 293.15 K. Open squares, these experiments; solid line, UNIFAC model.

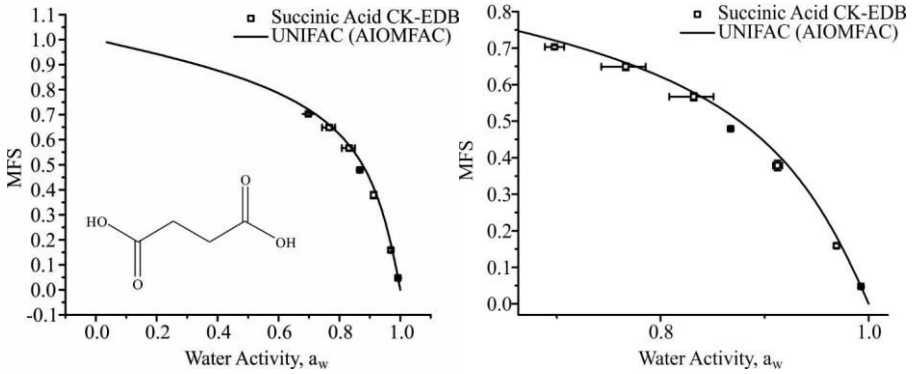

Table S13.1: Pure component refractive index (n_{melt}) is determined using molar refraction, assuming ideal mixing for calculation of the melt density (ρ_{melt}), from bulk data available in Cai et al. (2016). The variation of density as a function of the root of solute mass fraction ($MFS^{1/2}$ =x) is represented by polynomial fit parameters. *Upper* and *lower* refer to 95 % confidence limits for fits to experimental data, (Section 2.2 in manuscript).

			Polynomial fit ($\rho_{sol} = a + b_1x + b_2x^2 + b_3x^3 + b_4x^4 + b_5x^5 + b_6x^6$)						
	n_{melt}	ρ_{melt}/ g.cm^{-3}	a	b_1	b_2	b_3	b_4	b_5	b_6
Best	1.4928	1.4185	998.2	-1.96	324.69	-146.48	426.3	-373.62	191.37
Upper	1.4935	1.4249	998.2	-2.08	329.57	-155.12	447.91	-395.04	201.45
Lower	1.4920	1.4122	998.2	-1.85	319.93	-138.32	405.79	-353.36	181.79

Table S13.2: Tabulated experimental data points shown in **Fig S13.1.**

a_w	error a_w (+ve)	error a_w (-ve)	MFS	error MFS
0.69803	0.00919	0.00918	0.70299	0.00502
0.76653	0.0191	0.02355	0.64896	0.00963
0.83176	0.0191	0.02355	0.56672	0.01018
0.86728	0.00142	0.00142	0.47926	0.0025
0.91247	0.00444	0.0044	0.37868	0.01328
0.96915	0.00137	0.00136	0.15909	0.00637
0.99255	3.09E-04	3.16E-04	0.04733	0.00178

S14 Glutaric Acid Hygroscopicity

Figure S14.1: Hygroscopicity of Glutaric Acid, (Sigma Aldrich, Purity 99 %), at 293.15 K. Open squares, these experiments; solid line, UNIFAC model.

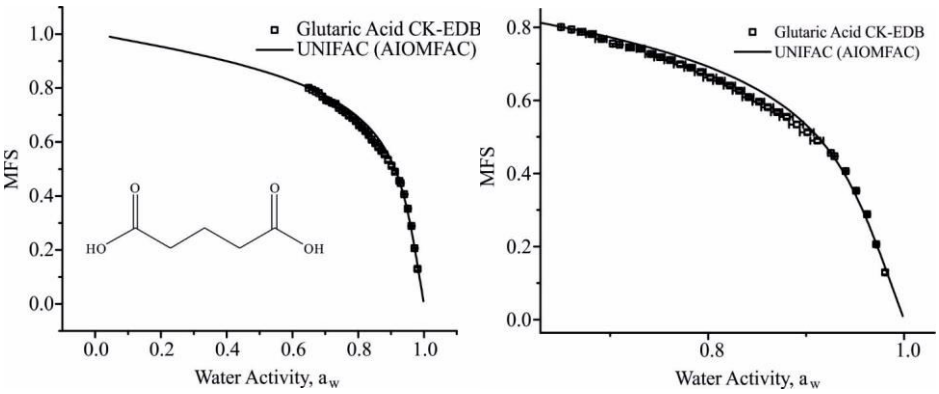

Table S14.1: Pure component refractive index (n_{melt}) determined using molar refraction where the melt density (ρ_{melt}) is determined using a polynomial fit of density to the square root of MFS ($MFS^{1/2}$ =x). Bulk values used are available in Cai et al. (2016). *Upper* and *lower* refer to 95 % confidence limits for fits to experimental data.

			Polynomial fit ($\rho_{sol} = a + b_1x + b_2x^2 + b_3x^3$)			
	n_{melt}	ρ_{melt}/ $g.cm^{-3}$	a	b_1	b_2	b_3
Best	1.4655	1.2745	997.5	-1.56	238.79	39.75
Upper	1.4660	1.2760	997.5	0.401	231.59	46.55
Lower	1.4649	1.2729	997.5	-3.53	245.98	32.95

Table S14.2: Tabulated experimental data points shown in **Fig S14.1.**

a_w	error a_w (+ve)	error a_w (-ve)	MFS	error MFS
0.64988	4.93E-04	6.03E-04	0.80052	2.01E-04
0.66053	5.88E-04	7.21E-04	0.79339	2.71E-04
0.67122	0.00348	0.00426	0.78724	9.92E-04
0.68089	0.00458	0.00561	0.78134	0.00256
0.69112	0.00522	0.00639	0.76761	0.00226
0.70268	4.02E-04	4.98E-04	0.75519	1.75E-04
0.70969	0.0019	0.00235	0.75207	8.79E-04
0.72069	0.00357	0.00441	0.74499	0.00276
0.73156	0.0038	0.00469	0.74131	0.003
0.74152	0.00467	0.00575	0.72636	0.00217
0.75089	0.00485	0.00598	0.71793	0.00185
0.76119	0.00482	0.00594	0.70997	0.00323
0.77157	0.00535	0.00659	0.69846	0.00478
0.7818	0.00495	0.0061	0.68945	0.00241
0.79242	0.00502	0.00618	0.6775	0.00399
0.80236	5.99E-03	7.39E-03	0.6624	0.00435
0.81173	5.37E-03	6.62E-03	0.65327	0.00271
0.82228	0.00521	0.00642	0.64016	0.00336
0.83171	0.00538	0.00662	0.62617	0.00336
0.84134	0.00521	0.00642	0.60886	0.0028
0.852	0.00538	0.00663	0.59616	0.00364
0.86106	0.00556	0.00684	0.58136	0.00487
0.87055	0.00521	0.00642	0.56748	0.00361
0.88031	0.00617	0.00761	0.5545	0.00465
0.89058	0.00635	0.00785	0.5337	0.00679
0.90142	0.00628	0.00777	0.51244	0.00601
0.91173	0.00596	0.00737	0.48949	0.00523

0.92543	1.50E-04	2.02E-04	0.45608	4.73E-04
0.92905	1.56E-04	1.58E-04	0.44732	6.46E-04
0.94053	3.86E-04	3.86E-04	0.40605	0.00233
0.95111	4.52E-04	4.52E-04	0.35279	0.00256
0.96227	3.42E-04	3.41E-04	0.28818	0.00275
0.97153	3.20E-04	3.20E-04	0.20634	0.00243
0.98066	8.31E-04	8.09E-04	0.12936	0.00558

S15 Adipic Acid Hygroscopicity

Figure S15.1: Hygroscopicity of Adipic Acid, (Sigma Aldrich, Purity 99 %), at 293.15 K. Open squares, these experiments; solid line, UNIFAC model.

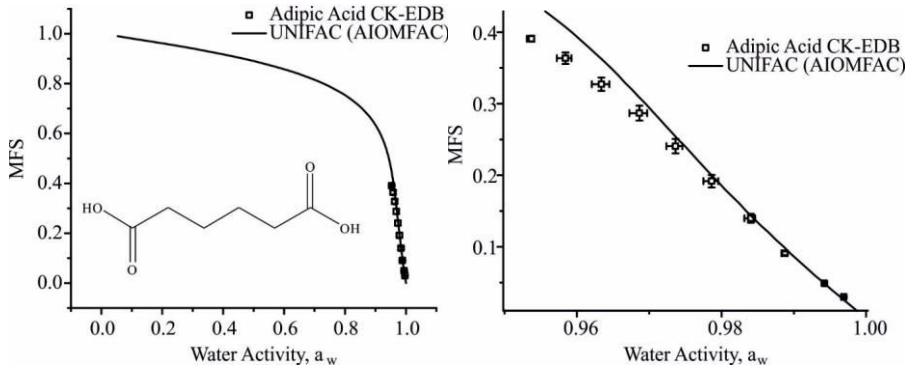

Table S15.1: Pure component refractive index (n_{melt}) is determined using molar refraction, assuming ideal mixing for calculation of the melt density (ρ_{melt}), from bulk data available in Cai et al. (2016). The variation of density as a function of the root of solute mass fraction ($MFS^{1/2}$ =x) is represented by polynomial fit parameters. *Upper* and *lower* refer to 95 % confidence limits for fits to experimental data, (Section 2.2 in manuscript).

			Polynomial fit ($\rho_{sol} = a + b_1x + b_2x^2 + b_3x^3 + b_4x^4 + b_5x^5 + b_6x^6$)						
	n_{melt}	ρ_{melt}/ g.cm^{-3}	a	b_1	b_2	b_3	b_4	b_5	b_6
Best	1.5052	1.2897	998.2	-0.483	232.81	-36.78	137.06	-96.59	55.48
Upper	1.5093	1.3192	998.2	-0.705	253.36	-53.41	183.61	-139.01	77.14
Lower	1.5012	1.2614	998.2	-0.323	213.1	-24.73	101.55	-65.53	39.14

Table S15.2: Tabulated experimental data points shown in **Fig S15.1.**

a_w	error a_w (+ve)	error a_w (-ve)	MFS	error MFS
0.95373	3.22E-04	6.26E-04	0.39071	0.00391
0.95843	8.35E-04	0.00118	0.36348	0.00812
0.9634	0.0011	0.00133	0.3272	0.00935
0.96865	0.00107	0.00138	0.28685	0.01043
0.97365	9.42E-04	0.00127	0.24062	0.01007
0.97863	9.10E-04	0.00114	0.1917	0.00876
0.98405	5.88E-04	8.82E-04	0.13977	0.00621
0.98877	3.13E-04	4.91E-04	0.09086	0.0027
0.99423	1.80E-04	3.02E-04	0.04898	0.00153
0.99692	1.66E-04	3.62E-04	0.02978	7.74E-04

S16 Pimelic Acid Hygroscopicity

Fig S16.1: Hygroscopicity of Pimelic Acid, (Sigma Aldrich, Purity 99 %), at 293.15 K. Open squares, these experiments; solid line, UNIFAC model.

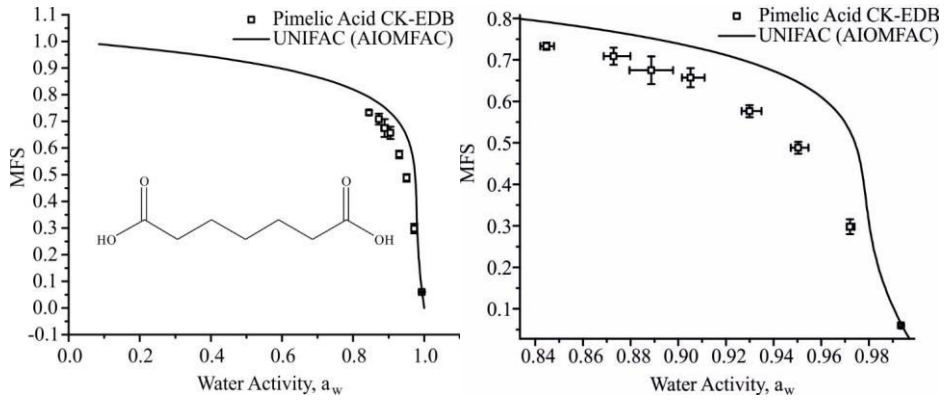

Table S16.1: Pure component refractive index (n_{melt}) is determined using molar refraction, assuming ideal mixing for calculation of the melt density (ρ_{melt}), from bulk data available in Cai et al. (2016). The variation of density as a function of the root of solute mass fraction ($MFS^{1/2}$ =x) is represented by polynomial fit parameters. *Upper* and *lower* refer to 95 % confidence limits for fits to experimental data, (Section 2.2 in manuscript).

			Polynomial fit ($\rho_{sol} = a + b_1x + b_2x^2 + b_3x^3 + b_4x^4 + b_5x^5 + b_6x^6$)						
	n_{melt}	ρ_{melt}/ g.cm^{-3}	a	b_1	b_2	b_3	b_4	b_5	b_6
Best	1.4917	1.2262	998.5	-0.184	188.18	-14.19	67.86	-37.91	23.94
Upper	1.4940	1.2435	998.5	-0.246	200.41	-18.89	83.16	-50.18	30.74
Lower	1.4894	1.2095	998.5	-0.136	176.23	-10.52	55.25	-28.29	18.47

Table S16.2: Tabulated experimental data points shown in **Fig S16.1.**

a_w	error a_w (+ve)	error a_w (-ve)	MFS	error MFS
0.84466	0.00317	0.00251	0.73296	0.0087
0.87279	0.00711	0.00413	0.70863	0.02048
0.88863	0.00919	0.00916	0.67508	0.03342
0.90517	0.00585	0.00361	0.65697	0.02274
0.92985	0.00504	0.00334	0.57632	0.01441
0.9503	0.00434	0.00304	0.48806	0.01436
0.97207	0.0019	0.00139	0.29782	0.01787
0.99347	2.49E-04	3.32E-04	0.06002	0.00268

S17 Methyl Malonic Acid Hygroscopicity

Fig S17.1: Hygroscopicity of methyl malonic acid, (Sigma Aldrich, Purity 99 %), at 293.15 K. Open squares, these experiments; solid line, UNIFAC model.

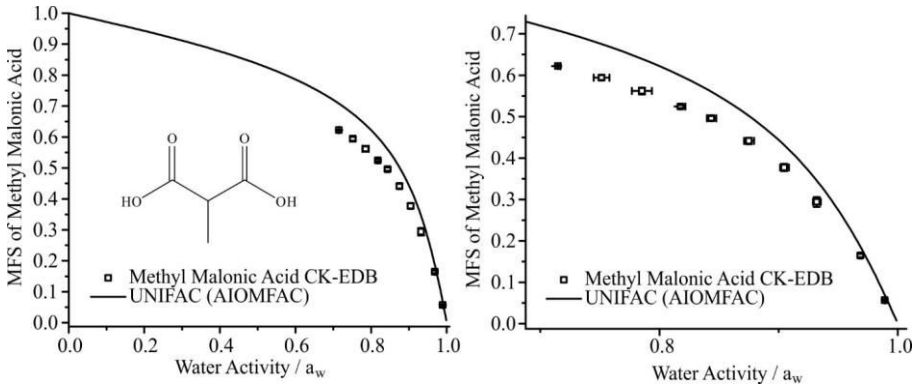

Table S17.1: Pure component refractive index (n_{melt}) is determined using molar refraction, assuming ideal mixing for calculation of the melt density (ρ_{melt}), from bulk data available in Cai et al. (2016). The variation of density as a function of the root of solute mass fraction ($MFS^{1/2}$ =x) is represented by polynomial fit parameters. *Upper* and *lower* refer to 95 % confidence limits for fits to experimental data, (Section 2.2 in manuscript).

			Polynomial fit ($\rho_{sol} = a + b_1x + b_2x^2 + b_3x^3 + b_4x^4 + b_5x^5 + b_6x^6$)						
	n_{melt}	ρ_{melt}/ $g.cm^{-3}$	a	b_1	b_2	b_3	b_4	b_5	b_6
Best	1.4817	1.3876	998.8	-1.45	301.28	-108.73	330.65	-279.56	146.61
Upper	1.4819	1.3902	998.8	-1.49	303.18	-111.53	337.82	-286.56	149.98
Lower	1.4815	1.3851	998.8	-1.42	299.45	-106.09	323.86	-272.94	143.43

Table S17.2: Tabulated experimental data points shown in **Fig S17.1.**

a_w	error a_w (+ve)	error a_w (-ve)	MFS	error MFS
0.71493	0.002	0.00248	0.62219	0.00155
0.75141	0.00657	0.00657	0.59428	0.00609
0.78527	0.0084	0.0084	0.562	0.00836
0.81777	0.004	0.00245	0.52434	0.00364
0.84355	0.00409	0.00369	0.49609	0.00573
0.875	0.00438	0.00401	0.44143	0.00784
0.90462	0.00402	0.00333	0.3774	0.00875
0.93201	0.00335	0.00317	0.29413	0.01184
0.96865	8.29E-04	8.90E-04	0.16472	0.0041
0.98911	4.09E-04	4.11E-04	0.05691	0.00203

S18 Methyl Succinic Acid Hygroscopicity

Figure S18.1: Hygroscopicity of methyl succinic acid, (Sigma Aldrich, Purity 99 %), at 293.15 K. Open squares, these experiments; solid line, UNIFAC model.

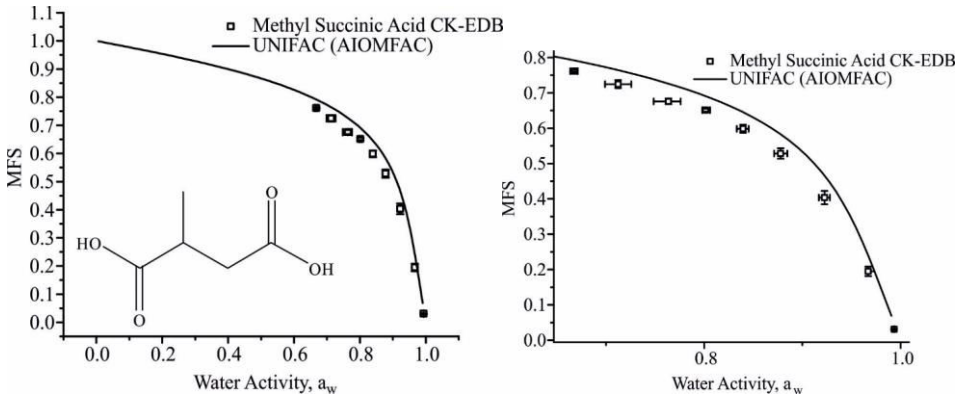

Table S18.1: Pure component refractive index (n_{melt}) is determined using molar refraction, assuming ideal mixing for calculation of the melt density (ρ_{melt}), from bulk data available in Cai et al. (2016). The variation of density as a function of the root of solute mass fraction ($MFS^{1/2}$ =x) is represented by polynomial fit parameters. *Upper* and *lower* refer to 95 % confidence limits for fits to experimental data, (Section 2.2 in manuscript).

			Polynomial fit ($\rho_{sol} = a + b_1x + b_2x^2 + b_3x^3 + b_4x^4 + b_5x^5 + b_6x^6$)						
	n_{melt}	ρ_{melt}/ $g.cm^{-3}$	a	b_1	b_2	b_3	b_4	b_5	b_6
Best	1.4779	1.3035	998.2	-0.572	242.3	-43.51	156.55	-114.16	64.69
Upper	1.4784	1.3090	998.2	-0.614	246.13	-46.62	165.26	-122.12	68.76
Lower	1.4774	1.2980	998.2	-0.533	238.48	-40.56	148.19	-106.58	60.79

Table S18.2: Tabulated experimental data points shown in **Fig S18.1.**

a_w	error a_w (+ve)	error a_w (-ve)	MFS	error MFS
0.66772	0.00345	0.00424	0.76125	0.00296
0.71234	0.0134	0.0134	0.72476	0.01132
0.7636	0.01237	0.01517	0.67596	0.00785
0.80135	0.00451	0.00326	0.65118	0.00447
0.83951	0.00575	0.00629	0.59855	0.01151
0.87778	0.00688	0.00657	0.52839	0.01469
0.92249	0.00567	0.00567	0.40343	0.01891
0.96705	0.00282	0.00249	0.19484	0.01368
0.99344	3.28E-04	3.47E-04	0.03075	0.00168

S19 Binary Aqueous Diethylmalonic Acid - Hygroscopicity

Fig S19.1: Hygroscopicity of diethylmalonic acid, (Sigma Aldrich, Purity 98 %), at 293.15 K. Open squares, these experiments; solid line, UNIFAC model.

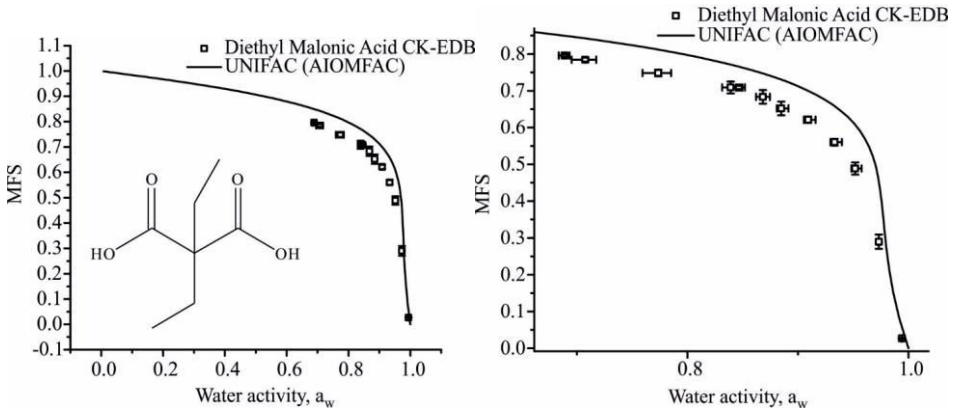

Table S19.1: Pure component refractive index (n_{melt}) is determined using molar refraction, assuming ideal mixing for calculation of the melt density (ρ_{melt}), from bulk data available in Cai et al. (2016). The variation of density as a function of the root of solute mass fraction ($MFS^{1/2}$ =x) is represented by polynomial fit parameters. *Upper* and *lower* refer to 95 % confidence limits for fits to experimental data, (Section 2.2 in manuscript).

			Polynomial fit ($\rho_{sol} = a + b_1x + b_2x^2 + b_3x^3 + b_4x^4 + b_5x^5 + b_6x^6$)						
	n_{melt}	ρ_{melt}/ $g.cm^{-3}$	a	b_1	b_2	b_3	b_4	b_5	b_6
Best	1.4854	1.2184	998.2	-0.161	182.82	-12.45	61.98	-33.36	21.37
Upper	1.4858	1.2219	998.2	-0.172	185.32	-13.25	64.69	-35.44	22.55
Lower	1.4850	1.2149	998.2	-0.151	180.32	-11.69	59.36	-31.37	20.24

Table S19.2: Tabulated experimental data points shown in **Figure S19.1.**

a_w	error a_w (+ve)	error a_w (-ve)	MFS	error MFS
0.68895	0.00441	0.00543	0.79565	0.00315
0.70762	0.01	0.01233	0.78448	0.00548
0.7737	0.01156	0.01425	0.7484	0.00901
0.83916	0.01287	0.00773	0.70902	0.01617
0.84654	0.00329	0.00246	0.70885	0.00435
0.86832	0.00637	0.0062	0.68324	0.01847
0.88499	0.00646	0.00418	0.65203	0.0186
0.90928	0.00665	0.00391	0.62123	0.00847
0.93317	0.00665	0.00374	0.56028	0.00907
0.95177	0.00586	0.00329	0.48861	0.01646
0.97321	0.00199	0.00152	0.28968	0.01912
0.99422	3.23E-04	3.66E-04	0.02697	0.00157

S20 2,2-Dimethyl Glutaric Acid Hygroscopicity

Fig S20.1: Hygroscopicity of 2,2-dimethyl glutaric acid, (Sigma Aldrich, Purity > 98 %), at 293.15 K. Open squares, these experiments; solid line, UNIFAC model.

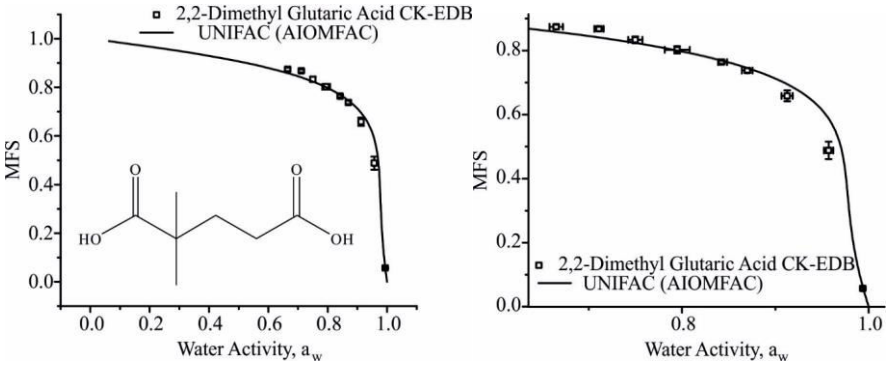

Table S20.1: Pure component refractive index (n_{melt}) is determined using molar refraction, assuming ideal mixing for calculation of the melt density (ρ_{melt}), from bulk data available in Cai et al. (2016). The variation of density as a function of the root of solute mass fraction ($MFS^{1/2}$ =x) is represented by polynomial fit parameters. *Upper* and *lower* refer to 95 % confidence limits for fits to experimental data, (Section 2.2 in manuscript).

			Polynomial fit ($\rho_{sol} = a + b_1x + b_2x^2 + b_3x^3 + b_4x^4 + b_5x^5 + b_6x^6$)						
	n_{melt}	ρ_{melt}/ $g.cm^{-3}$	a	b_1	b_2	b_3	b_4	b_5	b_6
Best	1.4881	1.2225	998.2	-0.174	185.75	-13.39	65.16	-35.81	22.76
Upper	1.4884	1.2248	998.2	-0.181	187.39	-13.93	67	-37.24	23.57
Lower	1.4878	1.2201	998.2	-0.166	184.04	-12.83	63.28	-34.36	21.94

Table S19.2: Tabulated experimental data points shown in **Fig S20.1.**

a_w	error a_w (+ve)	error a_w (-ve)	MFS	error MFS
0.66522	0.00707	0.00713	0.87406	0.00722
0.71105	0.00493	0.00494	0.8677	0.00654
0.74996	0.00758	0.00758	0.83334	0.01058
0.79488	0.01337	0.01338	0.80256	0.01126
0.84249	0.00573	0.00389	0.76365	0.00522
0.86987	0.00563	0.00574	0.73768	0.00728
0.91262	0.00592	0.00605	0.65854	0.01692
0.95695	0.00508	0.00491	0.48805	0.02723
0.99362	3.59E-04	3.74E-04	0.05685	0.00348

S21 2,2-Dimethyl Succinic Acid Hygroscopicity

Fig S21.1: Hygroscopicity of 2,2-dimethyl succinic acid, (Sigma Aldrich, Purity 99 %), at 293.15 K. Open squares, these experiments; solid line, UNIFAC model.

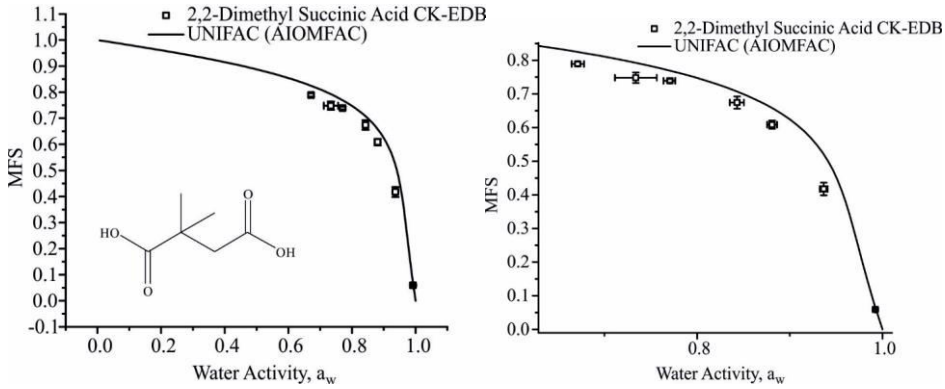

Table S21.1: Pure component refractive index (n_{melt}) is determined using molar refraction, assuming ideal mixing for calculation of the melt density (ρ_{melt}), from bulk data available in Cai et al. (2016). The variation of density as a function of the root of solute mass fraction ($MFS^{1/2}=x$) is represented by polynomial fit parameters. *Upper* and *lower* refer to 95 % confidence limits for fits to experimental data, (Section 2.2 in manuscript).

			Polynomial fit ($\rho_{sol} = a + b_1x + b_2x^2 + b_3x^3 + b_4x^4 + b_5x^5 + b_6x^6$)						
	n_{melt}	ρ_{melt}/ $g.cm^{-3}$	a	b_1	b_2	b_3	b_4	b_5	b_6
Best	1.4889	1.2710	997.9	-0.382	220.13	-29.13	114.09	-76.29	44.68
Upper	1.4897	1.2776	997.9	-0.419	224.73	-31.96	122.4	-83.53	48.48
Lower	1.4880	1.2644	997.9	-0.347	215.51	-26.48	106.23	-69.5	41.09

Table S21.2: Tabulated experimental data points shown in **Fig S21.1**

a_w	error a_w (+ve)	error a_w (-ve)	MFS	error MFS
0.6713	0.00663	0.00663	0.78921	0.00655
0.73389	0.02256	0.02256	0.74829	0.01579
0.77076	0.00564	0.00705	0.73908	0.00579
0.84308	0.00747	0.00776	0.67413	0.01818
0.88089	0.00536	0.00529	0.60846	0.01212
0.9367	0.00425	0.00424	0.41751	0.01893
0.99244	4.24E-04	5.93E-04	0.05911	0.00313

S22 2-Methyl Glutaric Acid Hygroscopicity

Fig S22.1: Hygroscopicity of 2-methyl glutaric acid, (Sigma Aldrich, Purity 98 %), at 293.15 K. Open squares, these experiments; solid line, UNIFAC model.

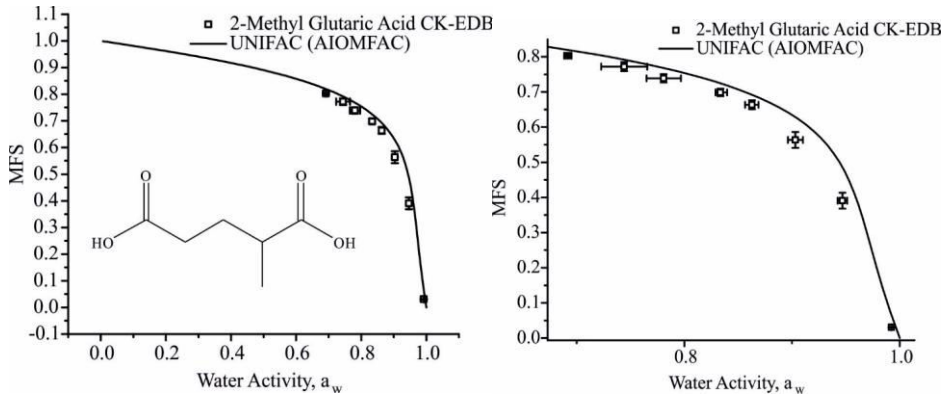

Table S22.1: Pure component refractive index (n_{melt}) is determined using molar refraction, assuming ideal mixing for calculation of the melt density (ρ_{melt}), from bulk data available in Cai et al. (2016). The variation of density as a function of the root of solute mass fraction ($MFS^{1/2}$ =x) is represented by polynomial fit parameters. *Upper* and *lower* refer to 95 % confidence limits for fits to experimental data, (Section 2.2 in manuscript).

			Polynomial fit ($\rho_{sol} = a + b_1x + b_2x^2 + b_3x^3 + b_4x^4 + b_5x^5 + b_6x^6$)						
	n_{melt}	ρ_{melt}/ $g.cm^{-3}$	a	b_1	b_2	b_3	b_4	b_5	b_6
Best	1.4866	1.2585	997.6	-0.319	211.59	-24.4	99.95	-64.16	38.24
Upper	1.4873	1.2648	997.6	-0.350	216	-26.78	107.1	-70.26	41.49
Lower	1.4858	1.2522	997.6	-0.290	207.17	-22.18	93.17	-58.44	35.17

Table S22.2: Tabulated experimental data points shown in **Fig S22.1**

a_w	error a_w (+ve)	error a_w (-ve)	MFS	error MFS
0.68925	0.00271	0.00334	0.80479	0.00208
0.72204	0.01005	0.01239	0.78383	0.00857
0.76123	0.01296	0.01422	0.75567	0.01704
0.78959	0.02339	0.02377	0.73478	0.02713
0.82836	0.01185	0.00726	0.70077	0.02018
0.84699	0.00634	0.00601	0.68658	0.01104
0.8785	0.00611	0.00622	0.63205	0.01527
0.91076	0.00612	0.00583	0.54437	0.02194
0.94004	0.00438	0.00438	0.4312	0.02071
0.98128	4.79E-04	0.0012	0.14884	0.0113
0.99285	2.24E-04	2.25E-04	0.02928	0.00106

S23 3-Methyl Adipic Acid Hygroscopicity

Fig S23.1: Hygroscopicity of 3-methyl adipic acid, (Sigma Aldrich, Purity 99 %), at 293.15 K. Open squares, these experiments; solid line, UNIFAC model.

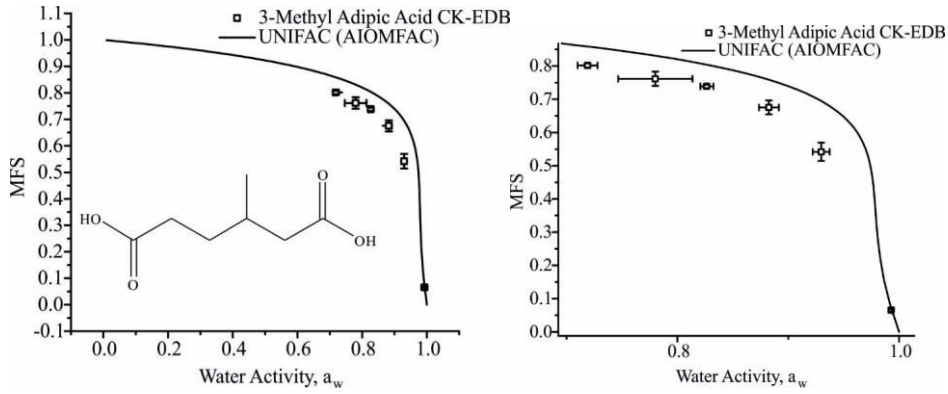

Table S23.1: Pure component refractive index (n_{melt}) is determined using molar refraction, assuming ideal mixing for calculation of the melt density (ρ_{melt}), from bulk data available in Cai et al. (2016). The variation of density as a function of the root of solute mass fraction ($MFS^{1/2}$ =x) is represented by polynomial fit parameters. *Upper* and *lower* refer to 95 % confidence limits for fits to experimental data, (Section 2.2 in manuscript).

			Polynomial fit ($\rho_{sol} = a + b_1x + b_2x^2 + b_3x^3 + b_4x^4 + b_5x^5 + b_6x^6$)						
	n_{melt}	ρ_{melt}/ $g.cm^{-3}$	a	b_1	b_2	b_3	b_4	b_5	b_6
Best	1.4865	1.2141	999.0	-0.147	179.19	-11.33	58.11	-30.42	19.69
Upper	1.4878	1.2243	999.0	-0.176	186.48	-13.59	65.86	-36.34	23.06
Lower	1.4852	1.2041	999.0	-0.121	171.99	-9.4	51.21	-25.33	16.75

Table S23.2: Tabulated experimental data points shown in **Fig S23.1.**

a_w	error a_w (+ve)	error a_w (-ve)	MFS	error MFS
0.71902	0.00897	0.00897	0.80154	0.00624
0.78015	0.03348	0.03347	0.7615	0.02149
0.82646	0.00615	0.00574	0.73848	0.00556
0.88266	0.00886	0.00907	0.67532	0.02097
0.92986	0.00748	0.00771	0.54185	0.02748
0.993	2.61E-04	3.72E-04	0.06527	0.00354

S24 3-Methyl Glutaric Acid Hygroscopicity

Fig S24.1: Hygroscopicity of 3-methyl glutaric acid, (Sigma Aldrich, Purity 99 %), at 293.15 K. Open squares, these experiments; solid line, UNIFAC model.

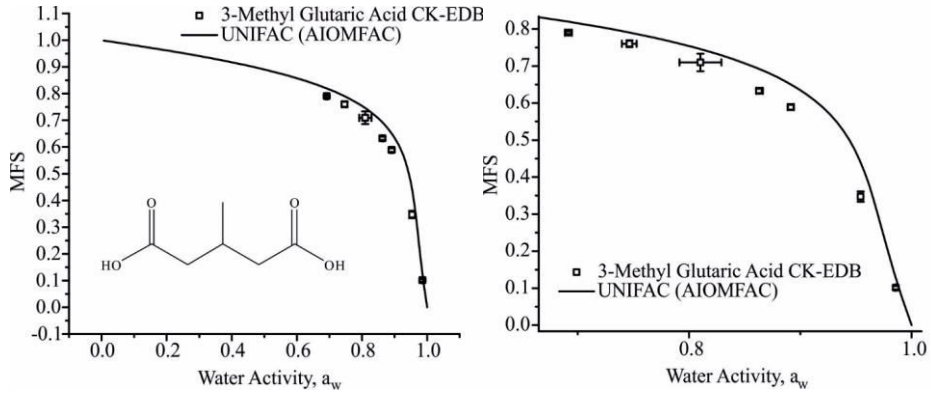

Table SI.24.1: Pure component refractive index (n_{melt}) is determined using molar refraction, assuming ideal mixing for calculation of the melt density (ρ_{melt}), from bulk data available in Cai et al. (2016). The variation of density as a function of the root of solute mass fraction ($MFS^{1/2}$ =x) is represented by polynomial fit parameters. *Upper* and *lower* refer to 95 % confidence limits for fits to experimental data, (Section 2.2 in manuscript).

			Polynomial fit ($\rho_{sol} = a + b_1x + b_2x^2 + b_3x^3 + b_4x^4 + b_5x^5 + b_6x^6$)						
	n_{melt}	ρ_{melt}/ $g.cm^{-3}$	a	b_1	b_2	b_3	b_4	b_5	b_6
Best	1.4819	1.2498	997.9	-0.277	205.29	-21.26	90.32	-56.07	33.89
Upper	1.4822	1.2531	997.9	-0.292	207.6	-22.37	93.74	-58.92	35.43
Lower	1.4816	1.2466	997.9	-0.264	203.04	-20.22	87.1	-53.39	32.44

Table S24.2: Tabulated experimental data points shown in **Fig S24.1.**

a_w	error a_w (+ve)	error a_w (-ve)	MFS	error MFS
0.69173	0.00299	0.00334	0.79013	0.0038
0.74649	0.00642	0.00683	0.76025	0.00932
0.81013	0.01887	0.01884	0.70959	0.02367
0.86283	0.00343	0.00213	0.63276	0.00618
0.89131	0.00283	0.00283	0.58884	0.00675
0.95411	0.00246	0.00245	0.3472	0.01394
0.98567	6.06E-04	6.09E-04	0.10123	0.00477

S25 3, 3-Dimethyl Glutaric Acid Hygroscopicity

Fig S25.1: Hygroscopicity of 3, 3-dimethyl glutaric acid, (Sigma Aldrich, Purity 98 %), at 293.15 K. Open squares, these experiments; solid line, UNIFAC model.

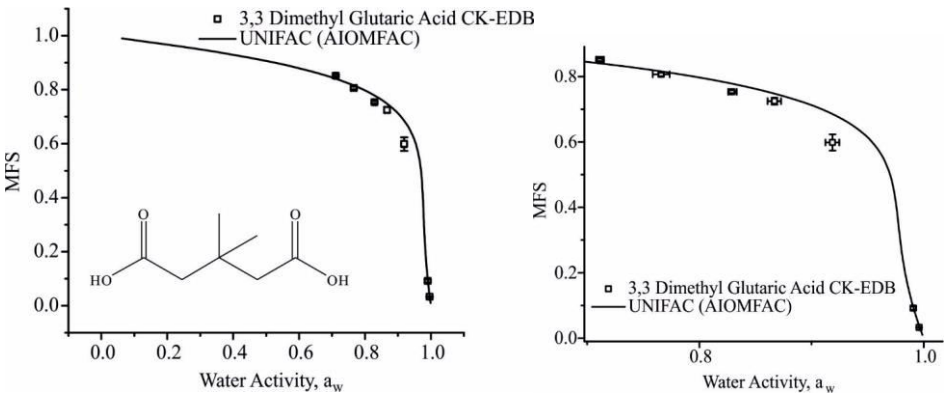

Table S25.1: Pure component refractive index (n_{melt}) is determined using molar refraction, assuming ideal mixing for calculation of the melt density (ρ_{melt}), from bulk data available in Cai et al. (2016). The variation of density as a function of the root of solute mass fraction ($MFS^{1/2}$ =x) is represented by polynomial fit parameters. *Upper* and *lower* refer to 95 % confidence limits for fits to experimental data, (Section 2.2 in manuscript).

			Polynomial fit ($\rho_{sol} = a + b_1x + b_2x^2 + b_3x^3 + b_4x^4 + b_5x^5 + b_6x^6$)						
	n_{melt}	ρ_{melt}/ $g.cm^{-3}$	a	b_1	b_2	b_3	b_4	b_5	b_6
Best	1.4903	1.2206	998.3	-0.167	184.33	-12.92	63.58	-34.59	22.07
Upper	1.4906	1.2231	998.3	-0.175	186.11	-13.5	65.55	-36.11	22.93
Lower	1.4900	1.2182	998.3	-0.160	182.61	-12.38	61.74	-33.18	21.27

Table S25.2: Tabulated experimental data points shown in **Fig S25.1.**

a_w	error a_w (+ve)	error a_w (-ve)	MFS	error MFS
0.71132	0.00345	0.00345	0.85176	0.00384
0.76078	0.006	0.00743	0.80912	0.00721
0.79151	0.01941	0.01942	0.79788	0.01562
0.83444	0.00416	0.00451	0.75169	0.00421
0.87055	0.00543	0.00565	0.71882	0.0105
0.91582	0.00545	0.00564	0.61641	0.02163
0.96018	0.00389	0.00389	0.39161	0.02576
0.99443	2.18E-04	2.83E-04	0.04485	0.00225

S26. PEG3 Hygroscopicity

Fig S26.1: Hygroscopicity of PEG3, at 293.15 K. Open squares, these experiments; solid line, UNIFAC model.

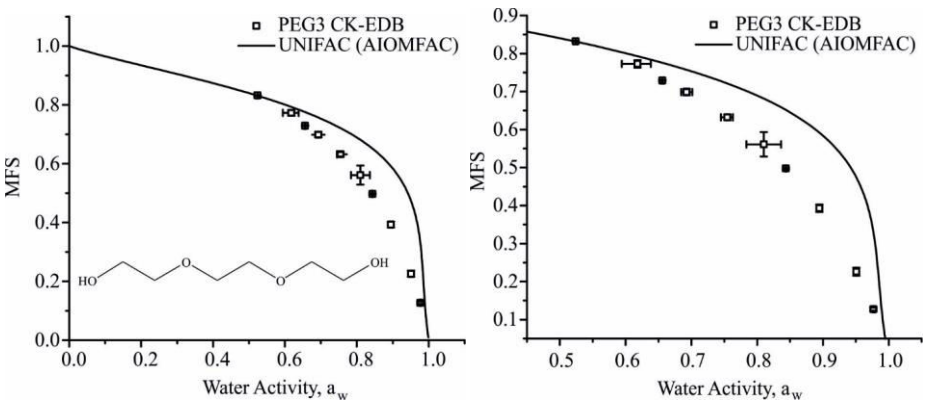

Table S26.1: Measured values of pure component melt density (ρ_{melt}) and refractive index (n_{melt}) (PEG3 is liquid), presented with parameterisation for solution measurements of density where x is the square root of MFS ($MFS^{1/2}$ =x). *Upper* and *lower* refer to 95 % confidence limits for fits to experimental data. Upper and lower limit on refractive index and density are determined by the error in the refractometer and by the densitometer respectively.

			Polynomial fit ($\rho_{sol} = a + b_1x + b_2x^2 + b_3x^3$)			
	n_{melt}	ρ_{melt}/ g.cm^{-3}	a	b_1	b_2	b_3
Best	1.4551	1.109	999.97	-75.75	431.63	-246.73
Upper	1.4552	1.122	999.97	-0.198	268.11	-144.15
Lower	1.4550	1.096	999.97	-151.31	595.15	-349.31

Table S26.2: Tabulated experimental data points shown in **Fig S26.1.**

a_w	error a_w (+ve)	error a_w (-ve)	MFS	error MFS
0.524	0.0024	0.00286	0.83232	0.00127
0.61806	0.02008	0.02389	0.77269	0.0098
0.65597	0.00198	0.00242	0.72923	0.00152
0.69291	0.00856	0.00856	0.69867	0.0088
0.75489	8.16E-03	0.01	0.63211	7.82E-03
0.81001	0.0263	0.0263	0.56113	0.03211
0.84347	0.00123	0.00119	0.49753	0.00229
0.89472	0.00416	0.00414	0.39303	0.01004
0.95087	3.07E-03	3.07E-03	0.22603	0.01048
0.97688	0.00201	0.00112	0.12742	0.00393

S27. PEG4 Hygroscopicity

Fig S27.1: Hygroscopicity of PEG4, at 293.15 K. Open squares, these CC-EDB experiments; solid line, UNIFAC model; blue line UManSysProp; red line adsorption isotherm model from Dutcher.

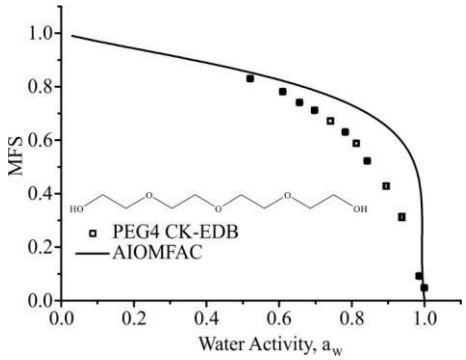

Table S27.1: Measured values of pure component melt density (ρ_{melt}) and refractive index (n_{melt}) (PEG4 is liquid), presented with parameterisation for solution measurements of density where x is the square root of MFS ($MFS^{1/2}$ =x). *Upper* and *lower* refer to 95 % confidence limits for fits to experimental data. Upper and lower limit on refractive index and density are determined by the error in the refractometer and by the densitometer respectively.

			Polynomial fit ($\rho_{sol} = a + b_1x + b_2x^2 + b_3x^3$)			
	n_{melt}	ρ_{melt}/ g.cm^{-3}	a	b_1	b_2	b_3
Best	1.4589	1.1271	999.97	-37.39	296.85	-130.68
Upper	1.4590	1.13412	999.97	-9.65	235.84	-92.25
Lower	1.4588	1.12338	999.97	-65.13	357.86	-169.11

Table S27.2: Tabulated experimental data points shown in **Fig S27.1.**

a_w	error a_w (+ve)	error a_w (-ve)	MFS	error MFS
0.52052	0.00336	0.00399	0.83006	8.065E-4
0.60966	0.00229	0.00278	0.78149	8.220E-4
0.65636	0.00166	0.00204	0.74058	0.00177
0.69735	0.00172	0.00212	0.71195	0.00154
0.74132	0.00556	0.00685	0.67145	0.00929
0.78212	6.975E-4	8.803E-4	0.63073	8.501E-4
0.81258	0.00536	0.00535	0.58791	0.00759
0.84243	0.00132	0.00111	0.52225	0.00213
0.89453	0.00427	0.00448	0.42827	0.01048
0.93766	0.00385	0.00376	0.31263	0.01217
0.98571	0.0013	0.00127	0.0918	0.00662
0.99969	0.00143	0.00156	0.0475	0.00252

S28 Erythritol Hygroscopicity

Fig S28.1: Hygroscopicity of erythritol (Sigma Aldrich 99 %), at 293.15 K. Open squares, these experiments; solid line, UNIFAC model.

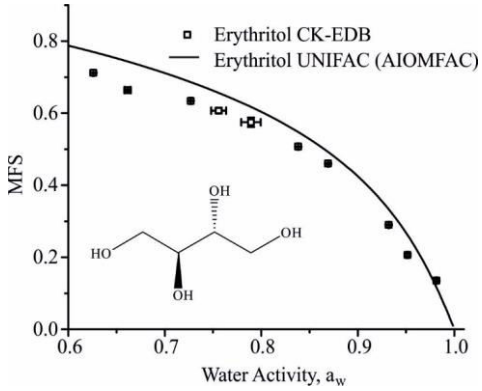

Table S28.1: Pure component refractive index (n_{melt}) is determined using molar refraction, assuming ideal mixing for calculation of the melt density (ρ_{melt}), from bulk data available in Cai et al. (2016). The variation of density as a function of the root of solute mass fraction ($MFS^{1/2} = x$) is represented by polynomial fit parameters. *Upper* and *lower* refer to 95 % confidence limits for fits to experimental data, (Section 2.2 in manuscript).

			Polynomial fit ($\rho_{sol} = a + b_1x + b_2x^2 + b_3x^3$)			
	n_{melt}	ρ_{melt}/ g.cm^{-3}	a	b_1	b_2	b_3
Best	1.5211	1.3754	998.6	58.46	37.98	278.66
Upper	1.5388	1.3813	998.6	60.21	33.79	286.94
Lower	1.5204	1.3695	998.6	56.75	42.03	27.049

Table S28.2: Tabulated experimental data points shown in **Fig S28.1.**

a_w	error a_w (+ve)	error a_w (-ve)	MFS	error MFS
0.62602	8.77112E-4	0.00107	0.71188	6.08334E-4
0.66147	0.0027	0.0033	0.66395	0.00226
0.72692	0.00104	0.00129	0.6342	6.57702E-4
0.75582	0.00775	0.00777	0.60723	0.00739
0.78929	0.01009	0.0101	0.57499	0.01315
0.83827	7.77253E-4	0.001	0.50705	9.72437E-4
0.86916	7.13427E-4	6.96511E-4	0.46004	0.00138
0.93195	2.64028E-4	3.52642E-4	0.28987	0.00175
0.95145	7.53773E-4	7.52526E-4	0.20621	0.00312
0.9815	5.76107E-4	5.56581E-4	0.13503	0.00279

S29 Sorbitol Hygroscopicity

Fig S29.1: Hygroscopicity of sorbitol (Sigma Aldrich ≥ 98 %), at 293.15 K. Open squares, these experiments; solid line, UNIFAC model. Data taken at RHs lower than indicated by the dashed black line show increased error in hygroscopicity retrieval due to the imposition of a kinetic limitation on water transport.

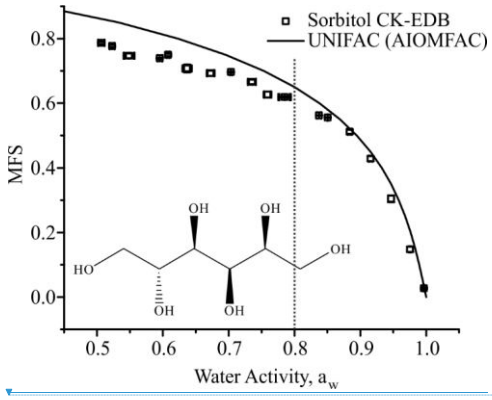

Deleted:

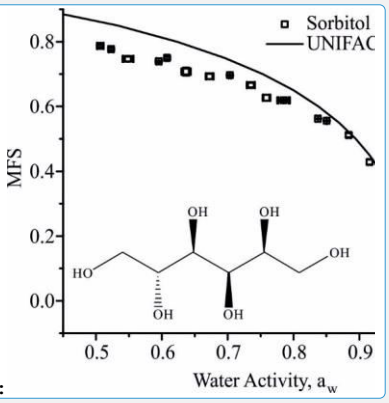

Table S29.1: Pure component refractive index (n_{melt}) determined using molar refraction where the melt density (ρ_{melt}) is determined using a polynomial fit of density to the square root of MFS ($MFS^{1/2}$ =x). Bulk values used are available in Cai et al. (2016). *Upper* and *lower* refer to 95 % confidence limits for fits to experimental data.

			Polynomial fit ($\rho_{sol} = a + b_1x + b_2x^2 + b_3x^3$)			
	n_{melt}	ρ_{melt}/ g.cm^{-3}	a	b_1	b_2	b_3
Best	1.5244	1.4231	997.8	8.6	286.1	130.7
Upper	1.5267	1.4333	997.8	24.74	234.56	175.54
Lower	1.5220	1.4128	997.8	-7.6	337.59	85.83

Table S29.2: Tabulated experimental data points shown in **Fig S29.1.**

a_w	error a_w (+ve)	error a_w (-ve)	MFS	error MFS
0.50647	0.00432	0.00512	0.78667	0.00341
0.52291	0.0031	0.00369	0.7771	0.00307
0.54873	0.00705	0.00838	0.74672	0.00731
0.59535	0.00322	0.00389	0.73916	0.00193
0.60809	0.0019	0.0023	0.74976	0.00343
0.63682	0.00605	0.00728	0.70773	0.01216
0.67255	0.00497	0.00601	0.69271	0.00773
0.7035	0.00148	0.00183	0.69648	0.00163
0.73531	0.00619	0.00619	0.66608	0.00694
0.75896	0.00493	0.00599	0.62673	0.00941
0.78492	0.00775	0.00958	0.61901	0.00237
0.83722	0.00384	0.0025	0.56241	9.55991E-4
0.85049	9.622E-4	8.165E-4	0.5556	0.00118
0.88386	0.00262	0.0027	0.51154	0.00629
0.91574	0.00253	0.00266	0.4286	0.0076
0.94681	0.00245	0.00245	0.30429	0.01053
0.97555	0.0014	0.00139	0.14769	0.00774
0.99655	0.00112	6.78573E-4	0.02751	0.00293

S30 D-(+)-Trehalose Dihydrate Hygroscopicity

Deleted: ¶
¶
¶
¶

Fig S30.1: Hygroscopicity of D-(+)-trehalose dihydrate (Sigma Aldrich ≥ 99 %), at 293.15 K. Open squares, these experiments; solid line, UNIFAC model. Data taken at RHs lower than indicated by the dashed black line show increased error in hygroscopicity retrieval due to the imposition of a kinetic limitation on water transport.

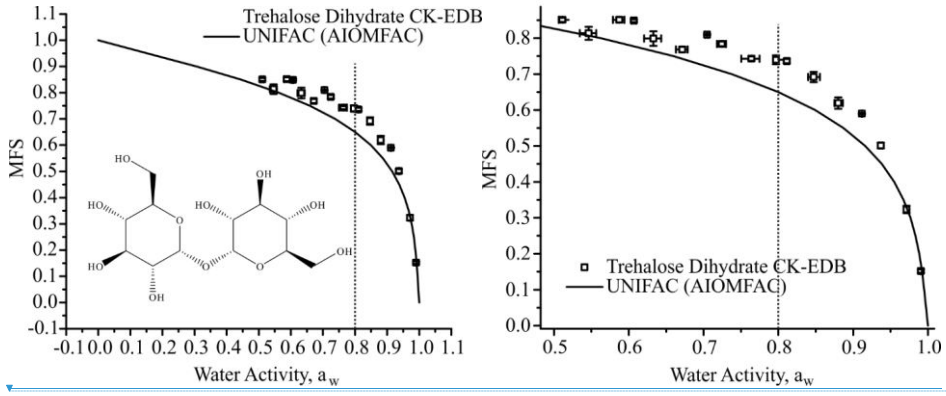

Deleted:

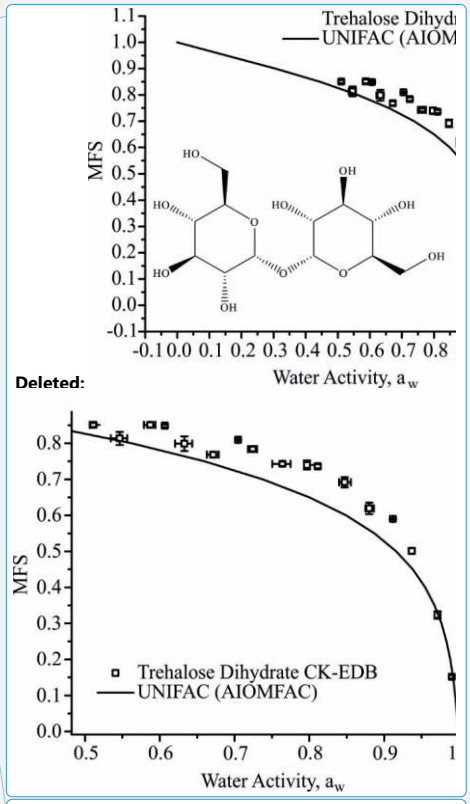

Deleted:

Table S30.1: Pure component refractive index (n_{melt}) determined using molar refraction where the melt density (ρ_{melt}) is determined using a polynomial fit of density to the square root of MFS ($MFS^{1/2}$ =x). Bulk values used are available in Cai et al. (2016). *Upper* and *lower* refer to 95 % confidence limits for fits to experimental data.

			Polynomial fit ($\rho_{sol} = a + b_1x + b_2x^2 + b_3x^3$)			
	n_{melt}	ρ_{melt}/ g.cm^{-3}	a	b_1	b_2	b_3
Best	1.5193	1.4682	997.8	8.2	284.3	177.8
Upper	1.5211	1.4734	997.8	11.6	269.79	194.19
Lower	1.5175	1.4629	997.8	4.87	298.84	161.43

Table S30.2: Tabulated experimental data points shown in **Fig S30.1.**

a_w	error a_w (+ve)	error a_w (-ve)	MFS	error MFS
0.51123	0.00397	0.0047	0.8511	0.00561
0.54636	0.01007	0.01196	0.81364	0.01816
0.5873	0.007	0.00844	0.85121	0.00732
0.60689	0.00263	0.00319	0.84879	0.00386
0.63303	0.01031	0.01244	0.79889	0.02031
0.67154	0.00716	0.00861	0.76858	0.00766
0.70479	0.00212	0.00262	0.80977	0.00199
0.72437	0.00577	0.00642	0.78413	0.00669
0.76384	0.01102	0.01364	0.743	0.00611
0.79679	0.00422	0.00225	0.7399	0.01219
0.81122	0.00282	0.00195	0.73624	0.0059
0.84712	0.00837	0.00721	0.69205	0.01427
0.88007	0.00598	0.00498	0.61945	0.01589
0.9118	5.25851E-4	5.4066E-4	0.58998	0.00159
0.93698	0.00204	0.00204	0.50101	0.00792
0.97142	0.00151	0.00149	0.3233	0.01015
0.99054	4.05516E-4	4.09208E-4	0.15195	0.00476

S31. Galactose Hygroscopicity

Fig S31.1: Hygroscopicity of (Sigma Aldrich ≥ 99 %), at 293.15 K. Open squares, these experiments; solid line, UNIFAC model. Data taken at RHs lower than indicated by the dashed black line show increased error in hygroscopicity retrieval due to the imposition of a kinetic limitation on water transport.

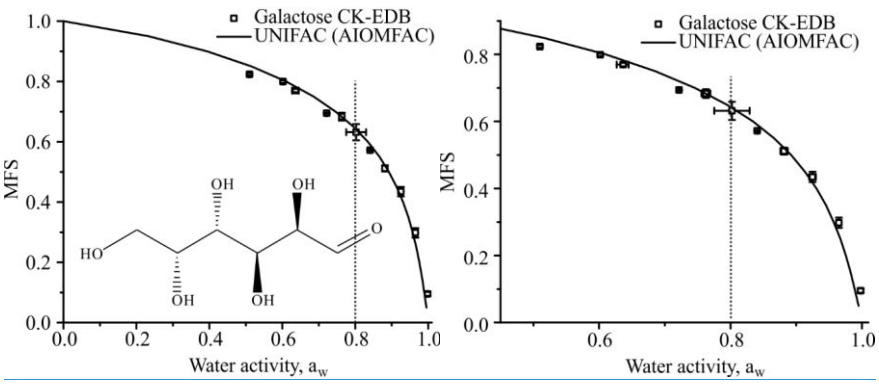

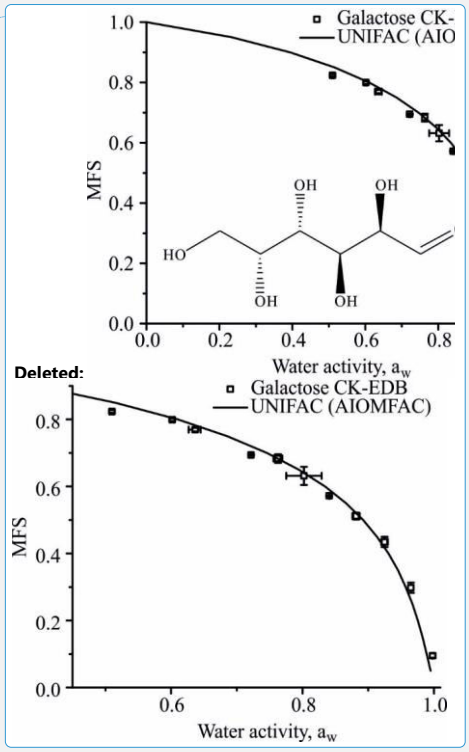

Table SI.31.1: Pure component refractive index (n_{melt}) is determined using molar refraction, assuming ideal mixing for calculation of the melt density (ρ_{melt}), from bulk data available in Cai et al. (2016). The variation of density as a function of the root of solute mass fraction ($MFS^{1/2}$ =x) is represented by polynomial fit parameters. *Upper* and *lower* refer to 95 % confidence limits for fits to experimental data, (Section 2.2 in manuscript).

			Polynomial fit ($\rho_{sol} = a + b_1x + b_2x^2 + b_3x^3$)			
	n_{melt}	ρ_{melt}/ g.cm^{-3}	a	b_1	b_2	b_3
Best	1.5885	1.6306	997.36	403.27	83.09	150.11
Upper	1.5892	1.6351	996.67	165.3	-284.07	752.22
Lower	1.5878	1.6261	997.37	399.69	83.4	145.36

Table S31.2: Tabulated experimental data points shown in **Fig S31.1.**

a_w	error a_w (+ve)	error a_w (-ve)	MFS	error MFS
0.50996	0.00287	0.0034	0.82372	0.00382
0.60189	0.00267	0.00323	0.7993	0.00405
0.63684	0.00839	0.01012	0.76963	0.0055
0.72183	0.0016	0.00199	0.69438	0.00194
0.76282	0.00662	0.00694	0.68348	0.01289
0.80226	0.02704	0.02704	0.6317	0.02723
0.84064	0.00138	8.91966E-4	0.572	0.00141
0.88152	0.00559	0.00561	0.51157	0.01025
0.92485	0.00483	0.00491	0.43437	0.01532
0.96504	0.00377	0.00374	0.29773	0.01536
0.99822	0.00115	7.88489E-4	0.09505	0.00656

S32 Xylose Hygroscopicity

Fig S32.1: Hygroscopicity of (Sigma Aldrich ≥ 99 %), at 293.15 K. Open squares, these experiments; solid line, UNIFAC model.

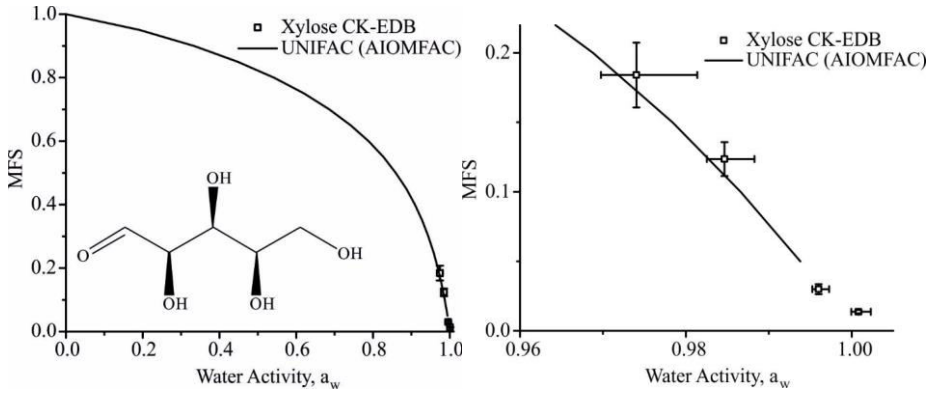

Table S32.1: Pure component refractive index (n_{melt}) is determined using molar refraction, assuming ideal mixing for calculation of the melt density (ρ_{melt}), from bulk data available in Cai et al. (2016). The variation of density as a function of the root of solute mass fraction ($MFS^{1/2} = x$) is represented by polynomial fit parameters. *Upper* and *lower* refer to 95 % confidence limits for fits to experimental data, (Section 2.2 in manuscript).

			Polynomial fit ($\rho_{sol} = a + b_1x + b_2x^2 + b_3x^3$)			
	n_{melt}	ρ_{melt}/ g.cm^{-3}	a	b_1	b_2	b_3
Best	1.5615	1.5626	996.73	127.69	-163.53	597.09
Upper	1.5619	1.5653	996.74	126.37	-159.45	591.57
Lower	1.5611	1.5598	996.72	128.97	-167.5	602.42

Table S32.2: Tabulated experimental data points shown in **Fig S32.1.**

a_w	error a_w (+ve)	error a_w (-ve)	MFS	error MFS
0.97404	0.00732	0.00429	0.1841	0.0233
0.98465	0.00361	0.00212	0.12356	0.01215
0.996	0.00127	7.43479E-4	0.02995	0.00361
1.00081	0.00148	8.71845E-4	0.01372	0.0012

S33 2,3-Dimethyl Succinic Acid Hygroscopicity

Fig S33.1: Hygroscopicity of 2,3-dimethyl succinic acid (Sigma Aldrich ≥ 99 %), at 293.15 K. Open squares, these experiments; solid line, UNIFAC model. (Density treatment for 2,2-dimethyl succinic acid used.)

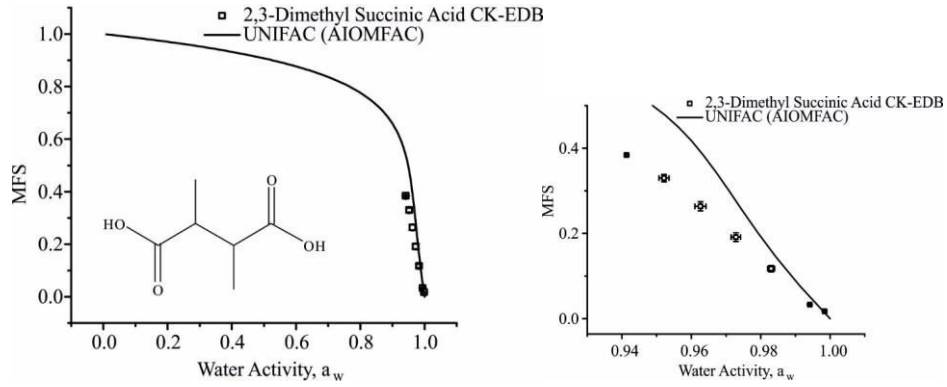

Table S33.2: Tabulated experimental data points shown in **Fig S33.1.**

a_w	error a_w (+ve)	error a_w (-ve)	MFS	error MFS
0.94132	5.11673E-4	5.12405E-4	0.38395	0.00207
0.95214	0.00144	0.00144	0.32979	0.00859
0.96262	0.00159	0.00159	0.26369	0.01065
0.97285	0.00138	0.00138	0.19135	0.01011
0.98303	0.001	0.001	0.11733	0.00731
0.99417	2.09751E-4	2.24291E-4	0.03301	0.00121
0.99844	2.59195E-4	4.09162E-4	0.01724	4.61378E-4

S34 Dimethyl Malonic Acid Hygroscopicity

Figure S34.1: Hygroscopicity of (Sigma Aldrich 98 %), at 293.15 K. Open squares, these experiments; solid line, UNIFAC model. (Density treatment for methyl succinic acid used.)

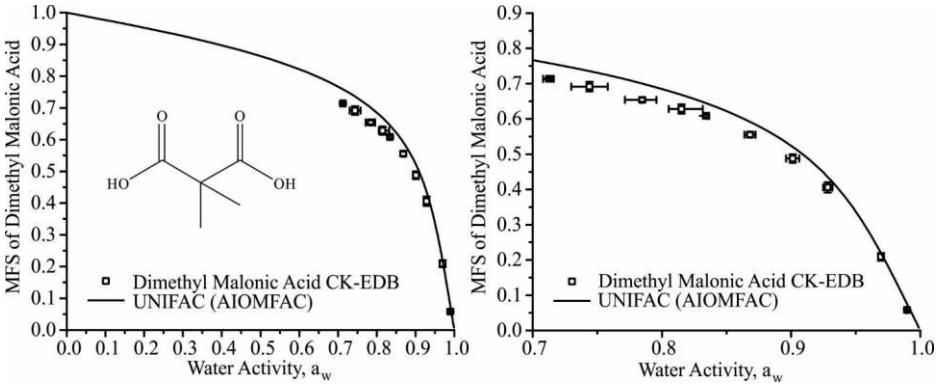

Table S34.2: Tabulated experimental data points shown in **Figure S34.1.**

a_w	error a_w (+ve)	error a_w (-ve)	MFS	error MFS
0.71262	0.00362	0.00449	0.7136	0.00301
0.744	0.0141	0.0141	0.69155	0.01343
0.78481	0.01088	0.01348	0.65412	0.00614
0.81516	0.01647	0.00985	0.62813	0.01311
0.83412	0.00246	0.00229	0.60844	0.00357
0.86818	0.00422	0.00426	0.5554	0.00729
0.90119	0.00509	0.00506	0.48761	0.01203
0.92833	0.00366	0.00365	0.40593	0.01475
0.96965	0.00157	0.00194	0.2089	0.01089
0.9897	4.75033E-4	4.76981E-4	0.05824	0.00271

S35 Aspartic Acid Hygroscopicity

Fig S35.1: Hygroscopicity of aspartic acid (Sigma Aldrich ≥ 99 %), at 293.15 K. Open squares, these experiments; solid line, UNIFAC model. (Density treatment for alanine used)

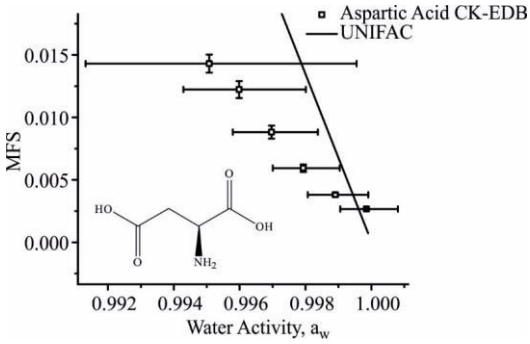

Table S35.1: Tabulated experimental data points shown in **Fig S35.1.**

a_w	error a_w (+ve)	error a_w (-ve)	MFS	error MFS
0.99507	0.00448	0.00375	0.01431	7.18E-04
0.99599	0.00202	0.0017	0.01223	6.83E-04
0.99697	0.00141	0.00118	0.00882	5.15E-04
0.99793	0.00111	9.28E-04	0.00594	3.01E-04
0.99891	0.001	8.39E-04	0.00381	1.64E-04
0.99985	9.52E-04	7.98E-04	0.00266	8.72E-05

S36 Asparagine Hygroscopicity

Fig S36.1: Hygroscopicity of asparagine (Sigma Aldrich ≥ 98 %), at 293.15 K. Open squares, these experiments; solid line, UNIFAC model. (Density treatment for alanine used)

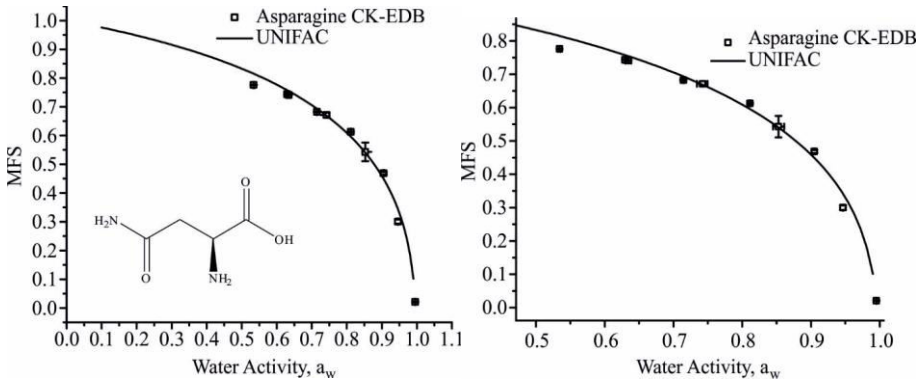

Table S36.1: Tabulated experimental data points shown in **Figure S36.1.**

a_w	error a_w (+ve)	error a_w (-ve)	MFS	error MFS
0.53409	0.00178	0.00213	0.77577	0.00129
0.62935	0.00189	0.0023	0.74326	0.00101
0.63444	0.00381	0.00465	0.74081	0.00101
0.71441	0.00113	0.0014	0.68254	0.00175
0.74237	0.007	0.00854	0.67146	0.00782
0.81123	8.45796E-4	8.49613E-4	0.61254	0.00185
0.85278	0.00812	0.00813	0.54286	0.03203
0.9048	0.00102	9.46055E-4	0.46853	0.00454
0.94641	0.00108	0.0011	0.3002	0.00693
0.9951	2.80427E-4	2.96722E-4	0.02083	0.00124

S37 Errors in Density and Refractive Index Parametrisations and their Impact on Hygroscopicity

Fig S37.1 Parametrisation for (a) density based on ideal mixing and bulk measured values for density up to the solubility limit and (b) refractive index predicted beyond the solubility limit using molar refraction. In both (a) and (b) dashed lines indicate the uncertainty envelope in the parametrisations. All bulk experimental values of aqueous density and refractive index are available in the supplementary information of Cai et al. (2016). In (c) measured equilibrium hygroscopicity curves are presented with upper and lower error envelope arising from the uncertainties in density and refractive index which is too small to be obvious.

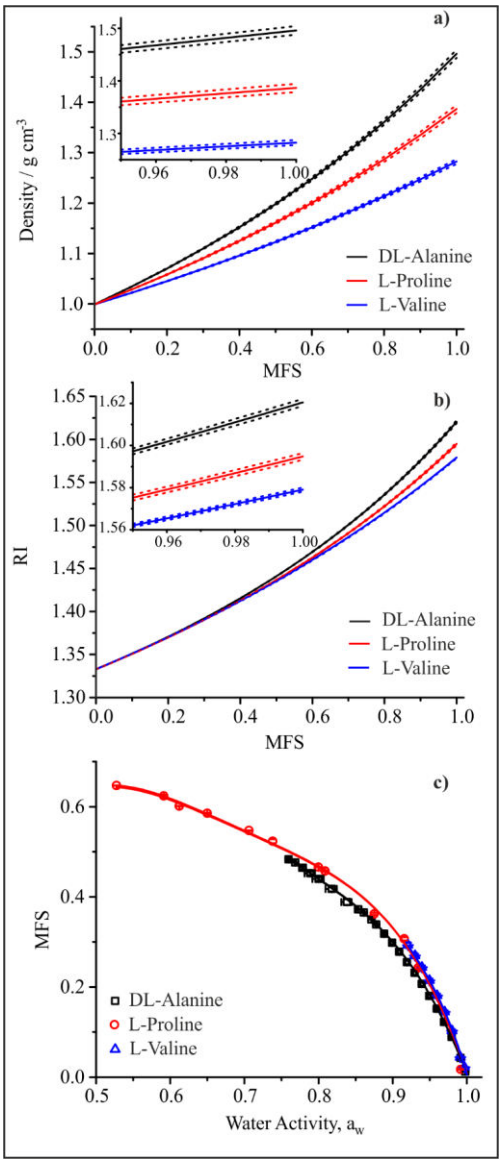
a)
Density / g cm^{-3}
MFS
DL-Alanine
L-Proline
L-Valine
b)
RI
MFS
DL-Alanine
L-Proline
L-Valine
c)
MFS
Water Activity, a_w
DL-Alanine
L-Proline
L-Valine

S38 ΔMFS for Simple Straight Chain Dicarboxylic Acids

Fig S38.1 The difference in mass fraction of solute (ΔMFS) between values predicted by UNIFAC and experimental values (a) oxalic acid, (b) malonic acid, (c) succinic acid and (d) glutaric acid.

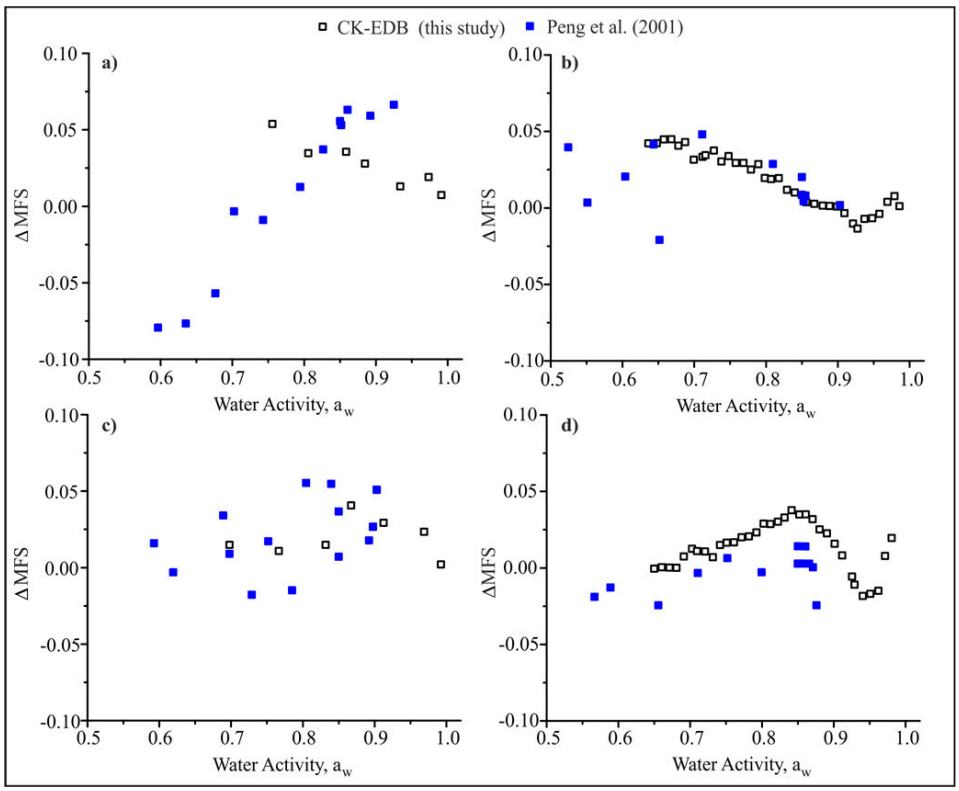

S39 Viscosity, Diffusion Constant and Timescale of Diffusional Mixing

The kinetic modelling framework used in the analysis of the droplet evaporation events is valid only in the absence of a bulk-kinetic limitation on near surface composition, i.e. the particle must be assumed to be homogeneous in composition. Such a limitation was obvious for hygroscopicity measurements of trehalose, galactose and sorbitol at RH's lower than 80 %. To ensure the measurements are not compromised by bulk diffusion, we consider two important factors.

Firstly, the impact of viscosity on the hygroscopicity retrievals becomes very obvious when we consider the consistency and uncertainty in the raw hygroscopic growth curves determined from different droplets evaporating into differing RHs. Droplets drying into different RHs reach different compositions at different times, and will retain different amounts of water because of different drying rates. This leads to an artificially low MFS at a particular RH which then slowly returns to the equilibrium curve overtime. Thus, an inconsistency is apparent between retrieved hygroscopic growth curves (or MFS vs a_w) when drying into different RHs. An example of this is shown in Figure S39.1, where we report unbinned hygroscopicity data for alanine (a non-viscous amino acid) and trehalose (viscous at RHs lower than 80%). It is clear here that the different portions of the hygroscopic curves retrieved from measurements at different RHs are consistent for alanine but not for trehalose. A further easy way to identify this retention of water in a particle that is not fully

equilibrated is simply to measure the much longer time-dependence in size once the initial evaporation of water has stopped. In droplets that have reached a bulk diffusion limitation, the existence of a kinetic limitation is apparent in a steadily decreasing size as water continues to leave over a timescale longer than 10 s.

Fig S39.1 a) Unbinned hygroscopicity data for the compound alanine. b) Unbinned hygroscopicity data for the compound trehalose. At 50 % RH trehalose has a viscosity of 3.8 x 10^5 Pa.s (Song et al. 2016).

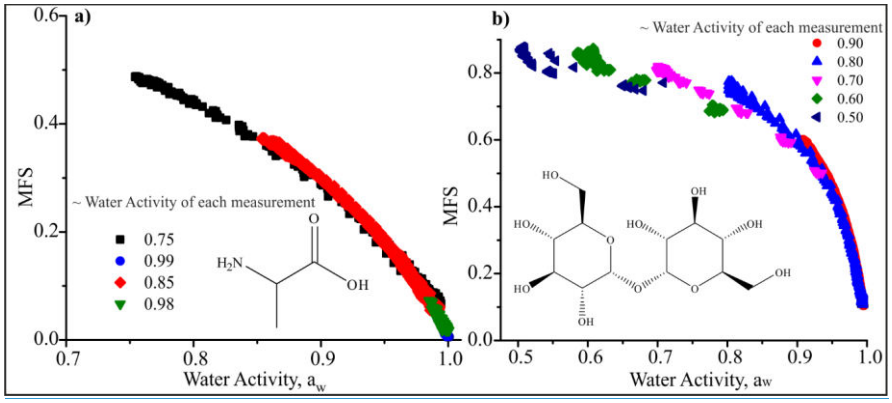

Secondly, we can determine the expected conditions under which we might expect problems to arise in retrieving hygroscopic growth curves from an evaporation measurement. Considering again trehalose at 80 % RH, an aqueous-trehalose droplet has a viscosity of 0.5 Pa.s, increasing to 3.8×10^5 Pa.s at 50 % RH (Song et al. 2016). Therefore, as the RH of the gas phase for the evaporation measurement is lowered, we can expect the increasing viscosity/decreasing diffusivity to become increasingly important. By contrast, for aqueous-carboxylic acid droplets, the viscosity never gets above 1 Pa s even at the driest RHs considered here (Song et al. 2016).

With these known dependencies of viscosity on water activity, we can estimate the timescale for diffusional mixing within a droplet, assuming that this provides an estimate of the timescale for an evaporating droplet to form a homogeneous mixture. This timescale must be considerably shorter than the evaporation timescale for our hygroscopicity estimations to be valid. First, the Stokes-Einstein equation is used to estimate the diffusion constant of water at varying viscosity (varying RH).

$$D = \frac{k_B T}{6\pi r_{mol} \eta} \qquad (1.1)$$

D is the diffusion constant, k_B is the Boltzmann constant, T is temperature, r_{mol} is the molecular radius of water (taken as 1.375 Å) and η is the viscosity. It should be noted that equation (1.1) is likely to provide a significant underestimate of the diffusion constant due to the failure of the Stokes-Einstein equation. At a viscosity of 100 Pa s, the diffusion constant for water in sucrose is already more than one order of magnitude larger than estimated from the viscosity (Power et al. 2013). However, using diffusion constants estimated from (1.1) will provide an upper limit on the diffusional mixing timescale. The timescale for diffusional mixing, τ, is then estimated using the expression

$$\tau = \frac{a^2}{\pi^2 D} \qquad (1.2)$$

where a is the droplet radius (set as 10 microns in this calculation).

We compare the diffusional mixing timescales for aqueous droplets of trehalose, NaCl, $NaNO_3$ and glutaric acid in the newly added supplemental Figure S39.2 (and repeated below). Given that we have been able to report accurate hygroscopic growth curves for $NaNO_3$ down to 50 % RH (see Rovelli et al. 2016 and the

response to referee 2), it is clear that a final viscosity at 50 % of ~ 0.1 Pa.s (Baldelli et al.) is insufficient to impede accurate measurement of the hygroscopicity. Indeed, this suggests that water transport in any aerosol droplet that maintains a viscosity lower than 0.1 Pa.s during drying should remain sufficiently fast to avoid a bulk diffusion limitation, permitting accurate hygrosocpicity measurements. As an example of the diacarboyxlic acids considered in this study, glutaric acid has a considerably lower viscosity at 50 % RH of ~ 0.01 Pa.s (Song et al. 2016), indicative of what we might expect for all such similar systems. By contrast, aqueous-trehalose droplets cross the 0.1 Pa.s viscosity threshold at a water activity of ~0.85 (Song et al. 2016), commensurate with the deviation and increased scatter in the hygroscopicity measurements reported above for this compound.

Deleted: i

Based on the two considerations above and to indicate clearly the water activity ranges over which we consider the hygroscopicity measurements to be valid for trehalose (S30), galactose (S31) and sorbitol (S29), we have added a dashed line to indicate where the data appear to become kinetically limited. We have added the following words to the captions of these Figures: "Data taken at RHs lower than indicated by the dashed black line show increased error in hygroscopicity retrieval due to the imposition of a kinetic limitation on water transport."

Again, we must reiterate that the true diffusion constants are generally found to be much larger than values estimated from the Stokes-Einstein equation. A droplet with a viscosity of 0.1 Pa s takes ~0.3 s to mix by diffusion based on our analysis here, but this is an upper limit on the timescale.

Fig S39.2 a) Viscosity of Trehalose, NaCl, NaNO3 and Glutaric Acid as a function of RH. b) Estimated diffusion constant as a function of RH. c) Timescale for diffusional mixing at the RH shown on x-axis. Dashed green line represents 1 second timescale for diffusional mixing.

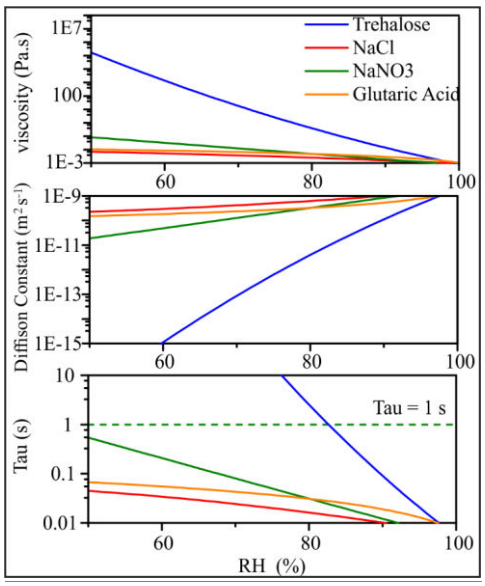

A. Baldelli, R. M. Power, R. E. H. Miles, J. P. Reid and R. Vehring *Effect of crystallization kinetics on the properties of spray dried microparticles,* Aerosol Science and Technology, 2016, 50:7, 693-704, DOI:10.1080/02786826.2016.1177163

R. M. Power, S. H. Simpson, J. P. Reid and A. J. Hudson, *The transition from liquid to solid-like behaviour in ultrahigh viscosity aerosol particles,* Chemical Science, 2013, 4 , 2597, DOI: 10.1039/c3sc50682g

Y. Chul Song, A. E. Haddrell, B. R. Bzdek, J. P. Reid, T. Bannan, D. O. Topping,, C. Percival, and C. Cai *Measurements and Predictions of Binary Component Aerosol Particle Viscosity* J. Phys. Chem. A 2016, 120, 8123−8137, DOI: 10.1021/acs.jpca.6b07835

Deleted: ¶